

stabilization and levitation. Our findings and methods for code development show encouraging results and suggest that further improvements to the design and calibration of our system should be explored in order to refine our proof-of-concept for specific applications.

MAGNETIC FIELD MANIPULATION
AS A MEANS OF STABILIZATION

By

Team MAGNET

Samer M. AbouSaleh
Nikhil Badami
James Nathaniel Foote
Adam I. Hurwitz
Alexander C. Johnson
David S. Kessler
José Fernando Lamas
Jesse D. Lynch
Robin Kimberly McFaul
Thomas A. Ogden
Shawn G. Rosofsky
Noah J. Wichrowski
Chungho P. Woo

Thesis submitted in partial fulfillment of the requirements of the Gemstone
Program University of Maryland, College Park
2017

Advisory Comittee:

Dr. Frank Coale,
Dr. Elisabeth Smela, Chair
Dr. Gilmer Blankenship
Dr. Daniel Lathrop
Dr. Robert Sanner

© Copyright by

Team MagNET

Samer M. AbouSaleh
Nikhil Badami
James Nathaniel Foote
Adam I. Hurwitz
Alexander C. Johnson
David S. Kessler
José Fernando Lamas
Jesse D. Lynch
Robin Kimberly McFaul
Thomas A. Ogden
Shawn G. Rosofsky
Noah J. Wichrowski
Chungho P. Woo

2017

This page intentionally left blank.

Acknowledgments

We would like to acknowledge all those that have helped us in our research: our former teammate Emma Holmes; our Mentor Dr. Frank Coale; our previous Mentor Dr. R. D. Gomez; and the Gemstone supporting staff: Dr. Kristan Skendall, Dr. Vickie Hill, Leah Tobin, and Jessica Lee. We would also like to thank our librarian Ms. Jesse Sigman; our former librarians Robin Dassler and Nevenka Zdravskovska; and expert advisors Dr. Jungho Kim, Dr. Bruce Jacob, and Mr. Martin Nelson. Finally, we would like to extend the most gracious of thanks to our Launch UMD donors, without whose contributions we would have been unable to support our research endeavors.

Contents

Acknowledgments	ii
Table of Contents	iii
List of Tables	vi
List of Figures	vii
List of Symbols	ix
1 Introduction	1
2 Literature Review	5
2.1 Overview	5
2.2 Magnets	6
2.2.1 Fundamental Concepts	6
2.2.2 Magnetic Dipoles	8
2.2.3 Earnshaw's Theorem	10
2.3 Spin-Stabilized Magnetic Levitation	11
2.4 Dynamic Magnetic Stabilization	13
2.5 Existing Examples of Magnetic Levitation	15
2.5.1 Levitron	15
2.5.2 Magnetic Bearings	17
2.5.3 Photolithography	18
2.6 Possible Applications of Magnetic Stabilization	19
2.6.1 Shock Absorption and Earthquake Protection	19
2.6.2 Centrifuges	20
2.6.3 Wind Turbines	21
2.7 Solenoids	22
2.7.1 Fundamental Concepts	22
2.7.2 Eddy Currents	24

2.7.3	Induction Motors	25
2.8	Circuits	26
2.9	Finite Element Method	27
2.9.1	Theory and Procedure	28
2.9.2	Applications of FEM	32
2.9.3	Software	33
2.10	Summary	34
3	Methodology	36
3.1	Overview	36
3.2	Research Questions and Planned Experimental Design	37
3.2.1	Properties of Levitation	37
3.2.2	Additions to Basic System	39
3.2.3	Optimization	41
3.2.4	Applicability	44
3.3	Magnet Mapping	45
3.4	Circuit Mapping	48
3.4.1	Existing Analog Circuit Analysis	48
3.4.2	Design of Dynamic Circuit Prototype	49
3.5	Prototyping	52
3.5.1	Prototype Overview	52
3.5.2	Solenoid Fabrication	54
3.5.3	Protective Case	56
3.5.4	Hall Effect Sensor Array	57
3.6	Control Theory	59
3.6.1	Modeling the System	59
3.6.2	Initial Compensator Design	62
3.6.3	Determining the Constants	63
3.7	Code Development	67
3.7.1	Sensor Readings	68
3.7.2	Control Algorithm	71
3.7.3	The Input Code	72
3.7.4	The Output Code	72
3.7.5	Debugging	72
3.8	Experimental Limitations	73
3.8.1	Practical Limitations	73
3.8.2	Empirical Limitations	75
3.9	Summary	77

4	Results and Analysis	78
4.1	Magnet Mapping	78
4.1.1	FEMM Models	78
4.1.2	Ring Magnet	80
4.1.3	Puck Magnet	82
4.2	Solenoids	83
5	Conclusions	87
5.1	Research Conclusions	87
5.2	Future Research	87
	Appendix A Magnetic Field Maps	89
A.1	Ring Magnet Axial Component	90
A.2	Puck Magnet Axial Component	94
A.3	Puck Magnet Radial Component	98
	Appendix B Magnetic Field MATLAB Analysis Code	100
	Appendix C Micro-controller Code	115
C.1	Main Code ADC	115
C.2	DAC-ADC Test Code	118
C.3	Control Code	122
	Appendix D Schematics and Design Drawings	124
	References	133

List of Tables

3.1	Solenoid Fabrication Materials	54
4.1	Solenoid Calibration Data	84

List of Figures

2.1	Example of a Hysteresis Curve	8
2.2	Tuned Mass Damper	14
2.3	Magnetic Diagram of the Levitron™	16
2.4	K-Type Brace	21
2.5	Diagram of a Solenoid	23
2.6	Hall Effect Sensor Graphic	26
2.7	Finite Element Mesh of Massachusetts	29
2.8	One-Dimensional Tent Functions	30
2.9	Numerical Solution by Finite Element Method	32
3.1	Puck Magnet Angle of Displacement	40
3.2	Measuring Puck Magnet's Axial Field Strength	46
3.3	Background Magnetic Field	47
3.4	Measuring Puck Magnet's Radial Field Strength	49
3.5	BJT Circuit Diagram	50
3.6	First Physical BJT Circuit	51
3.7	MOSFET Circuit Diagram	52
3.8	Assembled System Drawing	53
3.9	Hall Sensor Array	58
3.10	Compensator Bode Diagram	63
3.11	Ring Magnet Field Strength	64
3.12	Puck Magnet Field Strength	65
4.1	Magnetic Field FEMM Simulations	79
4.2	Axial Magnetic Field Modeling: Ring	80
4.3	Axial Magnetic Field Modeling: Puck	85
4.4	Solenoid Calibration: Magnetic Field and Current	86
A.1	Ring Magnet Axial Field at $z = 3.8$ mm	90
A.2	Ring Magnet Axial Field at $z = 14.2$ mm	91
A.3	Ring Magnet Axial Field at $z = 19.8$ mm	92

A.4	Ring Magnet Axial Field at $z = 27.2$ mm	93
A.5	Puck Magnet Axial Field at $z = 6.3$ mm	94
A.6	Puck Magnet Axial Field at $z = 13.2$ mm	95
A.7	Puck Magnet Axial Field at $z = 19.1$ mm	96
A.8	Puck Magnet Axial Field at $z = 24.4$ mm	97
A.9	Puck Magnet Radial Field at $z = 19.1$ mm	98
A.10	Puck Magnet Radial Field at $z = 236$ mm	98
A.11	Puck Magnet Radial Field at $z = 34.5$ mm	99
A.12	Puck Magnet Radial Field at $z = 44.2$ mm	99
D.1	Protective Case CAD Design	124
D.2	Assembled System Drawing	125

List of Symbols

Mathematical Symbols

- M the stiffness matrix in a FEM problem
- m_{ij} an entry in the stiffness matrix M , equal to $\int_a^b v'_i(x) v'_j(x) dx$
- $U_N(x)$ the one-dimensional FEM approximation of $u(x)$ with N interior nodes
- $V_D^{[a,b]}$ the set of all functions $v(x)$ possessing a piecewise continuous derivative and satisfying the Dirichlet condition $v(a) = v(b) = 0$

Physical Variables

- \mathbf{a} linear acceleration [m/s²]
- A_c cross-sectional area [m²]
- \mathbf{B} magnetic flux density [T] or [Wb/m²]
- \mathbf{F} force [N] or [kg·m/s²]
- \mathbf{H} magnetic field intensity [A/m]
- I electric current in a circuit [A] or [C/s]
- I rotational inertia [kg·m²]
- I_{tr} transverse rotational inertia [kg·m²]
- \mathbf{J} current density [A/m²]
- \mathbf{L} angular momentum [kg·m²/s]
- ℓ length [m]
- L_{sol} inductance of a solenoid [H] or [Wb/A]

\mathbf{M}	magnetization, the density of magnetic dipole moments	[J/T·m ²]
m	mass	[kg]
r	radius or radial distance	[m]
V	electric potential at a point in space or in a circuit	[V] or [J/C]
\mathbf{x}	position	[m]
ε	electromotive force	[V] or [J/C]
μ	magnetic permeability	[H/m] or [N/A ²]
μ_r	relative permeability of a material, μ/μ_0	
Φ_B	magnetic flux	[Wb] or [T·m ²]
ω	angular velocity	[Hz] or [s ⁻¹]

Constants

g	acceleration due to gravity	9.80665 m/s ²
μ_0	magnetic permeability of free space	$4\pi \times 10^{-7}$ H/m

Control Theory

B_0	ring magnet offset parameter	
B_2	ring magnet quadratic parameter	
c	solenoid constant, defined to equal $-12IA\kappa/z^5$	
$G(s)$	transfer function	
$H(s)$	compensator function	
s	Laplace space independent variable	
β	control modifier, defined such that $\beta^2 = 2\alpha/m$	
γ	gain modifier, defined to equal $2c\delta\mu_{puck}/(Im)$	
δ	displacement from center position for Taylor expansion of magnetic field	
κ	ferromagnetic core gain	
μ_{puck}	magnetic dipole moment of puck magnet	

Chapter 1

Introduction

Various systems, ranging in size from lab equipment to buildings, require critical components to remain static despite outside forces or moving internal parts in order to ensure their safety and increase their lifespan. Most current designs rely on strong foundations, springs, and dampers to achieve this static stability. However, these common systems lack a feedback loop. This omission prevents the systems from adapting to their respective environments, rendering the designs ineffective or inadequate under dynamic conditions.

We hypothesized that magnets could prove a viable solution to this problem, as electromagnets can create magnetic fields of varying strength. In order to assess the feasibility of this project, we reviewed current literature on magnetic levitation and stabilization technologies. Our initial research indicated that, based on the success of several simple systems, a device with real-time feedback from environmental factors could be used to create a stabilized magnetic levitation system by using permanent magnets and electromagnets in conjunction with a microcontroller to counter the inherent properties of magnets and gravity.

From this hypothesis, we designed a system that can measure the interaction between the base and the levitated magnet's field using Hall effect sensors and use that information to determine where in 3-D space the levitated object is relative to the base. The signals from the Hall sensors are in the form of a voltage measured in micorvolts, which correspond to the magnetic field strengths in each of the three Cartesian directions, giving the location in 3-D space of the levitating magnet. Using the measured location, the microcontroller then determines the necessary adjustments in position relative to the center to force the object back to the stable, central location. The microcontroller will then output a voltage, which is converted to a current using transistors, to one or more of the four individual inductors in order to stabilize the levitated puck magnet. The four inductors output magnetic fields proportional to the input current, meaning higher currents will result in stronger forces acting on the stabilized object. This process operates in real time on a 40Hz update cycle, chosen based on the control algorithm and style of coding, to continually adjust the magnetic field being output, assuring the stability of the levitated magnet.

In order to understand the challenges we would face in the design of our device, we analyzed the circuit of an existing simple, electric-powered, magnetic levitation system. The goal of this research was to understand how the device, that levitated a small magnet above a base of electromagnets, worked and potentially reverse engineer it, replacing hardware parts with a microcontroller to implement user control. After determining that the information we were collecting was not useful in generating a control algorithm, we de-

cided to gather data on the puck and ring magnets used by the previously mentioned existing system by scanning the magnets and mapping the fields in order to understand how the shapes of these magnets affect the shape of their respective magnetic fields. We then confirmed the scalability of our project by replicating the magnetic fields of these magnets using Finite Element Methods Magnetic software. We were able to verify the data gathered from the scans of our magnets through the computer modeling process, enabling us to more fully understand the order of magnitude of the magnetic field that our inductors have to be able to generate in order to do their job and assist with levitation. In order to do achieve levitation, we built and calibrated inductors to meet the required specifications of our chosen magnets. The inductors were then tested in three different circuits, testing whether or not our circuits were capable of outputting variable magnetic fields. We then developed a control algorithm based on the interaction of our magnetic components to be able to anticipate how the levitated magnet would act as well as how the system had to respond to keep the magnet levitating. The control algorithm was then used to write the code for the microcontroller to implement the control process to our prototype. The code was designed to adjust the current output to all four separate solenoids based on the magnetic field data from the Hall effect sensors. For future experiments, the code we wrote can be adapted to more complex mechanisms or scaled up for larger applications.

The research presented herein explores a novel method in developing a stabilization system using both permanent magnets and electromagnets in combination with a feedback loop to allow for real-time control of a levitating

object in space. Our research goal was to gather information and further calibrate and optimize the system in order to establish the limitations and benefits of this method of stabilization.

Chapter 2

Literature Review

2.1 Overview

Stabilization is an important aspect of structural and mechanical design. Stability is required for a table to remain standing or a car to function properly. Levitation is a key component in near-frictionless systems. Friction is caused by the contact between two surfaces, which can be eliminated through levitation. We combined these concepts to create a machine capable of actively levitating and stabilizing a magnetic object. The wealth of knowledge available in literature that pertains to control theory, circuits, and magnetic fields was explored and consolidated to design a functioning prototype. The following literature review provides the background information necessary for the design and implementation of our magnetic levitation system.

2.2 Magnets

2.2.1 Fundamental Concepts

Magnetic fields are produced by the movement of electric charges. In metals, elements that readily form positive ions (cations) and have metallic bonds, charges are unconstrained and may move freely in any direction. A random motion of charges produces competing effects, and there is no macroscopic magnetic field. Electrons in a permanent magnet, however, are aligned to a common axis of rotation, producing a net magnetic field [62]. Atomic orbitals are normally occupied by a pair of electrons having opposite quantum mechanical spins, but, in a permanent magnet, there are orbitals containing only one electron. Unpaired electrons that spin in the same direction contribute to an overall magnetic field.

A permanent magnet is a ferromagnetic material, like iron, that has been exposed to a sufficiently strong external magnetic field. The material then retains a constant field of its own even after the external field is removed. Other classes of magnetism include paramagnetic materials, whose electrons temporarily align themselves to form a magnetic field in the same direction as an applied magnetic force, and diamagnetic materials, which temporarily form a field in the opposite direction of an applied magnetic force [22].

When a ferromagnetic material is placed within an external magnetic field of strength \mathbf{H} , the electrons within the material align with that of the external field, provided the material is below a certain temperature known as the Curie point [69]. In turn, the magnetic moments of the electrons produce a new

magnetic field, denoted by the magnetization \mathbf{M} . As long as the external field remains, the ferromagnet will remain at maximum strength and add to the overall magnetic force. However, even after the external field is removed, the ferromagnet retains some of its own magnetic field, denoted by the total magnetic field, \mathbf{B} [69].

This phenomenon is known as hysteresis (see Figure 2.1). The relationship between \mathbf{B} , \mathbf{H} , and \mathbf{M} of a permanent magnet is given by the equation

$$\mathbf{M} = \frac{\mathbf{B}}{\mu_0} - \mathbf{H} \quad (2.1)$$

where μ_0 is the magnetic permeability of a vacuum [69]. The property where a ferromagnet maintains its residual magnetic field after being removed from an external field is called its retentivity. Up to a saturation point, a stronger applied field yields a greater residual magnetic field. However, after surpassing this saturation point, the residual field can no longer increase and the ferromagnet has reached its peak strength. Removing the ferromagnet's residual magnetic field requires that a secondary external field be applied in the opposite direction of the original field. The strength required to eliminate the residual field depends on the ferromagnet's coercivity [62]. Coercivity is a magnetic material's ability to resist changes in its magnetic properties, i.e. the ferromagnet's ability to retain a magnetic field without the original source of magnetism.

The practical uses of a magnet depends on its coercivity [62]. For example, magnetically "soft" materials (low coercivity) are often used in trans-

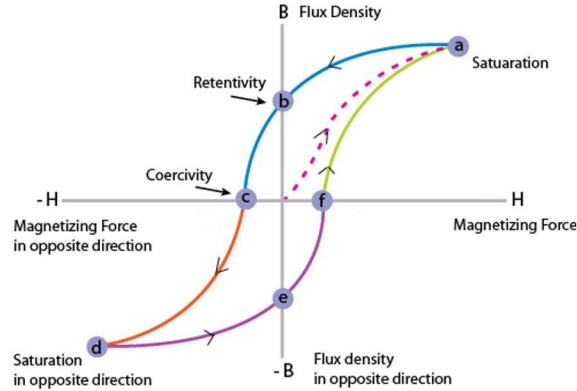


Figure 2.1: A qualitative hysteresis plot for a ferromagnetic material. Points c and f represent the same concept as well as points b and e; adapted from [60].

former cores and to amplify the field strength of electromagnets. On the other hand, magnetically “hard” materials (high coercivity), such as neodymium-iron-boron (NdFeB) magnets, are commonly used as permanent magnets.

2.2.2 Magnetic Dipoles

Most permanent magnets can be well approximated as magnetic dipoles as long as the magnets are separated by a significant distance. Dipoles can be envisioned as microscopic spheres with one side having a negative magnetic charge and the other side having a positive magnetic charge. This makes them relatively easy to describe mathematically [22]. The magnetic field of a dipole is given as

$$\mathbf{B}_{dip} = \frac{\mu_0}{4\pi r^3} [3(\mathbf{m} \cdot \hat{\mathbf{r}})\hat{\mathbf{r}} - \mathbf{m}] \quad (2.2)$$

or in spherical coordinates as

$$\mathbf{B}_{dip} = \frac{\mu_0 m}{4\pi r^3} [2 \cos \theta \hat{\mathbf{r}} + \sin \theta \hat{\boldsymbol{\theta}}] \quad (2.3)$$

where \mathbf{m} is the magnetic dipole moment vector, μ_0 is the magnetic permeability constant, r is radial distance from the surface of the magnet, and θ is the polar angle. This equation can be used in modeling magnetic systems and approximating the interactions between magnets, which is important for creating a control algorithm for a system using magnets.

The behavior of a magnetic dipole is well defined by a series of defining equations other than the basic equation that defines the magnetic field. The force on a magnetic dipole due to the field \mathbf{B} [22] is given as

$$\mathbf{F} = \nabla(\mathbf{m} \cdot \mathbf{B}). \quad (2.4)$$

The torque on a magnetic dipole [22] is given by

$$\boldsymbol{\tau} = \mathbf{m} \times \mathbf{B}. \quad (2.5)$$

Again, these equations are important in modeling the interactions between magnets, which is useful when attempting to write a control algorithm for a magnetic system. Permanent magnets can also be modeled as two plates of magnetic charge, called poles. Similar to electric charges, opposite poles attract one another and like poles repel one another[69]. However, the interaction between the magnetic poles is more mathematically complex than that

of electric charges, which introduces more difficulties when attempting to use magnetic forces for levitation or other applications. Approximating permanent magnets as magnetic dipoles significantly simplifies calculations of the dynamics of the magnets.

2.2.3 Earnshaw's Theorem

Creating the phenomenon of magnetic levitation is possible, but difficult to achieve due to the inherent properties of magnets. Simply positioning two magnets so that the like poles repel and opposes the force of gravity is not enough to keep the magnet afloat forever. In order to keep the magnet from flipping over and attracting to the magnet below it, a secondary motion is needed to keep the forces acting on the body in equilibrium. Different schemes will have varying effectiveness in achieving this goal, but some methods can be mathematically proven impossible. One such proof, formulated by Samuel Earnshaw in the 19th century, illustrates the inability of electromagnetic forces to stabilize a charged object [16].

Earnshaw's Theorem, in its most general form, may be stated as “no charged body can be in stable static equilibrium under the influence of electric forces alone” [37]. This is demonstrated by considering a point, \mathbf{p} , at which the net electromagnetic force is zero, so that

$$\frac{\partial V}{\partial x} = \frac{\partial V}{\partial y} = \frac{\partial V}{\partial z} = 0 \tag{2.6}$$

where V is the electromagnetic potential [16]. However, the fact that electro-

magnetic forces diminish by an inverse-square law requires that

$$\nabla^2 V = \frac{\partial^2 V}{\partial x^2} + \frac{\partial^2 V}{\partial y^2} + \frac{\partial^2 V}{\partial z^2} = 0 \quad (2.7)$$

hold at \mathbf{p} as well [16, 37]. If \mathbf{p} is a point of stability, all three second derivatives above are positive, which contradicts Eq. 2.7. Instead, at least one derivative must be negative, which makes \mathbf{p} a saddle point and, therefore, unstable.

Although Earnshaw's Theorem is commonly applied to electromagnetic systems, the mathematical derivation is the same for any inverse-square force field and can be generalized to any power law [11, 37]. Thus, it would seem that equilibrium ought to be difficult to achieve. However, this result refers only to static bodies so one may avoid the limitations described in Earnshaw's Theorem if the system in question is dynamic in some way. This is accomplished by introducing angular motion, or some other form of oscillation, which allows for stable equilibrium at the price of introducing time dependence [11].

2.3 Spin-Stabilized Magnetic Levitation

In spite of Earnshaw's conclusions, magnetic levitation is readily achieved by circumventing the phenomena described in the theorem. Spin-stabilized magnetic levitation (SSML) is a phenomenon by which a ring magnet's magnetic field (called the base field) can suspend a spinning magnetic object in levitation [18]. Although a statically levitated object would be prone to tip over and fall from the desired levitation point, a rotating object resists changes to its angular momentum and orientation. Thus, such an object can remain fixed

at a critical point in the magnetic field because its resistance to changing its orientation mitigates its tendency to become dislodged from the saddle point.

As it rotates, the levitated object's spin axis, which is tilted, will precess about the local magnetic field. For an angular velocity ω , the corresponding precession frequency is

$$\omega_p = -\frac{\boldsymbol{\mu} \cdot \mathbf{B}}{\|\mathbf{L}\|} = -\frac{\boldsymbol{\mu} \cdot \mathbf{B}}{I\omega} \quad (2.8)$$

where \mathbf{L} is the angular momentum of the levitated object, $\boldsymbol{\mu}$ is its magnetic dipole moment, \mathbf{B} is the local magnetic flux density, and I is levitated object's rotational inertia [83]. Higher precession frequencies allow the levitating object to align its spin axis to that of the base field quickly. Thus, due to the inverse relationship between ω and ω_p , higher angular velocities prevent the axis alignment. It can be shown that the maximum possible angular velocity for an object with mass m and effective radius r is approximately

$$\omega_{max} = \frac{1}{gr^2} \left(\frac{\boldsymbol{\mu} \cdot \mathbf{B}}{m} \right)^{3/2} \quad (2.9)$$

where g is acceleration due to gravity [83]. If I_{tr} is the transverse rotational inertia of the levitated object, the minimum angular velocity required for stability is

$$\omega_{min} = \frac{2}{r} \sqrt{\frac{I_{tr}}{I} \frac{\boldsymbol{\mu} \cdot \mathbf{B}}{m}} \quad (2.10)$$

The ratio of the levitated object's two principle moments of inertia is an important parameter for the system. Satisfying $\omega_{min} < \omega < \omega_{max}$ is a nontriv-

ial task, since the prerequisite condition $\omega_{min} < \omega_{max}$ is not trivial [83]. By combining Eqs. 2.9 and 2.10, we see that stable levitation is possible only if

$$\frac{\omega_{max}}{\omega_{min}} = \frac{\boldsymbol{\mu} \cdot \mathbf{B}}{2mgr} \sqrt{\frac{I}{I_{tr}}} \geq 1 \quad (2.11)$$

or, equivalently,

$$\frac{I}{I_{tr}} \geq \left(\frac{2mgr}{\boldsymbol{\mu} \cdot \mathbf{B}} \right)^2 \quad (2.12)$$

Even when Eq. 2.12 is satisfied, however, only a specific range of angular velocities results in system stability. In order to sustain SSML indefinitely, the system must maintain the levitated object's rotation between the lower and upper limits of Eqs. 2.9 and 2.10, usually by applying a force to counteract friction or drag.

2.4 Dynamic Magnetic Stabilization

Currently, several methods exist to stabilize a system utilizing levitating magnets. Like any other object in three-dimensional space, such a system possesses three translational and three rotational degrees of freedom [10]. According to Earnshaw's Theorem, a system comprised solely of static permanent magnets cannot achieve stable levitation, therefore an external force is needed to provide stability [16]. Such a force may serve either to dampen vibrations caused by the system or to return a displaced levitated object to equilibrium.

Many damping methods used for mechanical systems are also effective for magnetic levitation. Dashpots can mitigate the effects of vibrations in various

systems by harnessing the friction within viscous fluids in order to displace a system's kinetic energy [67]. Consequently, dashpots in the form of tuned mass dampers (TMDs) are widely used in various large structures to ensure that earthquakes and other geological disturbances cause minimal damage [92]. The optimal damping coefficient, c_{opt} , for a TMD in a floor-damper model (see Figure 2.2) is given by

$$c_{opt} = \sqrt{\frac{2m_1k_2}{1 + m_1/m_2}} \quad (2.13)$$

where m_1 and m_2 are the masses of the damper and floor, respectively, and k_2 is the floor spring stiffness [73, 93]. Despite their effectiveness, the use of viscous liquids is prone to leaks and expensive maintenance [92]. However, eddy current damping can be used in tandem with tuned mass dampers, which offers the advantage of lower maintenance costs without sacrificing performance.

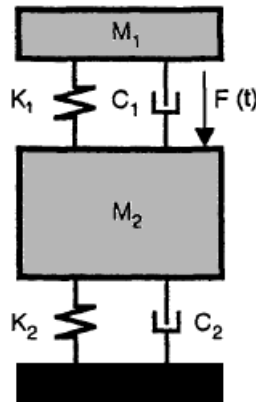


Figure 2.2: A schematic of a floor-damper model TMD; adapted from [93].

In specific configurations, electromagnets can also be effective dampers [68]. Circuits that incorporate electromagnets can be tuned to counteract

vibratory motion, which, in turn, enables them to respond to translational and rotational motion and return a levitating object to equilibrium. This makes it possible with certain configurations of circuit components and electromagnets to precisely control the movement of the stabilized object, leading to more control over the system.

2.5 Existing Examples of Magnetic Levitation

2.5.1 Levitron

The Levitron[™] is a magnetically levitating top, marketed as a toy, which demonstrates that a rotating object can achieve equilibrium in a static magnetic field as long as the magnetic force between the top and its base can counteract gravity and the top's angular momentum maintains its axis of rotation (see Figure 2.3).

This system depends solely on the interaction between a permanent ring magnet and a small puck magnet, leading to certain drawbacks inherent to the system. The top must be perfectly balanced in order to remain stably levitating. Any imperfections in this balance can cause the top to wobble and fail to maintain levitation [35]. Additionally, because the system is set in motion by mechanically imparting angular momentum to the top, there is no way to provide further energy to it after the initial spin, and air drag causes it to fall within minutes. There is also a low limit to the weight of a top that can be supported by the base magnet since the Levitron[™] uses a weak magnet in its base.

The Levitron Revolution[™] is a more advanced system that relies on dy-

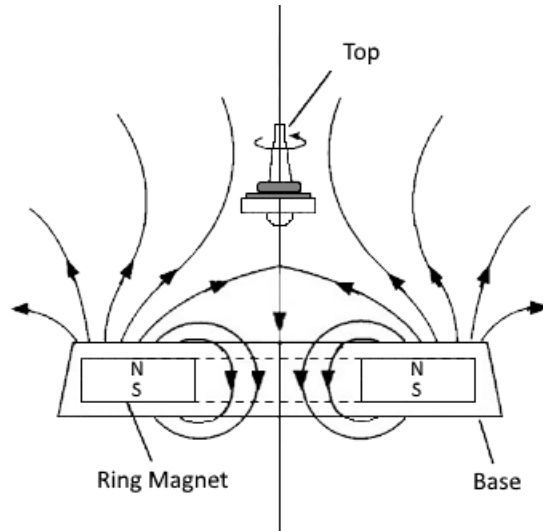


Figure 2.3: A schematic of the Levitron™ system; adapted from [35]. The top in this image is similar to the puck in the system discussed in this paper.

dynamic magnetic stabilization [11, 13]. It utilizes time varying electromagnetic solenoids alongside a permanent ring magnet to circumvent the effects of Earnshaw’s theorem and levitate a permanent-magnet puck. This device depends on a powered analog circuit that uses Hall effect sensors to create a feedback loop, which keeps the puck levitating [13].

During operation of the Levitron Revolution™, magnetic field measurements from an array of Hall effect sensors determine the location of the puck magnet. Based on the puck’s location, the circuit directs an appropriate amount of current through the solenoids to adjust the magnetic field of the base and keep the puck centered and stable [13]. Operating the solenoids at a duty cycle allows the system to impart force on the puck. At a high enough frequency, this counteracts the puck magnet’s tendency to flip over and attract to the magnet in the base [13].

One benefit of this system is its greater weight capacity compared to SSML. The added strength from the solenoids allows even a small system to support approximately half of a kilogram, which is two orders of magnitude greater than what the original Levitron™ can lift. Additionally, the puck can levitate for as long as the system receives power, as the solenoids continually exert force to counteract gravity and energy is not lost due to air resistance. Lastly, the dynamic system does not require a precisely symmetrical orientation of the puck magnet in order to function [8].

One drawback to a dynamic magnetic stabilization system is its external power requirement. Furthermore, being purely analog, the system is self-contained and does not permit external inputs to the controller. However, this system is sufficiently reliable and a suitable basic design for dynamic magnetic levitation on a small scale. For this reason, we have chosen to base our prototype design on improving the Levitron Revolution™ concept for further applications by converting it to a digital system that allows external input.

2.5.2 Magnetic Bearings

Magnetic bearings are designed to stabilize machines that rotate at high velocities. They consist of a shell, set around a rotor, which uses repulsive magnetic forces to restrict the freedom of the rotor to axial rotation with no pitch or yaw [45]. In order to achieve an equilibrium of magnetic forces and suspend the rotor without physical contact, most magnetic bearings implement active electromagnetic systems that determine the distance between rotor and bearing, adjusting the strength of the magnetic field accordingly [38]. Some

magnetic bearings instead use passive systems of superconducting magnets, which exhibit zero electrical resistance and divert magnetic field lines below a material-dependent critical temperature [4, 61]. Since there is no contact between moving parts, friction is eliminated from the system [38]. Magnetic bearings can support rotational speeds on the order of 10^4 rpm.

2.5.3 Photolithography

Another potential application of magnetic stabilization is for ultra-precision control of a specific stage or platform. This has immediate possibilities in semiconductor fabrication, as precision is critical for forming such features as channels only 14nm wide. Though this appears to be a viable technology worth developing [5, 96, 97], there is little impetus to develop it because there is only a niche area where a system this complex would be needed to replace what already exists. Hypothetically, there would be gains over piezoelectric actuation (the current method of precision movements of a stage), but the current technology is pervasive and widely accepted with almost all of the complications understood due to the amount of time that it has been in use.

Magnetic control of a stage could bring us closer to Ångström levels of precision, but the unique part of a magnetically levitated system is that its range would be on the order millimeters, as opposed to the current standard, which is limited to tens of micrometers [96]. Further, with a magnetically levitated system, the need for lubrication or mechanical linkage is entirely eliminated [97]. This prevents cascading between degrees of freedom and interdependent tolerance stack up [49]. Through the use of magnetic levitation,

these processes can be improved until prototypes can be mass produced with consistency, resulting in a means of achieving precise, six degree-of-freedom control.

2.6 Possible Applications of Magnetic Stabilization

2.6.1 Shock Absorption and Earthquake Protection

The subject of vibration mitigation in mechanical structures has received considerable interest due to its importance in engineering applications. There are three major categories of vibration control systems: active, semi-active, and passive. Passive systems achieve stabilization by means built into the system, without consuming external energy. However, once implemented, the mechanical properties of a passive system cannot be changed. Semi-active systems require a small amount of external power (less than 1 kW) in order to function, and active systems require a significant amount of power to function (at least 1 kW) [81, 86].

Linear tuned-mass dampers are a form of active control system that rely on a mass, spring, and damping mechanism to dissipate vibrational energy as heat [6]. The difficulty associated with using them is the amount of precision required, which necessitates constant fine tuning for the system to properly function. Another method, known as a nonlinear energy sink, adapts to the primary frequency of the vibrating system and relies on vanishing linear stiffness; a nonlinear restoring force works irreversibly to absorb the vibrational energy [6]. However, it is only possible to transfer specific quantized amounts of energy by this technique. Therefore, there is a limited achievable precision

because sufficiently small deviations will be uncorrectable.

A passive magnetic vibration absorber (PMVA) is a more recent application that uses only magnetic forces to mitigate vibrations. It can tune a vibrating system's linear and nonlinear stiffness via repulsive magnets and a series of correcting magnets located off its main axis. Furthermore, the system can be tuned to achieve different operational frequencies, which allows PMVAs to function in a variety of vibratory environments and makes them particularly desirable as an effective means of shock absorption [6].

Many theoretical and experimental research efforts have focused on implementing semi-active systems [81, 86]. One such system involves the use of a magnetorheological damper (MRD) installed with K-type braces, as seen in Figure 2.4 [84]. Low-power electric circuits continuously vary the magnetic field intensity in an MRD, which allows for rapid and reliable operation. Semi-active systems offer a balance between precision and energy requirements, which we have chosen for our design.

2.6.2 Centrifuges

Centrifuges are one of the many possible applications of our project. These common lab devices are used to rotate objects at high velocity. The friction caused by extended periods of rotation causes rotors to deteriorate over time and ultimately causes mechanical failure. Centrifuge failure from this damage is often expensive and sometimes extremely dangerous [27]. If paired with an effective method of imparting rotation, our magnetic levitation system has the potential to remove friction entirely from the centrifuge mechanism. By mag-

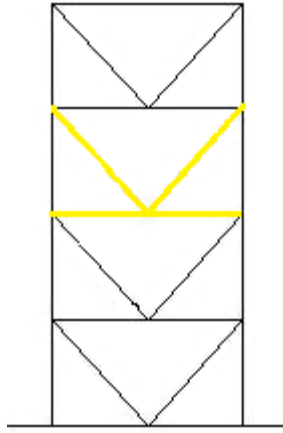


Figure 2.4: A diagram of a K-type brace, useful in dampening motion; adapted from [9].

netically levitating the rotor, it could be made to spin as quickly as necessary, as it would not be in physical contact with any surfaces. This would eliminate the damage caused by friction and also improve overall efficiency.

2.6.3 Wind Turbines

Another application of our project is power generation by vertically oriented electromagnetic generators, such as wind turbines. Electric generators with magnetically levitating rotors have the advantage of performing all energy transfer through a magnetic interaction between components rather than through mechanical energy transfer. This allows them to circumvent energy losses due to friction, mechanical wear, and material fatigue. Consequently, the rotors are able to operate more efficiently, last longer, and run with a lower rotational inertia and therefore take advantage of lower energy inputs. Wind turbines have a slow and constant rate of rotation and can be oriented to take ad-

vantage of magnetic levitation. More specifically, turbines can use a vertical orientation to take advantage of magnetic levitation and transfer energy without mechanical losses due to friction, or the wear of a mechanical rotor. These new turbines also would be able to take advantage of lower wind speeds than traditional wind turbines. In terms of their design, their levitating rotor would have a magnet which is rotating inside of a coil of copper wires and in that way generate electric power. There have already been many propositions for “maglev” wind turbines that use magnetic levitation to replace traditional ball bearings and gain the advantages described above. One proposition by Abbascia et al. describes such a design [1]. Their idea is to replace bearings with permanent magnets to levitate a rotor which can be spun by wind and produce electricity. They also add the use of additional technology called a single-ended primary inductor converter (SEPIC) that can regulate the varying voltage from the turbine to produce a steady DC output. Thus we can see the applications of stabilized magnetic levitation to wind turbines.

2.7 Solenoids

2.7.1 Fundamental Concepts

The basis for control in a dynamically levitating system is the feedback loop created by an electromagnet circuit in the base. An essential part of this dynamic levitation is the integration of solenoids into the base circuit. Solenoids and other inductors are, by definition, passive two-terminal electrical components that resist changes in current [15]. Solenoids create a magnetic field by running an electric current in a circle around a core, usually made of a ferric

material. This alters the magnetic alignment of the electrons within the core's atoms (see Figure 2.5).

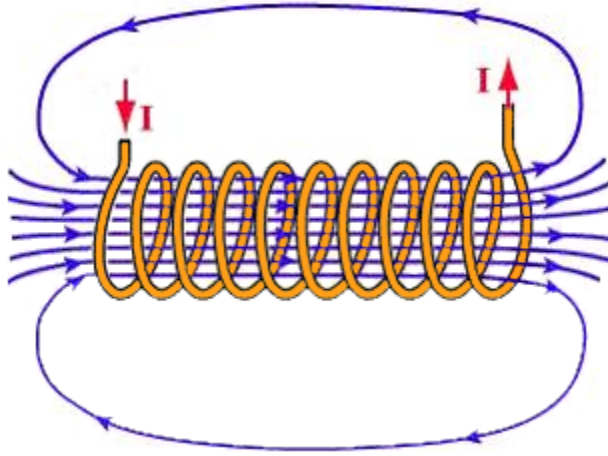


Figure 2.5: The current in a solenoid induces a magnetic field; adapted from [13].

Faraday's law of induction describes this phenomenon. A change in the magnetic flux, Φ_B , passing through a solenoid creates an electromotive force (EMF), ε , in the coil, and the magnitude of this force is equal to the rate at which magnetic flux changes [44, 47]. Additionally, Lenz's Law states that any current induced in this manner will itself induce a magnetic field that counteracts the original change in magnetic flux. In a coil of N loops, the induced EMF is additive, and it is possible to summarize the above information in a single equation:

$$\varepsilon = -N \frac{d\Phi_B}{dt} \quad (2.14)$$

The behavior of a solenoid depends on multiple design factors, including number of turns, length of coil, core material, and cross-sectional area. A

solenoid's inductance, L is defined as the ratio between the magnetic flux produced in the coil and the current that generates the flux [44]. In mathematical terms, a solenoid with N turns of wire, length ℓ , and cross-sectional area A_c has an inductance of

$$L_{sol} = \frac{\Phi_B}{I} = \frac{N^2 \mu A_c}{\ell} \quad (2.15)$$

where μ is the magnetic permeability of the core material [47]. In paramagnetic and diamagnetic materials, $\mu \approx \mu_0$, so the vacuum permeability is typically used as an approximation when this is the case [62]. Ferromagnetic materials, however, possess permeability values as high as 10^6 times greater than that of vacuum, so they are usually represented by a relative permeability $\mu_r = \mu/\mu_0$ [63].

Solenoids are classified based on their length and uniformity. A solenoid is called infinite if its length is sufficiently larger than its diameter; otherwise, it is finite. Independently, a solenoid may be formed by individual coils (discrete) or a cylindrical sheet of conductive metal (continuous) [15]. Solenoids may also be designated by the material present within their core. In this project, we are utilizing ferromagnetic core inductors.

2.7.2 Eddy Currents

Eddy currents, otherwise known as Foucault currents, are a byproduct of Faraday's law that function in a similar manner to solenoids [19]. Eddy currents flow in closed loops within conductors, perpendicular to the magnetic field and can be induced within nearby stationary conductors by a time-varying magnetic field created by a transformer or alternating current (AC) electro-

magnet. Lenz's law also applies to eddy currents [19]. By the properties of this law, an eddy current creates a magnetic field that opposes the field that created it, allowing it to react back onto the source of the external magnetic field. This can be viewed as a sort of magnetic inertia, as the electrons resist the movement by the magnetic field by imposing their own counteractive field. This reaction can either interfere with the main purpose of the magnetic field or be utilized as a stopping mechanism because eddy currents are a source of energy loss. The loss of energy due to eddy currents is experienced through the production of heat, which can damage circuit components if not monitored properly.

2.7.3 Induction Motors

Induction motors consist of two primary components: an external stator and an internal rotor [44]. Along the stator, several pairs of electromagnets are placed opposite one another and spaced equidistantly surrounding the rotor. These pairs of electromagnets are supplied with alternating currents in an out-of-phase manner, which creates a rotating magnetic field dipole. The magnetic fields induce current in wire coils attached to the rotor, which in turn create their own magnetic field. Due to interactions between the rotating dipole and the induced magnetic field, the rotor is forced to rotate. Because of this, the device creates torque and acts as a motor [44]. We initially considered creating a hybrid machine of an induction motor and our base levitation system to create something analogous to a frictionless motor. However, we chose to work first on the levitation aspect. Later, the team moved to do more work

with levitation rather than braiding in the implementation of a system that already exists and is fully functional.

2.8 Circuits

Hall effect sensors are circuit components that measure the voltage difference across an electrical conductor in order to determine magnetic field strength. Hall effect sensors are composed of a Hall effect transducer, which creates a Hall voltage in the circuit, and other circuit parts that add a bias [70]. This bias is used to fine-tune the Hall voltage of the sensor to give a precise measurement of the magnetic field. This is simply demonstrated in Figure 2.6 as obtaining a voltage difference from a plate that has become polarized by a nearby magnetic field.

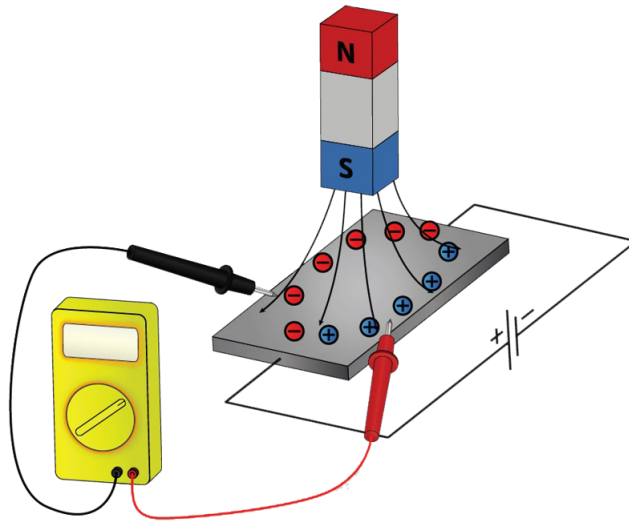


Figure 2.6: A simplified representation of Hall effect sensor operation; adapted from [64].

In order to locate our object in three dimensional space we chose to use a

three-dimensional triangulation system. By having three distinct fixed points of references, which is where the Hall effect sensors would be located, the team is able to collect magnetic field information in each of the three planes of standard Cartesian space, i.e. the xy , xz , and yz planes. The information gained will then be sent via our designed circuit to the microcontroller and put through our control algorithm to precisely determine the location of the magnet. This process is simplified when we assume that our system has not yet failed because then the levitated object can only exist within a certain area. This assumption that the object lies within the vertical projection of the ring magnet and is above the base eliminates one of the two possible solutions for our unbiased tri-axis sensors.

A microcontroller is a computer that has been scaled down to a single integrated circuit [39]. This system is used in place of an ordinary computer for convenience and easy access to input and output (I/O) ports. Microcontrollers are capable of outputting various digital signals, which can be converted into analog by an analog-to-digital converter (ADC). Implementing ADCs allows a microcontroller to interact with analog circuits.

2.9 Finite Element Method

When describing physical systems in the language of mathematics, a wide range of behaviors can be modeled by differential equations [85]. However, the majority of differential equations are nonlinear, inhomogeneous, or otherwise difficult to solve analytically. Various numerical schemes have been developed in order to approximate solutions to particular classes of ordinary and partial

differential equations. Finite Element Analysis (FEA) is one such numerical approach that finds applications in stress analysis, heat transfer, and electromagnetics [50]. The Finite Element Method (FEM) is typically applied to differential equations when the domain of interest possesses an irregular shape [85].

2.9.1 Theory and Procedure

This section will give an explanation of various mathematical concepts and tools that will be useful for the reader to better understand the approach to theory our team worked with, particularly regarding mathematical representations of boundary interactions and solving differential equations.

Before solving a differential equation by FEA, it is necessary to choose nodes based on an arbitrarily set standards by the team within the interior and on the boundary of the domain of interest [50]. These nodes are connected so as to partition the domain into “elements,” which Figure 2.7 demonstrates. When analyzing a two-dimensional domain, elements are usually taken to be triangular or quadrilateral; for functions of one variable, elements are intervals of the form $x_i < x < x_{i+1}$ [50].

The premise of FEA is that, by dividing the domain of interest into small pieces, one can approximate the solution to a differential equation by analyzing a simpler version of the problem [85]. Consider, for example, an analogous

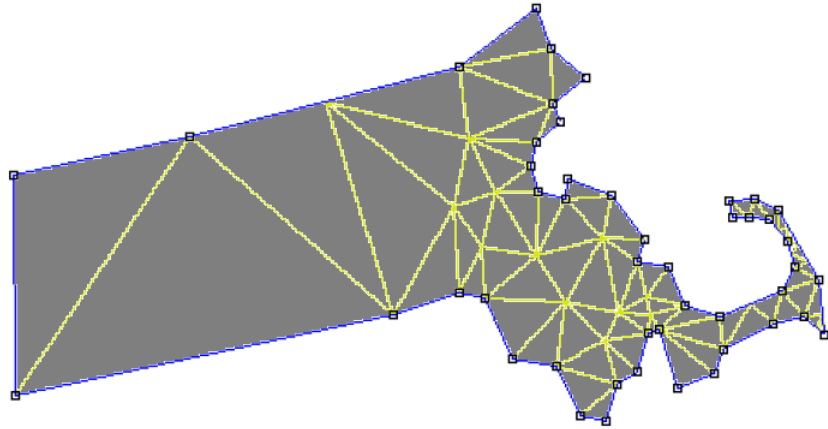


Figure 2.7: Triangular finite element mesh of a region in the shape of Massachusetts; from [55].

boundary value problem given by

$$\begin{cases} -u''(x) = f(x) \\ u(a) = u(b) = 0 \end{cases} \quad (2.16)$$

where f is a known function [23]. It can be shown that a solution to Eq. 2.16, $u(x)$, also fulfills the condition

$$\int_a^b u'(x) v'(x) dx = \int_a^b f(x) v(x) dx \quad (2.17)$$

for all functions $v(x) \in V_D^{[a,b]}$, that is, functions having a piecewise continuous derivative and $v(a) = v(b) = 0$ [23].

$V_D^{[a,b]}$ is an infinite set, which makes it impossible to individually verify Eq. 2.17 for every function that it contains. Therefore, the first set of equations is simplified by considering only a subspace of $V_D^{[a,b]}$ and approximating the

solution as a linear combination of basis functions [23, 85]. That is, for a set of N basis functions, $\{v_i(x)\}$, there are constants $\{\xi_i\}$ such that the approximate solution is given [85] by

$$U_N(x) = \xi_1 v_1(x) + \cdots + \xi_N v_N(x) \quad (2.18)$$

The form of these basis functions depends on the desired level of approximation, but the simplest and most common choice is to use linear “tent” functions, as seen in Figure 2.8 [2]. Each tent function corresponds to one node and is defined such that it equals one on its respective node and zero at all others [2, 85]. By this definition, it follows that $U_N(x_j) = \xi_j$ if x_j is the coordinate of node j [23].

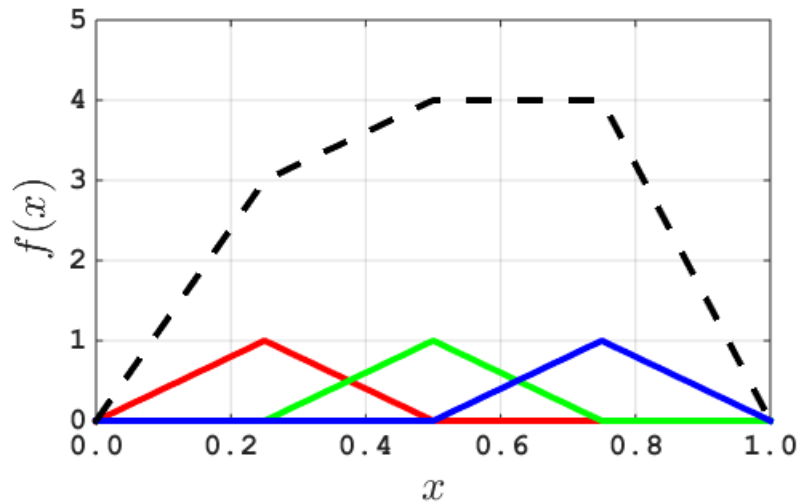


Figure 2.8: Three tent functions on the interval $[0, 1]$ and the linear combination $f(x) := 3\phi_1(x) + 4\phi_2(x) + 4\phi_3(x)$. Higher-dimensional tent functions are constructed analogously.

The goal of the FEM is thus to determine the values of the coefficients ξ_i . Combining Eqs. (2.17) and (2.18) yields [85] the following linear system

$$\int_a^b \left[\sum_{i=1}^N \xi_i v_i'(x) \right] v_j'(x) dx = \int_a^b f(x) v_j(x) dx \quad (2.19)$$

$$\sum_{i=1}^N \xi_i \left(\int_a^b v_i'(x) v_j'(x) dx \right) = \int_a^b f(x) v_j(x) dx \quad (2.20)$$

$$\sum_{i=1}^N m_{ij} \xi_i = f_j \quad (2.21)$$

where Eq. 2.21 defines the terms m_{ij} and f_j to equal the expressions in Eq. 2.20 that they replace. This may be expressed in matrix notation as

$$M \boldsymbol{\xi} = \mathbf{f} \quad (2.22)$$

in which M , called the stiffness matrix, is sparse (or filled with mostly values of zero) and tridiagonal (non zero elements are located on the main diagonal of the matrix, and 1 diagonal above and below that previously stated set of data) in the one-dimensional case [85].

Solving for the entries of $\boldsymbol{\xi}$ allows one to construct an approximation of $u(x)$. As Figure 2.9 demonstrates, even fairly coarse meshes yield qualitatively accurate solutions, which improve further as the element size is reduced. The procedure as a whole is the same for any number of independent variables: integrate the differential equation, approximate the solution as a linear combination of basis functions, and solve the resulting matrix equation for $\{\xi_i\}$ [50].

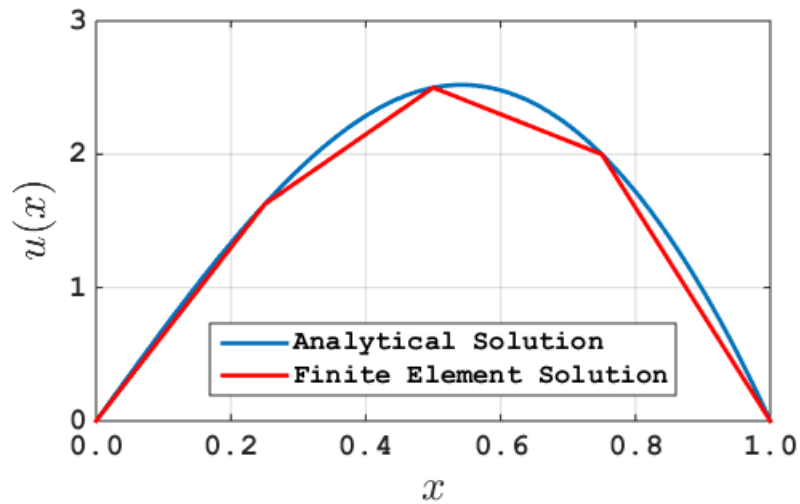


Figure 2.9: A comparison of analytical and FEM solutions to Eq. 2.16. Even with only $N = 3$ nodes, FEM produces a representation of the equations that maps the curve to an arbitrarily significant degree.

2.9.2 Applications of FEM

Initially designed by engineers in the 1940s, FEA is a software solution to represent various physical systems [50]. Furthermore, the FEM's utility is augmented by its ability to handle irregularly shaped domains, which are more difficult or less efficient when solved by a grid-based method [85]. FEA is typically used to solve problems in mechanical fields, such as stress and vibration, though it is also common in transport phenomena and gaining prevalence in bio-engineering settings [50].

In addition to those fields mentioned above, the FEM is suited for electromagnetic calculations. However, despite the fact that two-dimensional (2D) FEA is commonly used for addressing electrical systems and has proved effective at representing them, more complicated three-dimensional (3D) problems

have proven more difficult to produce with accuracy and are more computationally demanding [58, 59].

When modeling electromagnetic fields, one must take care to choose a finite element model that is designed for the behavior of the phenomena it describes. For example, certain modeling functions are incapable of predicting continuous fluxes where material properties change [58]. As a result, these models are inadequate for inhomogeneous media [58].

Further challenges are encountered when analyzing the behavior of electrically-powered devices, especially those that generate motion of some kind [59, 78]. Even in the absence of macroscopic motion, 3D systems may be underspecified in some cases, such as the “magnetizing current” method, where one must assume current density to be equal in all directions in order to eliminate extra degrees of freedom [59]. Although various methods exist to calculate the displacement, forces, and torques in such systems, mesh size and time step impose nontrivial effects on the stability and accuracy of solutions [78].

2.9.3 Software

Given the utility of FEA, there exists a plethora of software programs designed to implement the FEM to solve various differential equations. Such programs are usually specialized in order to handle a few specific types of problems. “Finite Element Method Magnetism (FEMM),” for example, is designed for two-dimensional and axisymmetric problems in electrostatics, magnetism, current flow, and heat transfer [55, 56]. The software uses linear basis functions on triangular elements and can handle a variety of common boundary conditions

[55].

When finding solutions, FEMM uses an approach where the differential equations are simplified by defining new quantities and applying known mathematical and physical laws [55]. For example, magnetostatic problems are governed by the following relationships:

$$\nabla \times \mathbf{H} = \mathbf{J} \quad (2.23)$$

$$\nabla \cdot \mathbf{B} = 0 \quad (2.24)$$

$$\mu \mathbf{H} = \mathbf{B} \quad (2.25)$$

where \mathbf{H} , \mathbf{B} , and μ are magnetic field intensity, flux density, and permeability, respectively, and \mathbf{J} is current density [55]. If a magnetic vector potential, \mathbf{A} is defined such that $\nabla \times \mathbf{A} = \mathbf{B}$, then Eqs. 2.23 through 2.25 reduce to

$$\nabla \times \left(\frac{1}{\mu} \nabla \times \mathbf{A} \right) = \mathbf{J} \quad (2.26)$$

which FEMM solves for \mathbf{A} and computes \mathbf{B} [55].

2.10 Summary

The existing literature on magnetic stabilization has shown this technology's potential utility in various applications. We determined that a proof-of-concept that showcased applicability of this technology would be the best way to contribute to the expansion of this field. The clearest way to accomplish this is to create a machine with adjustable parameters involving the position of the

levitating payload that could be fine-tuned to a variety of applications. The user-specified parameters in our system would enable us to investigate the applicability we believed the technology to have by implementing it in minor versions of the systems we deemed it would be applicable to. The adjustable parameters would benefit a variety of magnetic-stabilization systems, so we aimed for a system design that would have the widest applicability. The best way to implement modifiable parameters in a proof-of-concept was to have the entire system controlled by a microcontroller. These parameters would change constants in a control algorithm tailored to our system. The parameters could be determined through the magnetic field analysis with FEMM software. We theorized that we could use our analyses of a variety of magnets to show how effectively our system and would work with other magnet configurations. This would ensure that the system was adaptive enough to be used in large-scale applications like building stabilization, and smaller applications like centrifuges, which are approximated by increasing the strength and the size of the magnets and showing their interactions in a similar FEA model to the ones discussed in this paper.

Chapter 3

Methodology

3.1 Overview

Based on the information gathered from our literature review, we designed a series of experiments to gather data on a microcontroller-based magnetic levitation device and began designing and building components of our system. As the first step, we defined our necessary parameters, such as what we levitation and stability. Our initial approaches included investigating an established levitating system and studying the circuit used by that system, in the hope that we would be able to derive a system of equations that we could implement in our code. We also studied and mapped magnetic fields for the ring and puck magnets. We designed and created solenoids to fit our magnetic force requirements and our dimensional requirements. We then designed several circuits incorporating the solenoids into our system. Lastly, we created a control algorithm based on known constants such as ring magnet field strength, shape, and ideal puck magnet position. The team also implemented this algorithm into code. Our processes relating to each of these activities are described below.

3.2 Research Questions and Planned Experimental Design

3.2.1 Properties of Levitation

Can we achieve stable levitation? In order to qualitatively evaluate our prototype, levitation was defined as the ability of the system to counteract the force of gravity on the puck magnet without physical contact. Whether this can be achieved for a specific system depends solely on the puck and ring magnet combination, not on the control algorithm. Failure to levitate would imply that the magnets are too weak to counteract the force of gravity on the puck.

In order to test if levitation can occur for a given puck and ring magnet pair, we first placed the ring magnet on the table. Then, the tester held the puck in the palm of their hand and slowly lowered the puck magnet towards the ring magnet. If the puck magnet feels weightless, that indicates the puck and ring magnet combination is capable of levitation. Although this point seems trivial, it is important to ensure that our magnet pair can generate a sufficient force in opposition to gravity before continuing experimentation.

Stable levitation is defined as the capability of the system to suspend the puck magnet in the air for a significant period of time—as defined in the subsequent section—without noticeable lateral movement. In other words, does the puck magnet stay centered? To ensure that the puck magnet stays in its optimal position, a test rig was designed, utilizing four lasers and four light sensors. This test would be performed with the four lasers arranged in a 2x2 grid, where the center box of the grid represents the “zone of levitation.” The

puck would be placed in the center of the grid, and if the puck magnet moved in the xy-plane, it would break the laser beam, blocking the light from the sensor. When the light is blocked, the sensor will indicate the exact moment that the puck magnet deviates from the zone and how many times this happens. A small deviation in the position does not guarantee that the magnet will fall, so those instances can be ignored or the dimensions of the zone of levitation can be altered.

For how long can we sustain levitation? Our test for stable levitation was meant to determine the effectiveness of the control system utilized in the design. Before running this test, we needed to define what would be considered a “significant period of time,” a “noticeable rotation,” and a “noticeable lateral translation.” For our purposes, we set values of 10 seconds, 1° of rotation, and 0.5 cm from the axis of symmetry, respectively, subject to change after further analysis and experimentation.

When running our test for stable levitation, we would start by assembling the control system with the ring magnet in place and checking that the microprocessor was outputting to the data logging system. Then we would place the puck over the ring magnet and release it to begin the levitation. Next, we would record the amount of time the puck levitates and note any unusual behavior for the puck. We would consider the puck to have stably levitated if it remained levitating for more than 10 seconds. To ensure precise measurements, when the puck is dropped, a stopwatch would be started. Force sensors would be set on the surface of the magnetic base to detect when the

puck moved towards the base and when it made contact with the base or ground. Once the sensors detect contact being made, the timer would stop. Due to the high probability of the puck making contact with the magnetic base, most of the force sensors would be placed on the base itself. The objective was to make the puck levitate as long as the magnetic base is turned on. After the experiment, we would analyze the angle and translation data to ensure that those requirements were satisfied as well.

3.2.2 Additions to Basic System

Can we implement user-defined displacement? Currently-existing magnetic stabilization systems, while successful in maintaining an object in place, do not offer any additional control mechanisms. A microcontroller-based system offers the potential to allow user-specified translation and rotation of a levitated object by overlaying a series of signals in addition to the base control algorithm. Such signals could alter the magnetic force exerted on the levitated object so as to cause it to move as desired. Knowing that we want to impart a magnetic force to displace the puck magnet, we would determine how much current needs to flow through the solenoids. Once we have established that, we would calculate the corresponding signals that need to be sent to the microcontroller to achieve that goal.

What is the maximum recoverable deviation in puck position or angle? An ideally stable puck will levitate parallel to the ring magnet and above its center. However, real systems must compensate for disturbances

in puck position and orientation. These operations require knowledge of the maximum angle with the base from which the puck can recover (see Figure 3.1). Furthermore, the stability limit with respect to translational deviations must also be considered. This experiment would be carried out by adjusting the puck angle, tilting manually with respect to the base, and observing whether or not it can recover, filming the entire process in the plane of the levitating puck. By gradually increasing the magnitude, we would find the limits of recoverable angles. The angles would be measured by recording the vertical displacement of the puck's edge and using trigonometry.

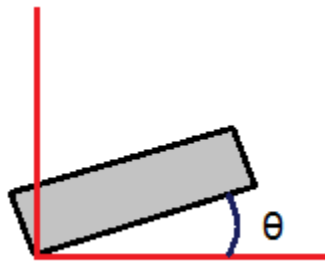


Figure 3.1: The puck magnet displaced at an angle θ from a horizontal orientation.

Can a wall of stators be implemented? Manipulation of a levitated object may be extended to further functionality. A ring of solenoids placed around the device at levitation height can alter the local magnetic field and impart rotational inertia to the levitated object. Thus, such a stator wall around the device causes the system to behave like an asynchronous motor, provided that the additional forces do not interfere with levitation. If a levitated object can be made to rotate by this method, the properties of such levitation

(maximum angular velocity and torque ranges) are important in judging the usefulness of the system.

3.2.3 Optimization

What is the most effective sensory system? There are a few ways to measure the height of the puck. The first option involves using a capacitive sensor that can measure the distance of conductive objects from it. The sensor would be oriented at the base of our device pointing up toward the load. We would then use a computer to gather data from the sensor. The second method involves using a photoelectric (laser) sensor to measure the height. Like the capacitive sensor, this sensor would be oriented so that it faces upwards towards the load. The data received from the sensor would be used by a micro-controller to determine the height of the puck. The final possible method would be to use hall effect sensors. Hall effect sensors measure the strength of the magnetic field surrounding them. We would measure the change in field strength from adding the puck to the system to determine the height of the puck. For our purposes, we decided to go with the photoelectric sensor set up.

How much power is required to operate the system? An important aspect of any powered electronic system is the energy required to keep the system running. In order to test the various states at which our system will exist, we must repeat our tests for 3 main states. These states are passive (no puck present), natural corrective (stabilizing puck with no extraneous forces),

and forced incorrect position (puck held at a point that is not inherently stable). In addition to this information, if we intend to overlay other signals, we must measure the power consumption in these states.

Power is defined as energy divided by time and is measured in Watts. In our experiment, we would consider power in two ways: the power through the inductors and the total power of the entire apparatus. Three distinct experiments, each with two sets of data collection, are required with an additional collection of data that is independent of what state the system is in for signal overlay.

For each state, both a voltmeter and ammeter must be included in line with the main power for the inductors and the power source from the wall in order to capture total consumption. For each case, we would generate a graph of both variables and multiply each point together, taking a 5-point weighted average to smooth noise. For the offset case, we would need to construct an apparatus to hold the puck in a set displaced position; an easy way to do this is to modify our dropping system to an off centered point. For the other two states, all that is required is a system that levitates. If these tests go smoothly, we may be able to expand to a fourth set of tests for an input of a destabilizing impulse and see the power spike associated with a specific force.

Will heating of components pose operational difficulties? Solenoids are susceptible to temperature changes due to the currents traveling through low resistance wiring. This necessitates investigation into both temperature dependent properties (Ohmic resistance) and burnout. Burnout is defined

to be an operating temperature at or above 100° C. All heat generated is assumed to be Joule heating. Temperatures would be measured in degrees Celsius and would be taken in each of the four states previously tested in power consumption. We would compare data collected to the theoretical values of heating found with current and the resistance of the coils.

In order to collect data, we would bond a thermistor to each coil and excite the system to the four states listed above. The various temperatures produced over time would be recorded and graphed, and we would cease the experiment when the system reaches steady state. We would prematurely end the experiment if it appears that the system is approaching burnout, as we do not intend to test until failure. This test, in combination with our power tests, can be used to observe the effect of temperature change vs. resistance. The thermistors provide a plot of temperature at all points, and our power measurements (voltage and current) would allow us to solve for resistance, yielding a resistance vs. temperature plot characteristic curve.

What is the maximum supportable weight? Two possible techniques were considered for this test. The first possible method is continuously adding weight in small intervals before lowering the puck into its stable levitation point. An alternative possibility involves writing an input in our algorithm that calls the weight and modifies the starting field output in order to have the puck levitate at the ideal height. In this experiment, "weight" refers to the gravitational force acting on the mass we would be levitating. Our goal is to determine how much mass we can levitate before the gravitational force

becomes stronger than the opposing magnetic force. If we use the physical test, we would weigh the puck to get a baseline payload. Then we would stack weights on top of the puck until the puck and payload is unable to levitate. If we want to be more exact, we could mathematically characterize the repelling forces of the puck, the ring magnet, and the solenoids in the vertical direction. At that point, we would find the maximum and minimum restorable force as well as the maximum downward force that can be counterbalanced.

For the computational test, we would write in a function that modifies the magnetic field strength based on a weight input. This test would proceed through trial and error until the desired levitation height could be achieved with any given weight below the maximum. If a weight could not achieve the desired levitation height regardless of the output from the electromagnets, it would be considered above the maximum supportable weight. Additionally, we could also run some computer simulations with the FEMM software in order to simulate the interactions of the magnetic fields of the puck and ring magnets. For practicality purposes, we decided upon the physical test.

3.2.4 Applicability

Does it work for any system of magnets? Reproducibility is a crucial element of any research project. In order for researchers to further investigate the product, a detailed record of the creation of the code, algorithms, and physical mechanisms for the specific system must be kept. This will help with the implementation of different magnets in the design, which is necessary for the advancement of the product. This could be tested theoretically using a

series of control algorithms and the specific data applying to different magnets. The information could then be verified using physical experiments.

What safety concerns are important? Whenever a product is being built, user safety is a major point of emphasis. The greatest risk faced with the levitation of a magnet would be an extremity being caught in between the puck and ring magnet in the event of instability. To measure the potential damage, we could conduct a test utilizing a force sensor, then let the system fail by allowing the puck magnet to fall onto the sensor. The sensor would calculate how much force the magnet potentially imparts on a finger. If this force is sufficient to cause notable harm, a warning should be printed on the device to keep all appendages away from the base while the machine is in use. Another risk is the effect that the large magnets have on pacemakers and other medical devices [77]. These devices begin to falter in the presence of approximately 0.5 mT of magnetic field. Being in close proximity to our magnets can result in experiencing magnetic fields greater than 0.5 mT. Therefore, knowledge of the force as it decays over distance is needed in order to determine the level of protection required when operating our product.

3.3 Magnet Mapping

Before constructing our device, we mapped the magnetic field of our magnets in order to better understand the resulting system. We used a LakeShore magnetic field sensor to sweep a Hall effect sensor within a 2D plane at a series of fixed heights above the magnet to determine the magnetic field strength

and shape (Figure 3.2). The exact heights were not chosen for the sake of the values themselves, but rather with the intention of observing the shape of the magnetic fields over a range of heights. We postulated that any series of heights a sufficient distance apart (we used 0.25 in) would provide us with enough data enough data to characterize field evolution with distance from the magnet. Thus, we obtained precise maps of the ring and puck magnets' fields (see Apendex) at multiple relative positions and insight into the decay of the magnetic fields with distance. [76].

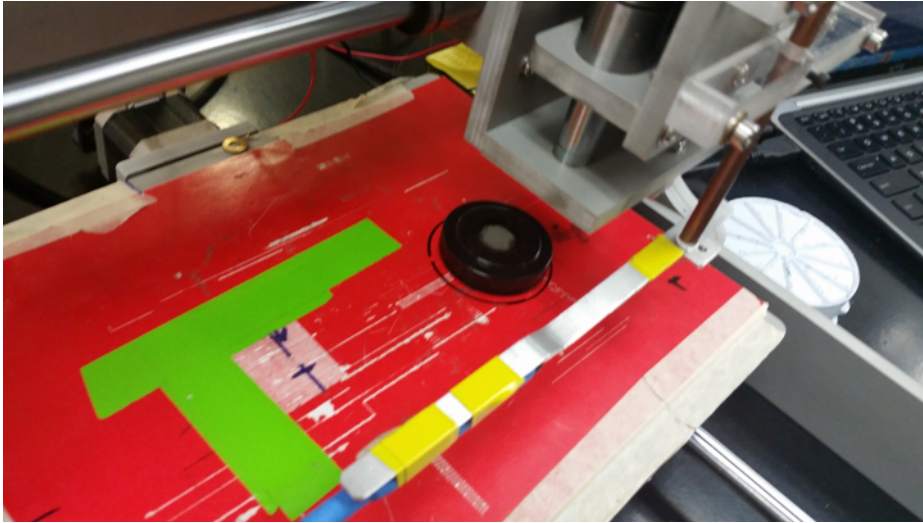


Figure 3.2: Experimental setup used to scan the magnetic field of the puck magnet with a movable Hall effect sensor [76].

We scanned the background magnetic field at the levitation height of 0.7in to characterize its effects on our measurements (Figure 3.3) and calibrated the LakeShore equipment by measuring ten replicates at each of eight points relative to the puck magnet. We applied a linear fit to these data, which we used to convert dimensionless Hall effect sensor readings to measurements of

magnetic field strength [76].

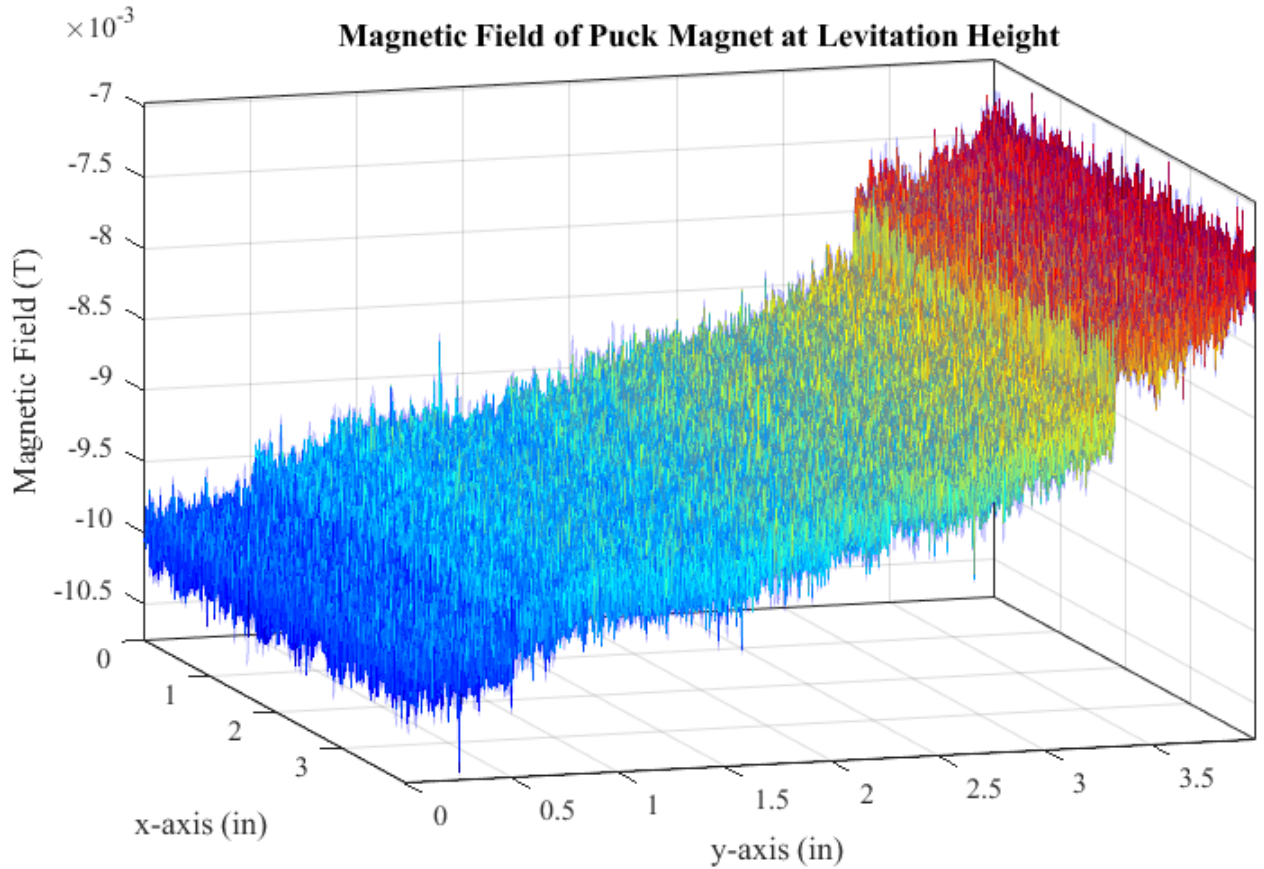


Figure 3.3: Surface plot of the background magnetic. The background is slanting in the positive direction, indicating that the background magnetic is systematically stronger in that direction. This asymmetry in the background field may explain breakdowns of cylindrical symmetry in the data from the scans of the puck and ring magnets.

We measured the ring magnet's axial field at points 0.15, 0.56, 0.78, and 1.07 in. above its top face. Axial field scans for the puck magnet were taken at 0.28, 0.52, 0.75, and 0.96 in. To obtain the radial field, the puck magnet was placed on its side (see Figure 3.4). Then, we performed 2D scans of the

magnetic field at constant height at a starting distance of approximately 0.25 in. These scans were performed at heights of 0.75, 0.93, 1.36, and 1.74 in. We hoped that these scans would provide us with the decay of the puck's radial field vs distance. However, the approximately 0.25 in. starting distance from the puck was found to differ between scans, which meant we were unable to extract meaningful data from these scans. To have more consistent radial magnetic field measurements, we would need a better means of securing the puck and controlling the starting position of the scanner. All distance measurements were obtained with an electronic calipers and are subject to an uncertainty of ± 0.05 in., and the uncertainty in the magnetic field strength was found to be negligible by comparison. The ± 0.05 in. uncertainty in the distance measurements was obtained by attempting to measure the distance between the magnet and the probe multiple times and taking the standard deviation.

3.4 Circuit Mapping

3.4.1 Existing Analog Circuit Analysis

While researching current systems of levitation and stabilization, we identified the Levitron Revolution as a simple example of what our system hoped to accomplish. In order to better understand the example and possibly gain some insight into what we wanted our system to emulate, we tried to reverse engineer the system and study the circuit components of the Levitron and how they interact with each other. However, we were not able to gain any significant information while doing this exercise, and learned that a reverse-engineering

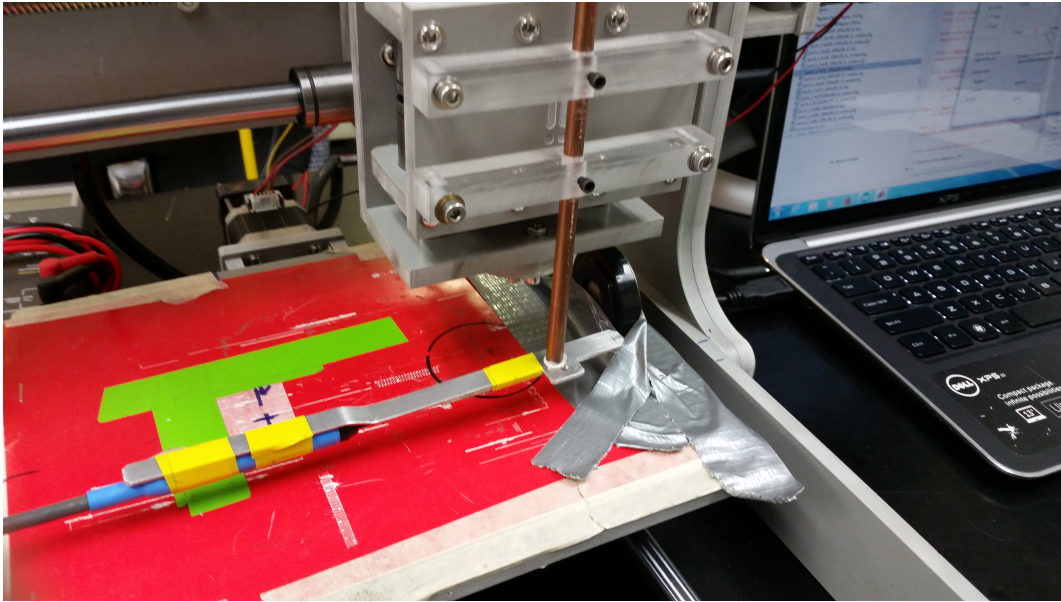


Figure 3.4: Experimental setup used to scan the magnetic field of the puck magnet with a movable Hall effect sensor [76].

or mapping effort is an ineffective way of translating a circuit to code. While we were able to see the major circuit components, we were unable to see how the circuit performed at a more precise level. However, we were successful in grasping the big concepts and what the circuit needed to do, but not exactly how to do it. These concepts were two analog op amps were controlled by an analog switch, amplification of signal with the banks of transistors, thermal safety fuse, and the use of solenoids.

3.4.2 Design of Dynamic Circuit Prototype

We transitioned to a focusing on designing a circuit tailored to our needs. Members of the team designed two circuits that could cause the inductors to emit magnetic fields. The first circuit utilized a NPN Darlington pair. We

chose to use a Darlington pair because our selected microcontroller outputs 10-40 mA, but our solenoids require a current on the order of an Ampere. It should be noted that there are two kinds of Darlington pairs, one with two NPN bipolar junction transistors (BJT) and one with two PNP BJT's. We chose to use NPN because it requires a small positive bias current to flow to the base. Whereas PNP requires negative current flowing from the base to ground. Based on the equipment available to the team, it was easier to utilize a NPN Darlington pair. The second circuit integrated a metal-oxide semiconductor field-effect transistor (MOSFET). The MOSFET accomplishes the same things as the Darlington pair circuit, but it is safer to use because regulating voltages are safer than currents. The MOSFET also has a faster response rate.

NPN Darlington Circuit

Below is the standard circuit diagram of the NPN Darlington circuit that the team used.

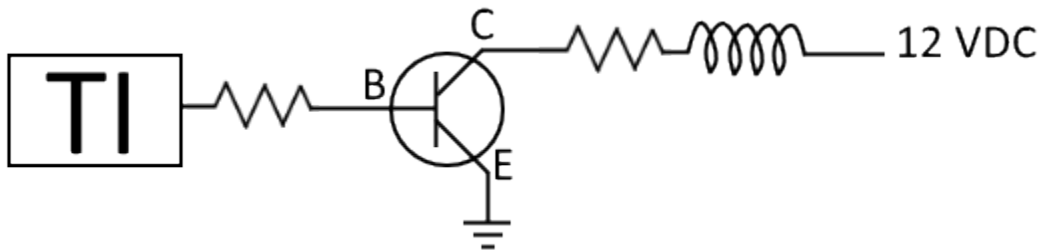


Figure 3.5: Darlington pair circuit used to test the initial setup and read from Hall sensors.

The team built this circuit and tested it by introducing another mag-

netic object in the presence of the inductor and measuring the current flowing through the inductor. The NPN Darlington pair that the team used was manufactured by ON Semiconductor and is called a Darlington Transistor 10A, 80V Bipolar Power NPN [66]. The data sheet is provided in Appendix D.

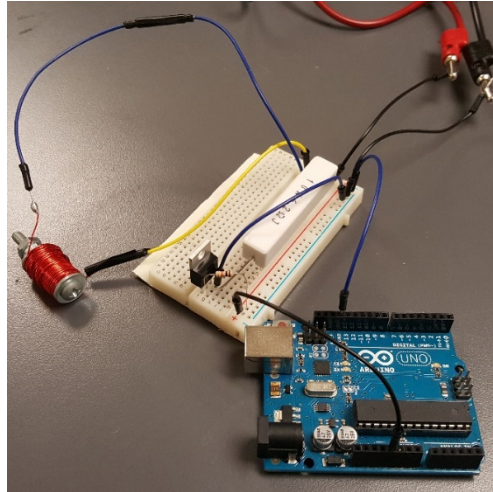


Figure 3.6: The first physical iteration of our circuit design.

The team ran simple pulse width modulating code on the microcontroller, which is depicted as the box labeled “TI” in Figure 3.6. This code results in a varying voltage from the microcontroller. That varying voltage value in turn results in a varying current flowing through the inductor via pulse width modulation. The team confirmed that the current flowing through the inductor was varying using a constant voltage source. The team knew that this circuit succeeded in emitting a magnetic field from the inductors because the magnetic object was attracted to the inductor.

MOSFET Circuit

The team designed and built the circuit shown in figure 3.7 to test the viability of a MOSFET utilizing circuit. The MOSFET that the team implemented is an N-channel power MOSFET. The specification sheet for this MOSFET is in the bibliography [31, 66].

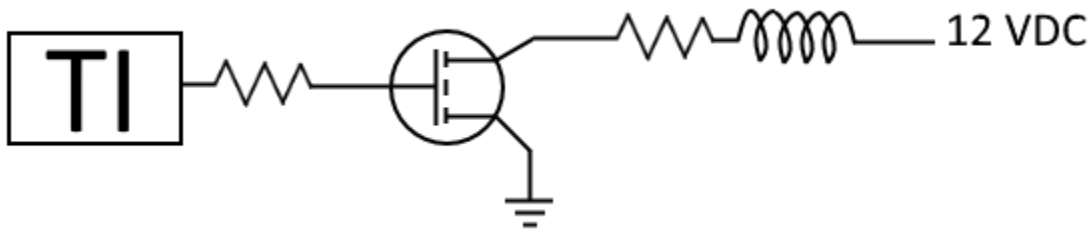


Figure 3.7: Diagram for an *N*-channel MOSFET circuit.

Once the circuit was built, the team ran a test identical to the one used for the NPN Darlington pair circuit to see which circuit would result in a higher magnetic force output. The results were also successful in this case, ie the MOSFET circuit output . The current flowing through the inductor was varying and the magnetic object was attracted to the inductor, confirming that there is a magnetic field being emitted from the inductor.

3.5 Prototyping

3.5.1 Prototype Overview

The aluminum case was fabricated using three slabs of aluminum. The base slab was left untouched while the other two slabs were cut with a hole saw and

metal cutting circular saw. A Tungsten Inert Gas (TIG) welder was used to combine the three pieces into one. Four small squares of aluminum were also cut and welded to the bottom of the case in order to raise the magnet and allow the passage of wires. Four small holes were also drilled into the center of the case. The magnet was placed in the case and the four solenoids were placed in the middle of the magnet. A section of the solenoids were fitted into the small holes that were drilled in the center for stability purposes. The cross was made using three pieces of printed circuit board (PCB) cut and arranged as shown in Figure 3.9. Hall effect sensors were soldered on the PCB board and the structure was placed in the middle of solenoids, so that each solenoid was separated from the others.

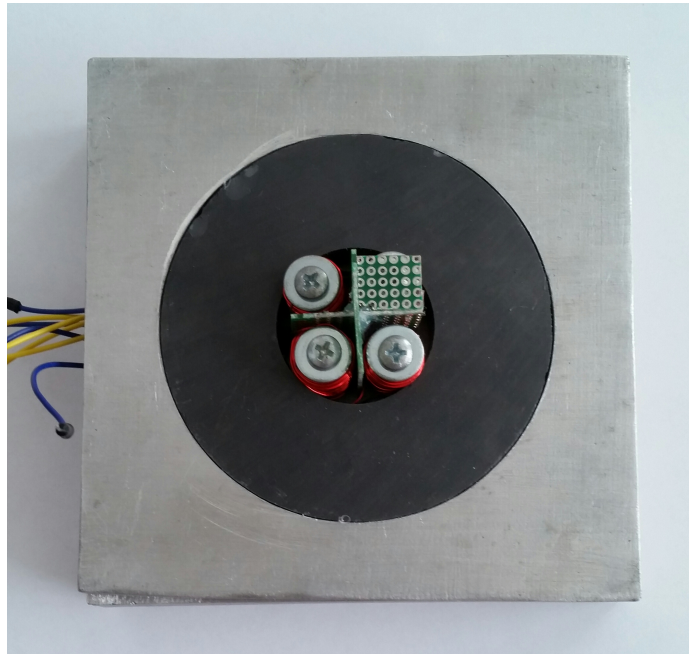


Figure 3.8: A photo that displays the placement of the ring magnet, solenoids, and PCB.

3.5.2 Solenoid Fabrication

Required Materials

In order to have the electromagnets that we needed for levitation meet all of the implied pre-requisite requirements for our research questions, we decided that custom fabrication of the solenoids was required. Most of the materials needed for this process are readily available in a typical machine shop. The only unique items needed were the custom built Electromagnet Maker Machine (created by Martin Nelson of Quince Orchard High School) and magnet wire. Magnet wire is enameled wire is a copper or aluminum wire coated with a very thin layer of insulation. The core sizes were selected to be 0.64 cm diameter by 3.8 cm long, the maximum possible size for 4 cores to fit in the center of the void of our ring magnet (4.45 cm in diameter). This size was selected to maximize inductance, directly proportional to diameter of electromagnet, while still allowing four solenoids to fit within the center of the ring magnet. We chose to use 4 solenoids for the multifaceted symmetrical properties.

Table 3.1: A list of the materials used to fabricate each solenoid.

Item	Quantity
Electromagnet Maker Machine (EMM)	One (1)
Power Drill	One (1)
24-Guage Magnet Wire	Ten (10) meters per EM
Pliers	One (1) Pair
Screw Cores (1/4" by 1.5")	One (1) per EM
Washers (1/2")	Two (2) per EM
Nuts (1/4")	Two (2) per EM
Lock-Washers (1/4")	One (1) per EM
Masking Tape	9 cm
Wire Cutters	One (1) Pair

Procedure

To fabricate the solenoids, we first took the screw that we needed to make an electromagnet (EM) and tape was then wrapped around the screw until the threads were entirely covered to prevent the threads from digging into the magnet wire and potentially altering the wrapping process or breaking through the insulating coating. We then slid a washer onto the screw until it bumped up against the head of the screw. A nut was placed, then lock-washer, then nut on the screw. The nuts were tightened against each other in order to lock the lock-washer, preventing unexpected movements while wrapping. The screw was loaded into the bit tip of the EM and the magnet wire extended an excess of 6 in. (15.24 cm) past the screw.

Next, we tied a knot around one end of the taped area (between the washers) and attempted to wind the screw by hand. If the wire wasn't wrapping, we tightened the knot at the top with pliers, taking care not to scratch off the protective coating. We trimmed all but 3-4 in. (7.62-10.16 cm) of the excess wire off and then bent it along the axis of shaft rotation. The power drill was loaded onto the machine and the bit tip fastened around the drive shaft. We made sure the drill was in the forwards setting and then slowly eased the drill on because the slower and with more care the rotations are done, the neater and more powerful the EM will be. We assisted this feed with our hands, even though the machine automatically guides the wire, for a higher quality.

At the end of pass down the length of the core, we paid extra attention to the wrapping process when the magnet wire started to double back on itself because the process was most likely to derail here. This process was

repeated for each layer to achieve desired amount of wraps, 9 layers of 30 wraps. This desired amount was determined by the fact that the solenoid was limited in size by the interior diameter of the ring magnet. For our purposes, we could not exceed a diameter of 0.6 inches (1.52 cm), so we used the washer to determine when the number of wraps reached the maximum diameter. We then stopped the drill and pulled the magnet wire tight if it was not already and then clipped the EM from the spool with at least 6 in. (15.24 cm) of excess wire on the EM and knotted the two ends around each other as this made it less likely that either lead fatigues and breaks off due to repeated bending before installation. An optional step is to further insulate the EM's by placing shrink tubing around them and heating them in order to hold all of the wiring in place, which we elected not to do for our prototype. This procedure was derived from prior experience of a team member.

The finished product was a set of four solenoid all wrapped 1 inch (2.54 cm) high and 0.6 inches (1.52 cm) wide. Each layer of wrapping was approximately 29 ± 2 coils. There were nine layers laid on each electromagnet. There is variation in thickness due to imperfect hand wrapping but overall they are approximately the width of the washers.

3.5.3 Protective Case

In designing the protective case, measurements of the ring magnet were first taken to determine the necessary size of the case. With the measurements, a CAD file of the prototype (Appendix D) was created to visualize the protective case. The case was fabricated using aluminum because it is a durable

non-ferromagnetic material and would have negligible impact on the magnetic field of the ring magnet. In the fabrication process, three 12.7 cm square, 2.54 cm thick sections were cut from a bulk of aluminum. The bottom of the three section was left as is and acted as the base of the case. The middle and top sections had a hole slightly larger than the ring magnet drilled through the center of them to house the ring magnet. The middle section had a segment removed on one of the sides leading into the hole to allow for the passage of wires. Four 1.25cm aluminum cubes were fabricated to attach to the bottom section and raise the ring magnet to allow for the passage of wires from underneath. The sections were tested to make sure that the magnet had no horizontal movement within the case and that the aluminum was flush with the magnet. The bottom and middle segments were welded together along with the four raisers while the top section was left whole to allow for easy access to the magnet and the components within. Four holes were drilled through the center of the case to rigidly secure the solenoids. The case was topped off with a piece of foam in order to protect the puck magnet from slamming into the base in the event that accidents occurred.

3.5.4 Hall Effect Sensor Array

We started building the prototype by creating an array for the Hall effect sensors from two pieces of printed circuit board (PCB), based off of a similar model name the Levitron [35]. The array was assembled by cutting the PCB into three pieces and arranging them so that they formed an XYZ coordinate system. The PCB was then bonded together using standard Gorilla Glue

and three Hall sensors attached using soldering paste, one in each direction of measurement (Figure 3.9). We used a soldering iron to connect the three pins of the Hall effect sensor to precut holes in the PCB. Wires were fed through the holes in the board and soldered in place, creating permanent connections for the pins.

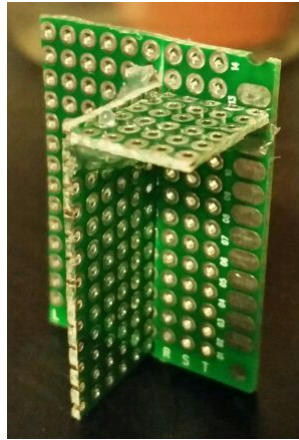


Figure 3.9: The circuit board on which the Hall effect sensors were mounted for measuring magnetic field strength.

We tested the Hall effect sensors by connecting them to an Arduino and analyzing the output of the serial monitor. We ensured that the readings varied in the presence of different magnetic fields by placing several different magnets next to the Hall probes and observing the changes in readings from the Arduino. In order to test the magnetic field strength of our electromagnets, we powered the electromagnets using the external power source. The external power source was set to output a constant 6 V to the electromagnet, with an LED in parallel to indicate when the electromagnet was receiving power. To determine the electromagnet's effect on the magnetic field of the system

(ring and puck already in place), we used the Hall effect sensor to measure the magnetic field first with only the puck magnet, and then with the puck magnet while the electromagnets were turned on.

After building this most basic prototype, it was clear that the PCB was not the optimal way to meet our needs because the Hall sensor leads physically did not line up with the standard spacing on the PCB. We therefore determined that we needed to etch our own circuit board instead. This method is more complicated, but much more exacting because it is a customized, unique design, generated explicitly for our project rather than a standard component. We designed the circuit to be printed using a program called Eagle, then planned to use that as the blueprint for our new array, but did not complete this process. (The following is how we would have completed the process.) We printed out the circuit and overlay it on a piece of copper-coated board and coated the parts we needed to stay with a protective layer to adhere them. Then, the whole board would be dipped into a solution to finalize the circuit board. To finish the array, holes would be cut in the board to fit the circuit components like the Hall sensors, and the components soldered in place.

3.6 Control Theory

3.6.1 Modeling the System

In order to develop our control algorithm we began by modeling the movement of the puck magnet using the following equation of motion (EOM)

$$\frac{d^2\mathbf{r}}{dt^2} = \frac{\mathbf{F}_M + \mathbf{F}_S}{m} \quad (3.1)$$

Where m is the mass of the puck magnet. This is a differential equation that describes the radial acceleration \mathbf{r} of the puck magnet as a result of the forces imposed by the ring magnet and the solenoids. These are shown as \mathbf{F}_M and \mathbf{F}_S respectively. To use this EOM, our next next step was to create models of F_M and F_S , that accurately described the radial forces on the puck magnet. However to simplify these models, we neglected changes in puck orientation or height. Our justification for this simplification was that changes in the levitation height and orientation are actually the consequence of small radial changes in position of the puck magnet. Thus controlling the radial position should be effective for active control. [44]. However, we intended to include the effect of levitation height and orientation if the simplified control strategy was insufficient.

The data obtained from the puck magnet matched our FEMM simulation well, so we were able to use the ring magnet's simulation data at levitation height in order to model the interaction between the two. At a levitation height of approximately 0.70 in (18 mm), this field could be approximated as a quadratic. This yielded the following expression for the ring magnet's axial field strength, $B_{ring,z}$

$$B_{ring,z} = B_2 r^2 + B_0 \quad (3.2)$$

where r is the radial distance from the center of the magnet, and B_0 and B_2 are constants. In order to convert magnetic field strength into force exerted

on puck magnet, we modeled the puck as a magnetic dipole, such that

$$\mathbf{F}_{\text{ring}} = \nabla(\mu_{\text{puck}} \cdot \mathbf{B}) \quad (3.3)$$

$$F_{\text{ring},r} = \mu_{\text{puck}} \frac{\partial B_{\text{ring},z}}{\partial r} \quad (3.4)$$

$$F_{\text{ring},r} = 2\mu_{\text{puck}} a r \quad (3.5)$$

where μ_{puck} is the magnetic dipole moment of the puck. We define the control modifier, β , such that $\beta^2 := 2B_2 \mu_{\text{puck}}/m$ and obtain the following ODE

$$\ddot{r} - \beta^2 r = 0 \quad (3.6)$$

where r , is still the radial distance from center.

In order to implement this model, we assumed that each solenoid in our array behaves as magnetic dipoles as done in [22] and produces a magnetic field of equal magnitude and opposite direction to that of the solenoid across from it. Finally, we were assumed that the deviation of the puck from the center of the ring magnet was sufficiently small to approximate the magnetic field as a Taylor expansion centered about a point at distance δ away from the solenoids. These simplifications enabled us to express the field of the solenoids as

$$B_{\text{sol},z} = \frac{c}{2} \left[(r - \delta)^2 - (r + \delta)^2 \right] \quad (3.7)$$

where the solenoid constant is defined $c := -12IA\kappa/z^5$, where I is the current passing through the solenoid, A is area of the solenoid, z is height above the solenoid, and κ is the ferromagnetic core gain.

From Eq. 3.7, we obtain the following expression for the vertical component of the magnetic force exerted by the solenoids

$$\mathbf{F}_S = -2c\delta\mu_{puck} \quad (3.8)$$

Combining the above results, we conclude that

$$\ddot{r} - \beta^2 r = \frac{2c\delta\mu_{puck}}{m} \quad (3.9)$$

$$= \gamma I(r) \quad (3.10)$$

where

$$\gamma := \frac{2c\delta\mu_{puck}}{Im} \quad (3.11)$$

is called the gain modifier.

3.6.2 Initial Compensator Design

Using Laplace transforms, we derived the following transfer function for our system:

$$G(s) = \frac{1}{(s - \beta)(s + \beta)} \quad (3.12)$$

We used MATLAB's control toolbox to design a compensator from Bode plots in Fig. 3.10, root-locus plots, and simulation step responses. We found that the compensator characterized by

$$H(s) = \frac{\gamma\kappa(s + \beta)(s + 0.5\beta)}{s(s + 5\beta)} \quad (3.13)$$

stabilized the system while reducing the problem to solving for constants β and γ .

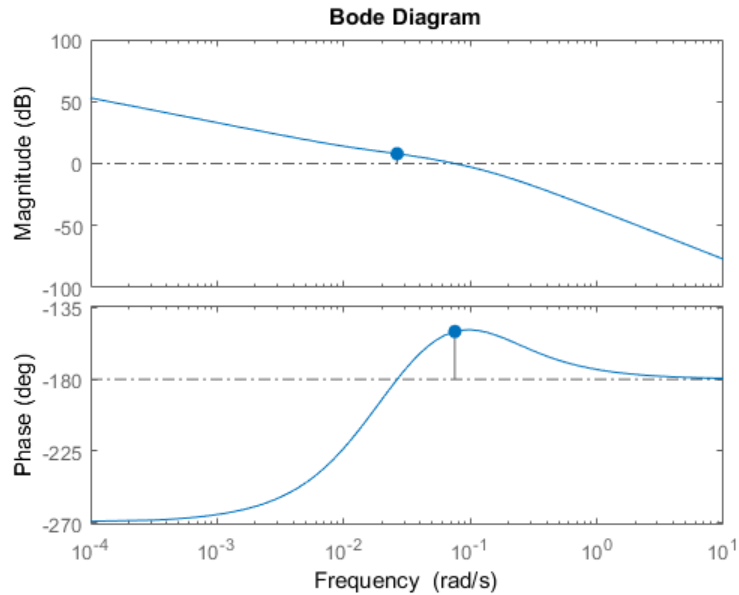


Figure 3.10: The Bode diagram of our proposed compensator for the system discussed above.

3.6.3 Determining the Constants

The Control Modifier β

To find $\beta = \sqrt{2\mu_{puck}a/m}$, we needed to calculate a , m , and μ_{puck} . Of these, m was the simplest and merely determined by weighing the puck. We found that

$$m = 0.086 \text{ kg} \tag{3.14}$$

Next, we needed to find a , the quadratic constant of the ring magnet. To

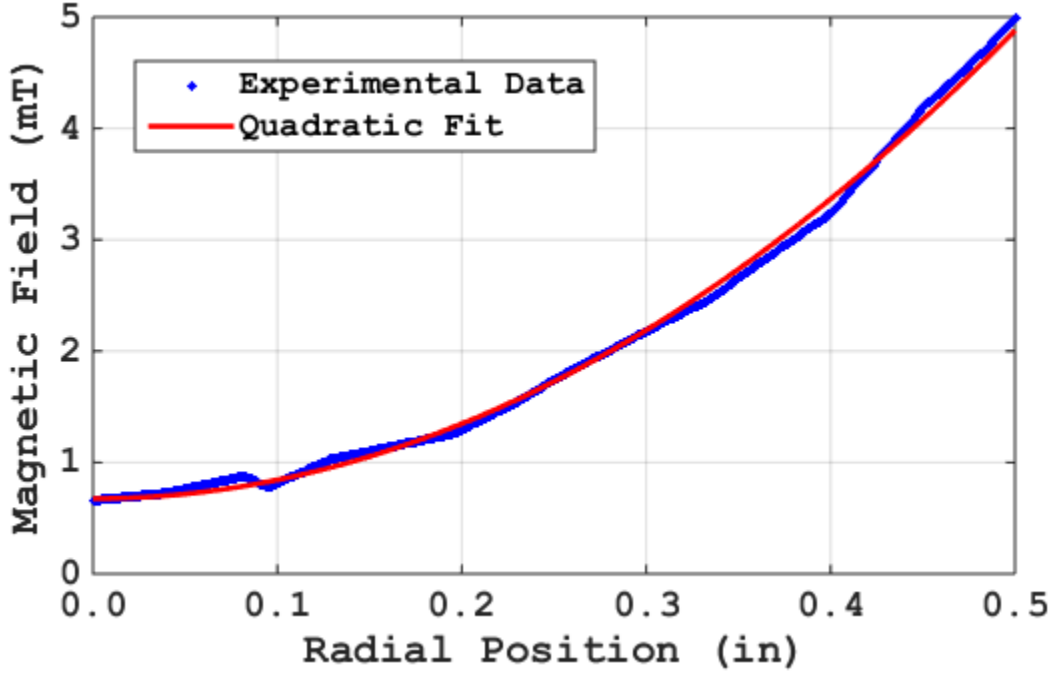


Figure 3.11: Quadratic fit of ring magnet simulation data at a height of 0.7 in.

do this, we performed a least squares fit of the FEMM simulation of the axial field of the ring magnet to a second order polynomial fit, restricting the linear coefficient to be zero at the levitation height of 0.7 in (1.78 cm) (Fig. 3.11). Linear fits were performed for each of these , and a was found to have the following value

$$a = 0.017 \text{ T/in}^2 \quad (3.15)$$

Finally, we needed to fit the μ_{puck} to the data. We assumed the puck to be a dipole, which has axial field at a constant height of approximately

$$B_z(r, z) = \frac{-6r^2\mu_{puck}}{z^5} + C = b(z) \cdot r^2 + C \quad (3.16)$$

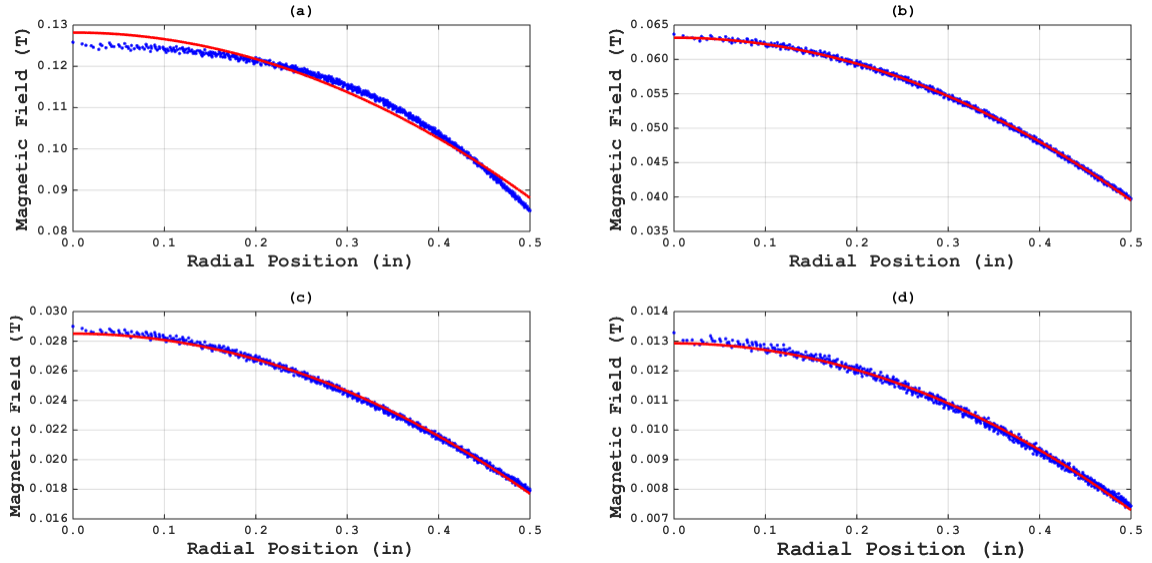


Figure 3.12: Quadratic fits of the puck magnet’s field strength at four heights: (a) 0.28 in., (b) 0.52 in., (c) 0.75 in., (d) 0.96 in.

where C is a constant. We then found the constant in front of the r^2 term for as height of 0.28 in (7.11 mm), 0.52 in (13.21 mm), 0.75 in (19.05 mm), and 0.96 in (24.38 mm), each ± 0.05 in, by performing a quadratic fit (Fig. 3.12.

Then we set

$$\mu_{puck} = \frac{-bz^5}{6} \quad (3.17)$$

We wanted to most closely resemble the dynamics of the puck, so we approximated

$$\mu_{puck} = 0.025 \text{ A} \cdot \text{in}^2 \quad (3.18)$$

Combining these expressions together, we find

$$\beta = \sqrt{\frac{2\mu_{puck}a}{m}} = 0.0313 \text{ s}^{-1} \quad (3.19)$$

The Gain Modifier γ

In order to calculate $\gamma = 2\mu_{puck}c\delta/m$, we first needed values of c and δ . Our device design fixes the value of δ :

$$\delta = 0.3 \text{ in} \tag{3.20}$$

In order to determine c , the proportionality constant between the magnetic field strength at levitation height and the input current, we calibrated our solenoids' current vs magnetic field at levitation height curve. This was done for each of our four solenoids by using the LakeShore magnetic field scanner to measure the magnetic field at the center of the solenoids at the levitation height of 0.7 in. Then a current source was run through the solenoid in series with a ceramic resistor, and we measured magnetic field strength at currents ranging from 0.00 to 1.00 A in increments of 0.10 A. Linear fits were performed for each of these fits and c was the slope of the solenoid. We note that one of the solenoids' data was disregarded because it significantly diverged from the rest indicating poor construction and has since been remade and will soon be retested to make sure it is working properly. The slopes of the rest of the solenoids were averaged together and the average value of c was found to be

$$c = -0.0034 \frac{\text{T}}{\text{A} \cdot \text{in}^2} \tag{3.21}$$

Combining these results yields

$$\gamma = -5 \times 10^{-5} \frac{\text{in}}{\text{s}^2 \cdot \text{A}} \quad (3.22)$$

3.7 Code Development

We utilized the TI C2000 Launchpad microcontroller for our coding environment. This system was chosen after considering several microcontroller options due to its advantages in real-time operating functionality. The team originally used hardware and software interrupts, a prioritized signal that communicates directly with the computer processor. These interrupts let the processor know that there is a task that needs to be completed immediately, with more important interrupts taking precedence over those with less urgency. We chose this approach due to the need to be highly responsive to instantaneous changes in magnetic field. However, this approach was difficult to implement.

Implementing a program that revolves around interrupts requires the use of threads. A computer thread provides information to the computer CPU on how to execute a certain set of instructions. The coding sub-team did not have the requisite knowledge to use threads for the interrupts. After consulting with an expert, the sub-team decided to implement the code using a new approach. This new approach proved much simpler to implement since it involved using a control loop that processed our sensor data at a rate of 40 Hz. After creating the general framework for the code, we focused on more specific aspects of the code.

3.7.1 Sensor Readings

The first step in implementing a control mechanism is reading sensor measurements for input to the algorithm. We wrote a program to convert magnetic field strength readings from the Hall effect sensors into an estimate of the puck magnet's position. This required compensating for disturbances from the solenoids and interpolating the puck's position from data describing its magnetic field.

We developed a quadratic approximation for the puck's magnetic field by least squares regression based on experimental data. At a levitation height of 0.07 in (1.8 mm), the field is given by

$$B_{puck} = -0.042r^2 + 0.061r - 0.0003 \quad (3.23)$$

where B_{puck} is in Teslas and r is in inches. B_{meas} is the measured magnetic field and is composed of two parts, B_{sol} , the magnetic field generated by the solenoid, and B_{puck} . The following expression gives us a way to find the position of the puck magnet from a measurement of the magnetic field strength:

$$-0.042r^2 + 0.061r - 0.0003 - B_{meas} + B_{sol(i)} = 0 \quad (3.24)$$

Solutions to Equation 3.24 can be calculated using the quadratic equation. The correct solution for the radial position will be the lesser of the two solutions, since we intellectually know the approximation we are using is the concave down side of a negative parabola.

However, as is shown, the magnetic field of the solenoids varies with current, and this has to be accounted for. In order for the microcontroller to accurately calculate the puck magnet's position, it must always have accurate knowledge of the magnetic field coming from the solenoids, so that this effect can be filtered out. The calibration data could be used for this, but this wouldn't provide great resolution and would make it very difficult to get accurate position measurements. Thus we decided that we would analytically determine the magnetic field around the solenoids in order to have informed knowledge of their magnetic output.

To begin modeling the magnetic field around the solenoids, we began using the Biot-Savart Law:

$$\vec{\mathbf{B}} = \frac{\mu_0}{4\pi} \int \frac{I d\vec{\ell} \times \hat{r}'}{|\mathbf{r}'|^2} \quad (3.25)$$

where $\vec{\mathbf{B}}$ is the magnetic field, $d\vec{\ell}$ is an infinitesimal length of current, and \mathbf{r}' is the displacement vector from the current element to the point where the field is being evaluated. This describes the magnetic field created by an element of current while accounting for orientation, proximity, and magnitude of the current. Using this law, an expression was created for the strength of the magnetic field surrounding a circular current loop at an arbitrary point in space. This expression is shown below, where each equation shows the axial and radial components of the field respectively.

$$B_x = \frac{i\mu_0}{2\pi\sqrt{R^2 + 2Rr + r^2 + x^2}} \left[\frac{E[k](R^2 - r^2 - x^2)}{(R^2 - 2Rr + r^2 + x^2)} - K[k] \right] \quad (3.26)$$

$$B_r = \frac{i\mu_0 x}{2\pi r\sqrt{R^2 + 2Rr + r^2 + x^2}} \left[\frac{E[k](R^2 + r^2 + x^2)}{(R^2 - 2Rr + r^2 + x^2)} - K[k] \right] \quad (3.27)$$

Where B_x and B_r are the axial and radial components of the magnetic field in Teslas, i is the current in amps, R is the radius of the current loop, r is the radial position of the arbitrary point in space, x is the axial position of the arbitrary point space, k is a grouping parameter defined as

$$k = \sqrt{\frac{4r}{R(1 + \frac{r}{R})^2 + \frac{x^2}{R^2}}} \quad (3.28)$$

and $K[k]$ and $E[k]$ are the complete elliptical integrals of the first and second kind, respectively. Now to model the field of the solenoids, we can treat the solenoids as an infinite sum of infinitesimally small circular current loops. Mathematically, this means we can make small adjustments to the above equations and then integrate them over the length of the solenoids to get equations that describe the magnetic field of the solenoids at an arbitrary point in space. We do this by replacing B_x and B_r with infinitesimal components of the magnetic field dB_x and dB_r . We then replace i with infinitesimal components of current along the length. We do this by replacing i with $(Ni/L) dx$, where N is the number of loops, and L is the length of the solenoid. The resulting equations are shown below

$$dB_x = \frac{\mu_0}{2\pi\sqrt{R^2 + 2Rr + r^2 + x^2}} \left[\frac{E[k](R^2 - r^2 - x^2)}{(R^2 - 2Rr + r^2 + x^2)} - K[k] \right] \frac{Ni}{L} dx \quad (3.29)$$

$$dB_r = \frac{\mu_0 x}{2\pi r\sqrt{R^2 + 2Rr + r^2 + x^2}} \left[\frac{E[k](R^2 + r^2 + x^2)}{(R^2 - 2Rr + r^2 + x^2)} - K[k] \right] \frac{Ni}{L} dx \quad (3.30)$$

We can then integrate these equations along the length of the solenoids to get an expression of the magnetic field of the solenoids at an arbitrary point

in space. However, because our hall sensors will be fixed in space relative to the solenoids, the only variable we will be left with is current i . Thus after this integration, we will get linear equations with respect to current that have constants that are the result of the integration of the above equations. The above equations were integrated in matlab, and the resulting linear equations are shown below

$$B_x(i) = 2.066i - 2.392 \times 10^{-7} \quad (3.31)$$

$$B_r(i) = 0.0011i + 3.882 \times 10^{-19} \quad (3.32)$$

These are the simple linear equations that describe the output of the magnetic field, in Teslas, for a given input current in amps. With these equations, it is possible to accurately measure the position of the puck magnet, and this paves the way for developing the implementation of the control algorithm

3.7.2 Control Algorithm

The first step in developing our code was implementing the control algorithm. We used the derived values of the control theory constants to update our algorithm and develop code that could be compiled and run. Most of this can be seen in the `main.c` and `control.c` files located in Appendix C. These files define a function to calculate the position of the puck and the control function necessary to calculate the appropriate output to the pins. The `findPos` function uses the readings taken from the hall probes and certain constants in order to calculate the position, y . This value is later passed as a parameter to the control function, which also takes parameters y_d , x , A , B , C ,

and D in order to apply the standard control algorithm to both calculate the output and modify the x vector for the next iteration of the algorithm.

3.7.3 The Input Code

The input code is displayed in Appendix C. The function `ConfigureADC()` configures the ADC hardware by initializing one of the four ADCs present on the team's Launchpad and sets it to have 12 bit resolution. This function also powers up the relevant ADC. The function `SetUpADCSoftware()` initializes which channel on the selected ADC the team will be using, as well as configuring the interrupt related to that channel. Finally, the `sample()` function reads in sensor data and stores it.

3.7.4 The Output Code

The output code initially set up the three DAC pins, specifically pins 25, 24, and 29, to output 5V. The control algorithm was implemented with the code and was ready for calibration. The pins were outputting in hexadecimal which were then converted to base 10, which would allow us to know exactly what voltage was being output, which ensures quick refinement of our formula.

3.7.5 Debugging

Code writing for any TI micro controller is done through their integrated development environment (IDE), code composer studio (CCS). CCS is based on a popular IDE called Eclipse, which has a powerful debugging system. The system allows the user to create break points in the code and move through

the code line by line, as well as see any expected output for each particular line of code. This system thus allows the user to see which line specifically is not working correctly and fix the problem.

3.8 Experimental Limitations

3.8.1 Practical Limitations

A common issue encountered with all prototyping is that the parts any team wants to use are not inherently compatible, especially if these parts are being using in a new fashion. This was the case for constructing the magnetic field detection system. The set of three orthogonal Hall Sensors had to be mounted to a substrate both mechanically and electrically compatible. This proved to be a challenge because this is typically achieved with custom printed circuit boards for a final product, but while we were in a fluid design phase this would have been a waste of resources and time, because if the design deviates at all, the entire custom board has to be scrapped. The other issue was that the Hall Sensors needed to be as close to perfectly orthogonal as possible. This was a structural challenge as well as an alignment challenge, and to complicate matters further, in order to yield the best reading possible, the sensors had to be as tightly grouped as possible. Our design used simple perforated circuitry board that was first slotted so two pieces fit at a 90 degree angle and then a shelf that was braced against the other two parts was made to give the third dimension. Then came the imperfections associated with how tiny the transducers are and the need to solder the leads by hand. This in and of itself was difficult, but in order to use the board only two of the three leads

naturally aligned while the solder had to be stretched in order to reach the next lead. We acknowledge that this will degrade the readings that we take, but believe it to be within a small enough bound to be negligible. There were also concerns raised that with such short leads and the difficulties of hand soldering that the heat exposure from the soldering iron would cause the sensors to lose functionality, but again from the preliminary results our team believes that no damage was caused.

The team could also have benefited from professionally made electromagnets. What we used for the prototyping were hand wound solenoids. This inherently introduces more variability than a machine wound counterpart. As explained earlier, there was variability in both the number of wraps per length as well as variability in the number of wraps from the outside to the core along the radial direction. This caused a variability in the inductance and by extension in the fields that are produced when used as electromagnets as the team intends. Corrections can be made by running every hand-made solenoid through a series of controlled current settings and fluctuations, their results can then be matched up to create individual scaling factors. This scaling term introduced, if kept simple, would be linear but this makes the assumption that over the range of use the output exhibits a linear response. Hypothetically we could take enough data to fit a second order or greater function but in the interest of simplicity and ability to implement, linear was the final choice. Preliminary data show that of the best grouping of solenoids there was not greater than a 50% divergence from average though this is a large range that at a later date can be further refined. This can be then included in the sta-

bilization code with a coefficient, at worst, between 0.75 and 1.25 in order to calibrate the effectiveness of each solenoid against the average ideal value.

The largest difficulty that we faced in code development was with choosing the device that we wanted to program. For several months, we believed that our project was much more computationally demanding than it actually was. For this reason, we were mostly experimenting with using different versions of Raspberry Pi computer modules. When we had a better grasp of our control algorithm, we realized that programming a microprocessor to do what was essentially a single procedure would not give us any major benefits over a microcontroller, as long as the microcontroller was sufficiently powerful. This ended up drastically delaying code development, as most of the low-level aspects of our code were inherently system-specific.

The algorithm itself and the constants we calculated and applied in our code all require further testing with a fully-implemented system before we can truly report their limitations and areas for potential improvement.

3.8.2 Empirical Limitations

As previously mentioned in the design of experiments section, we intended to use lasers and light sensors to determine whether the puck magnet was levitating stably. While this method would be effective, it is not without its limitations. First, the positions of the light sensors and lasers. The center of the grid, or pound symbol, will be a rectangle and the dimensions of that rectangle must be larger than the dimensions of the levitating puck magnet, but not too large. The critical dimensions of this rectangle are completely

dependent on the positioning of the light sensors and lasers. The rectangle must be larger than the puck magnet because if the rectangle is smaller, then the test will register that the puck magnet is constantly unstable. However, the rectangle cannot be too large, otherwise the sensors may not detect when the puck magnet is off-center, rendering the test useless. Second, the puck magnet is bound to reverberate as the system works to keep the puck stably levitating. These vibrations are difficult to predict. The vibrations may be relatively large, which may result in the test registering the puck magnet as unstable, however if the puck magnet is still levitating after that vibration, then it should be considered stable. Depending on the frequency of the reverberations, this issue may occur often. The team will need to use engineering judgment to differentiate between what the test considers as unstable and what actually is unstable.

The primary source of error in determining the maximum angular displacement will arise from difficulty in applying the displacement consistently. Without a mechanism to precisely alter the angle of the payload, the produced data sets may lack the repetition of trials needed for rigorous analysis. This is particularly significant in light of the possibility that there might not be one maximum angular displacement, as the ability of the system to restore itself may depend partially on environmental or chaotic factors. Furthermore, uncertainty will be present in each measurement due to resolution limitations of the digital protractor. However, it is unlikely that this uncertainty will be notable in comparison to that caused by random environmental factors.

3.9 Summary

With the information gained in the literature review, the team was able to stake a direction and design a large variety of tests in order to define success of our prototype. We first strove to understand what our exact set of magnetic field pairings looked like in a series of mappings, and make conjectures as to what the field strength would be for magnets of similar geometries. After mapping, we graphically represented this information, and the team found it easier to define the fields that we need to produce. In an effort to have a more accurate starting point we attempted to reverse engineer an existing levitation device, this did not lead to the desired results. The knowledge that we did gain from reverse engineering did not lead to a completed set of equations, due to circuit analysis as we hoped, but rather a concrete idea of what components and what exact type of component ordering was required. With a full circuit diagram theoretically implemented, the team moved onto the control algorithms where we found a way to mesh the expected field values, controlling circuit components, and expected physical levitation location. Lastly, the implementation of this control theory into code of a microcomputer would allow for full real time control over the stabilization. The team was excited for where our designs could take us and real-time manipulation of a levitating object.

Chapter 4

Results and Analysis

Due to setbacks in our research, we did not complete as many tests and produce as much physical data as we expected. However, the tests we ran were important steps toward our end goal. One of the large tests the team pursued was mapping our ring magnet. The goal of this was to create a lookup table for the puck position based on magnetic field readings from our Hall effect sensors. The other major test was to calibrate the solenoids. Since the team manufactured the solenoids by hand, rather than purchasing them commercially, there were likely to be inconsistencies in the wrapping and, thus, the magnetic fields produced, it was important to test the solenoids to determine necessary scaling factors for each.

4.1 Magnet Mapping

4.1.1 FEMM Models

Finite Element Method Magnetics (FEMM) software allows for modeling of 2D magnetostatics problems including those with axial symmetry [56]. After modeling the geometry and materials, and applying the desired boundary con-

ditions, the program numerically approximates the magnetic fields by dividing the area into thousands of triangles referred to as nodes. Then, the program numerically integrates Maxwell's equations inside each node. Upon computing the fields, the software generates a 2D model, which shows magnet fields at any point in the region of interest.

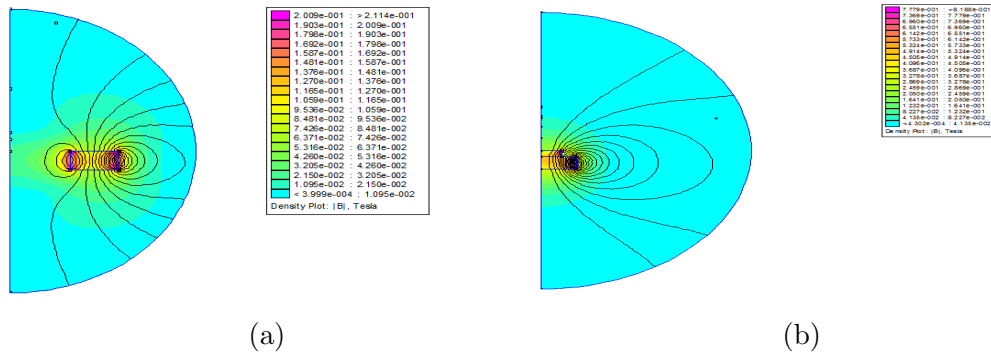


Figure 4.1: A half cross section of a FEMM simulation of (a) our ring magnet and (b) our puck magnet. The black curves are magnetic field lines.

FEMM was used to model the geometry of the ring magnet (Figure 4.1a) and the puck magnet (Figure 4.1b). For each magnet, a variety of magnetic alloys were tested to see how well the material agrees with the data. The we believed ring magnet to be a single magnetic alloy based on its appearance. However, we thought that the puck magnet is composed of two separate alloys stacked on top of each other due to its shape. To determine the material with the closest resemblance to the measured fields, the FEMM models with various different materials were plotted together with the data in a single plot for each scan. This plot displayed the axial magnetic field of the ring magnets vs radial distance from the axis of symmetry the geometry (Figs. 4.2 and 4.3).

4.1.2 Ring Magnet

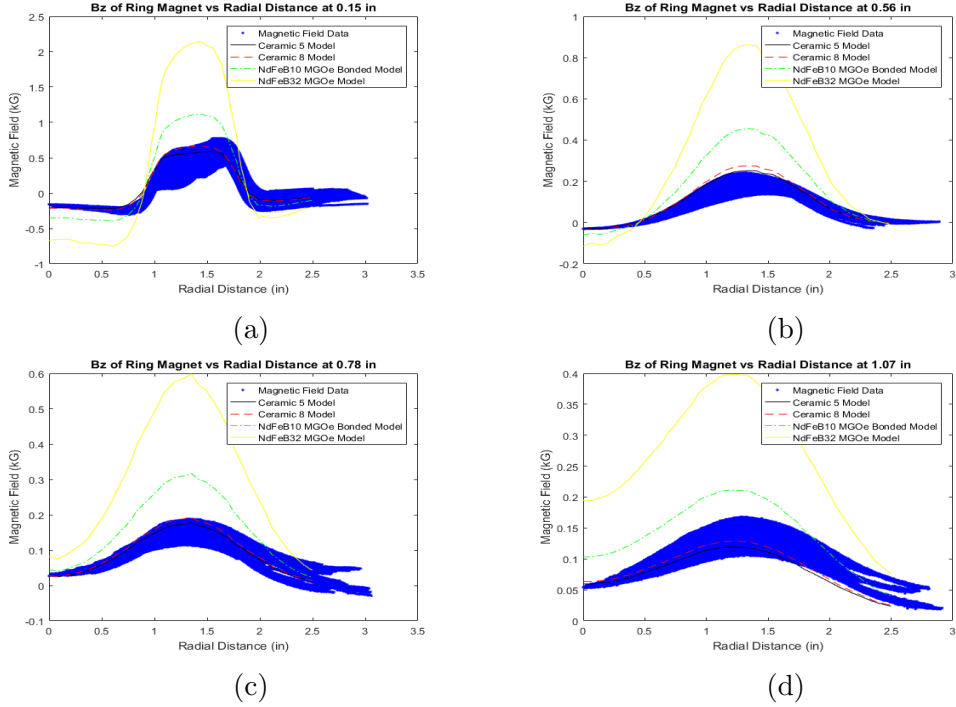


Figure 4.2: The images depict the decay of the axial magnetic field as the distance from the axis of symmetry of the ring magnet increases. These plots compare the experimental data to the the numerical models of the ring magnet’s geometry for various materials. These materials include ceramic 5, ceramic 8, NdBF₁₀ (Bonded) MGOe, and NdBF₃₂ MGOe. The heights plotted are 0.15 in. (a), 0.56 in. (b), 0.78 in. (c), and 1.07 in. (d). The blue line representing the data had an uncertainty roughly equivalent to the thickness of the line as can be treated as an error bar in the data.

When plotting the numerical models against the experimental data, the data needed to be converted from a Cartesian grid into a single variable expressing field strength in terms of distance from the center. In effect, this allows us to test the axial symmetry assumption that was built into the numerical models by observing the thickness of the experimental data’s line. In

turn, this thickness serves as the uncertainty in the magnetic field data. In addition, a background magnetic field was noted during each measurement. Moreover, the background magnetic field fluctuated noticeably from measurement to measurement. Therefore, a different free offset parameter was added to the magnetic field data measured at each height. In the case of Fig. 4.2 axial magnetic field, this offset was applied to match the ceramic 5 model as best as possible.

We note that this data did not always line up with itself as in the case of the ring magnet. This lack of symmetry is partially due to the asymmetric background discussed previously. In addition, the ring magnet appeared chipped at a portion on its upper face, which made the magnetic field noticeably weaker on that portion. This can be seen in Fig. 4.2 where the center of the graph appears very thick.

From Fig. 4.2, it was determined that ceramic 5 model best matches the data as it stays nearest to the experimental data. Although the ceramic 8 model also performs well, it slightly overshoots the maximum of the 0.56 in. plot. We should note that when the offset was adjusted to better agree with the ceramic 8 model, the 0.56 in. data would no longer have an overshoot at the maximum of the field. However, this caused the model to diverge from the data distances near the axis of symmetry. As for the two NdFeB alloys, we note that they fail due to significantly overshooting the data. Thus, we conclude that the ceramic 5 model best models the data.

4.1.3 Puck Magnet

The experimental data were converted from a Cartesian grid into a 1D function of radius in a similar matter as before. Although an offset was applied to this data set, it was done to ensure that at long distances from the puck, the field approaches zero. This was not possible with the ring magnet as it did not go to zero at the furthest points away from the magnet at which data were collected.

From looking at Figure 4.3, we note that there was no combination of materials that agreed with the data. The closest material combination was $m1$ =Stainless Steel 430 and $m2$ =NdBFe52 MGOe. However, the model's magnetic field decays too quickly to match the data. This is most prominently observed in the 0.28 in. measurement of the field. We note that the deviation between this model and the data decreases as the height of the measurement increases. However, none of the other tested combinations of materials even came close to matching the data. These results seem to indicate that the FEMM software may have difficulty modeling different materials that are in close proximity to each other.

From this analysis, we determined the materials that most closely model the ring and puck magnets. Moreover, it was noted that the FEMM simulations very accurately recreate the field of the puck magnet. Due to the noisiness of the ring magnet data and the accuracy of the simulation, it was recommended that future analysis of the field use the FEMM simulation as opposed to the magnetic field data. However, the puck magnet simulation failed to accurately capture the field from the data. Therefore, it was concluded

that future analysis of the puck magnet's field only use the simulations in the far field limit and require the use of data to compliment the use of FEMM simulations to complement the data especially in the near field limit.

4.2 Solenoids

After the creation of the solenoids, we checked that they were capable of producing similar magnetic forces given similar current, potentially modified with a correction coefficient. We began by prepping the materials and equipment. We created a circuit comprised of a power supply with a ceramic resistor (rated at 6.2 Ω , 10 W load limit) to prevent overheating.

The voltage on the power source was set to 12 Volts and the solenoids were labeled as S1, S2, S3, and S4. We zeroed a LakeShore gaussmeter and set it to the kG range, which provides values with an uncertainty of $\pm 1 \times 10^{-5}$ kG. After prepping, we placed the solenoid on the LakeShore machine and used duct tape to hold it at a constant position and orientation. We cleared the area of magnetic objects and centered the device's probe above solenoid S1 at a height of 0.68 in. above the solenoid. The machine was turned on and we measured the magnetic field of S1 for currents ranging from 0.00 A to 1.00 A in increments of 0.10 A. We repeated this procedure for the other solenoids.

Figure 4.4 shows that solenoids S2, S3, and S4 are in agreement with each other with only minimal deviations, but S1 produces a magnetic field approximately 60% weaker in magnitude, compared to the others. This difference suggests poor construction, possibly resulting from an internal stripping allowing current to bypass parts of the solenoid (see Figure 4.4 and Table 4.1).

Table 4.1: Calibration data for the first four manufactured solenoids.

Solenoid One			Solenoid Two		
I (A)	B (G)	V (V)	I (A)	B (G)	V (V)
0.00	-5.60	0.01	0.00	-2.50	0.01
0.10	-2.40	0.78	0.10	-5.00	0.78
0.20	-3.63	1.55	0.20	-8.13	1.55
0.30	-4.50	2.31	0.30	-11.59	2.32
0.40	-6.13	3.09	0.40	-15.24	3.09
0.50	-7.79	3.87	0.50	-18.78	3.86
0.60	-9.47	4.65	0.60	-22.21	4.63
0.70	-11.15	5.42	0.70	-25.44	5.38
0.80	-12.77	6.19	0.80	-28.48	6.15
0.90	-14.31	6.96	0.90	-31.22	6.90
1.00	-15.74	7.75	1.00	-33.76	7.66
Solenoid Three			Solenoid Four		
I (A)	B (G)	V (V)	I (A)	B (G)	V (V)
0.00	-2.90	0.01	0.00	-1.20	0.02
0.10	-5.69	0.81	0.10	-4.46	0.85
0.20	-9.22	1.61	0.20	-8.56	1.69
0.30	-13.19	2.42	0.30	-12.75	2.52
0.40	-17.30	3.22	0.40	-17.00	3.35
0.50	-21.22	4.02	0.50	-21.22	4.18
0.60	-24.85	4.87	0.60	-25.05	5.60
0.70	-28.04	5.65	0.70	-28.35	5.79
0.80	-30.87	6.43	0.80	-31.33	6.61
0.90	-33.20	7.21	0.90	-33.74	7.42
1.00	-35.46	8.01	1.00	-35.69	8.22

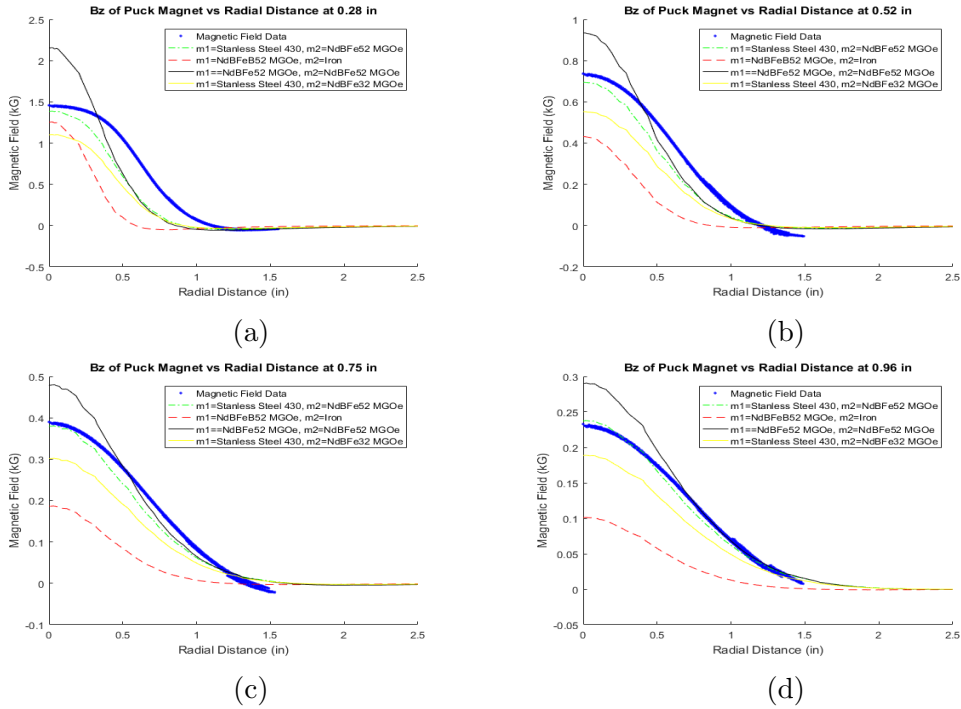


Figure 4.3: The images depict the decay of the axial magnetic field as the distance from the axis of symmetry of the puck magnet increases. These plots compare the experimental data to the the numerical models of the puck magnet's geometry for various materials. The puck model was modelled as a composite of two different cylindrical magnets. The material on the top magnet was denoted by m1 and the bottom magnet was denoted by m2. The heights plotted are 0.28 in. (a), 0.52 in. (b), 0.75 in. (c), and 0.96 in. (d). The blue line representing the data had an uncertainty roughly equivalent to the thickness of the line as can be treated as an error bar in the data.

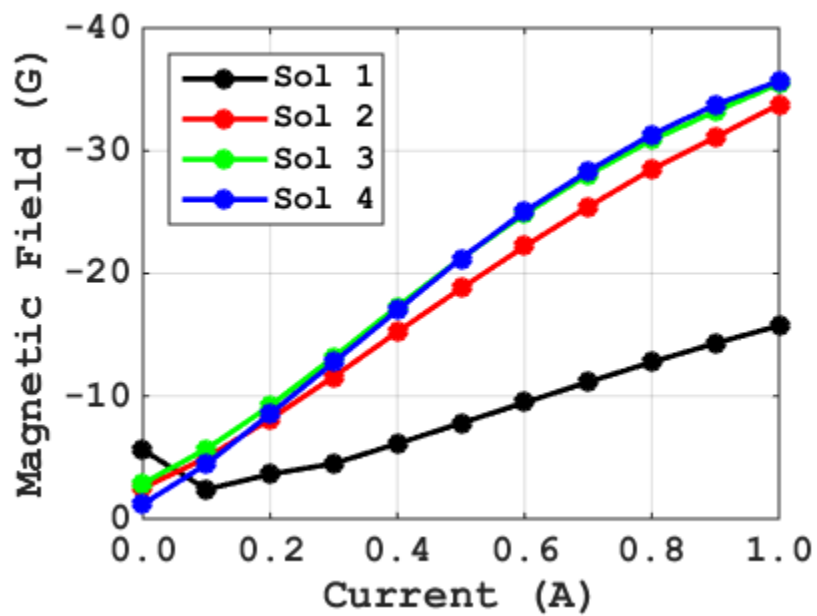


Figure 4.4: A plot of magnetic field strength as a function of current for the four solenoids that we manufactured. Sol 1 shows noticeable deviation from the other three.

Chapter 5

Conclusions

5.1 Research Conclusions

The overall goal of our research was to create a device that could stably levitate a puck magnet as an initial proof-of-concept that could be used to assess the feasibility of multiple practical applications of similar magnetic stabilization systems. With our research we determined that our device design is conceptually sound. The considerations we made during its creation have left a detailed record of the optimal research and development steps taken to create a magnetic stabilization device. More specifically, our research shows that the stabilization of a levitating magnet can be treated as an inverted pendulum problem, which could greatly expand the accessibility of magnetic stabilization research.

5.2 Future Research

The future research into magnetic stabilization devices will benefit heavily from our methods. We have itemized the process of constructing the device, and

have detailed a potential algorithm to use for the system. We have simplified the research process of future teams by detailing our biggest successes and roadblocks.

The magnet analysis software and hardware used in our research provide valuable information for teams using the same research configuration, and denote specific procedures to replicate this data collection for any pair of magnets. While further testing and calibration would have to be done to implement the code and design of our device, our research lays the groundwork for future researchers to explore the limitations of this device. Future research should be focused on the specific applications and scalability of the technology, with more time devoted to testing now that the steps for prototyping are clearly set out.

Appendix A

Magnetic Field Maps

The following color maps represent data collected from the LakeShore magnetic field measurement device (see Section 3.3). Data were recorded in a grid format, and the distance between adjacent measurements was $40\ \mu\text{m}$. In particular, the scans for ring axial, puck axial, and puck radial magnetic fields were squares of side 102 mm, 51 mm, and 64 mm, respectively.

The results show that material imperfections or damage cause observable deviations in a magnet's magnetic field (see Figure A.1, where a chip in the ring magnet locally reduces the field strength approximately six-fold). Furthermore, the spatial gradient is as steep as $160\ \text{kG/m}$ at the physical boundaries of the ring magnet, but only $20\ \text{kG/m}$ for the puck magnet. Lastly, the decay of the field strength with distance from the magnet is demonstrated by the sharper apparent resolution of the maps taken at closer positions.

A.1 Ring Magnet Axial Component

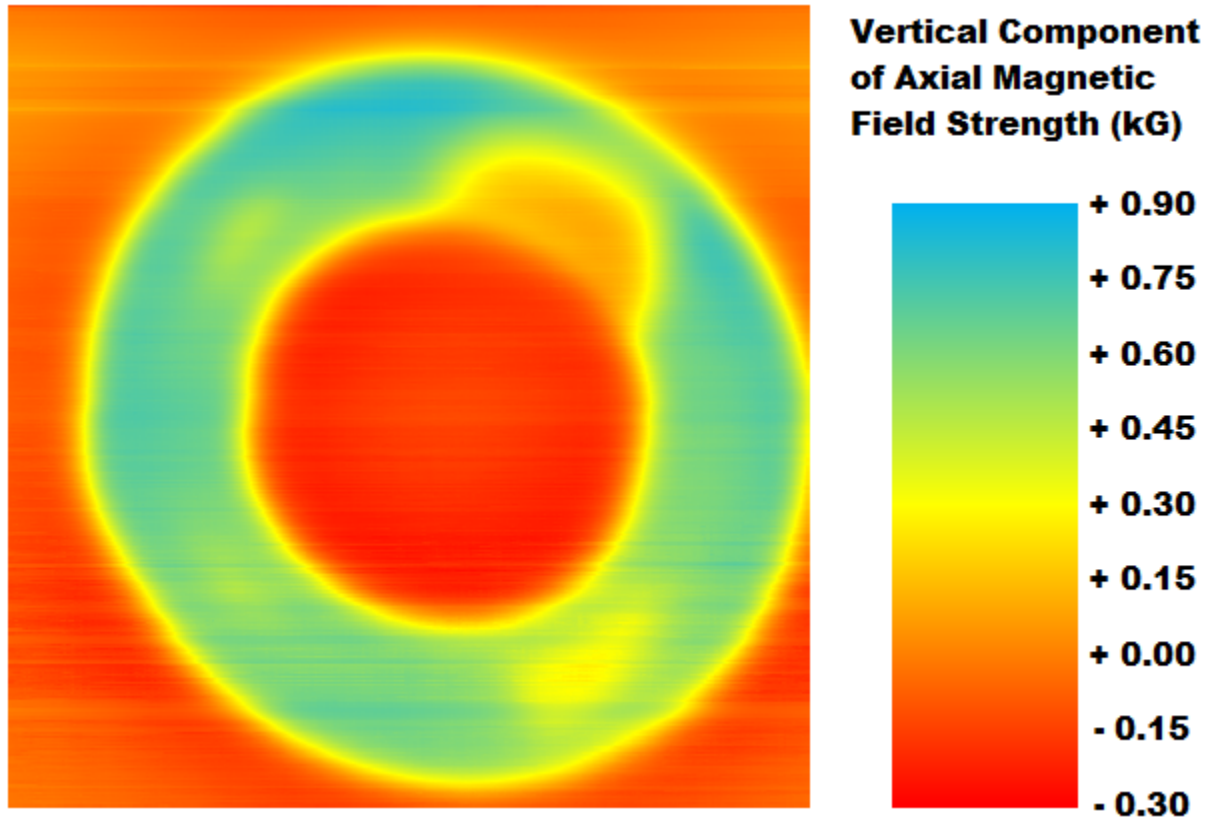


Figure A.1: Ring Magnet Axial Field at $z = 3.8$ mm.

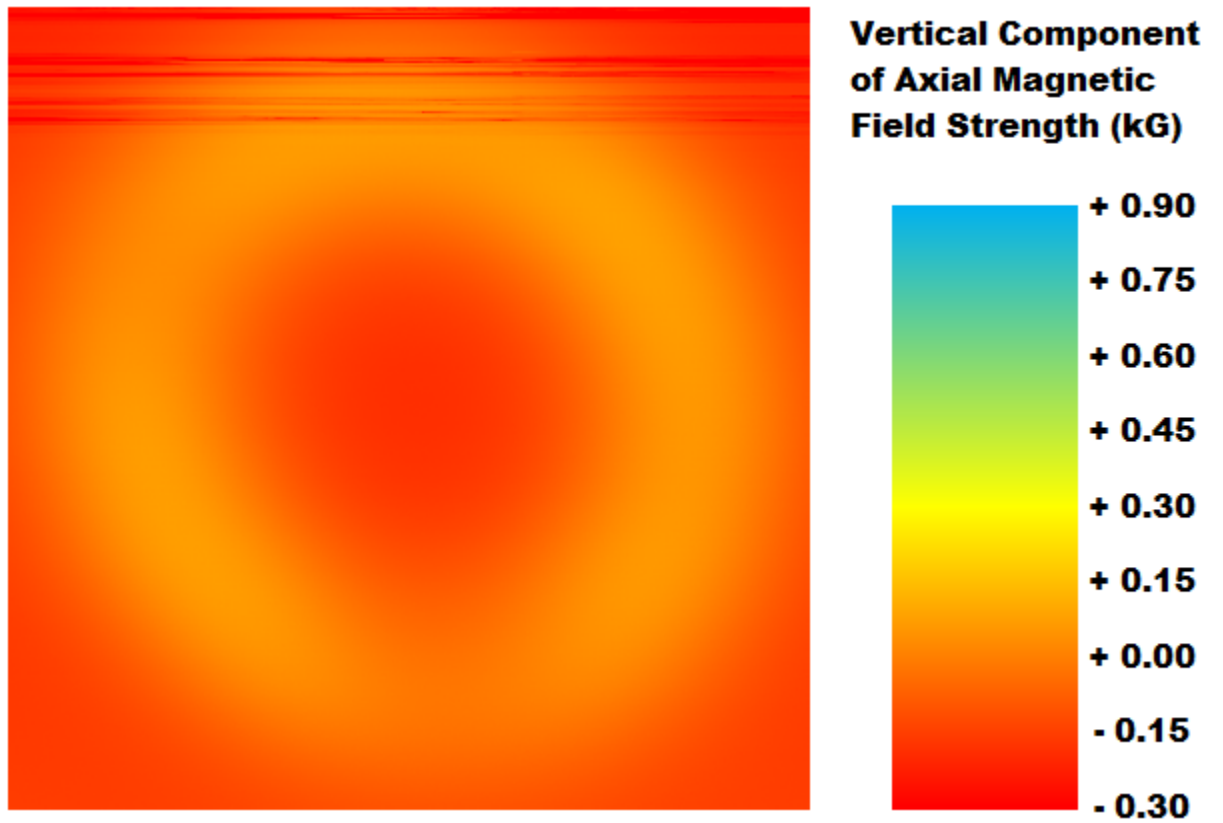


Figure A.2: Ring Magnet Axial Field at $z = 14.2$ mm.

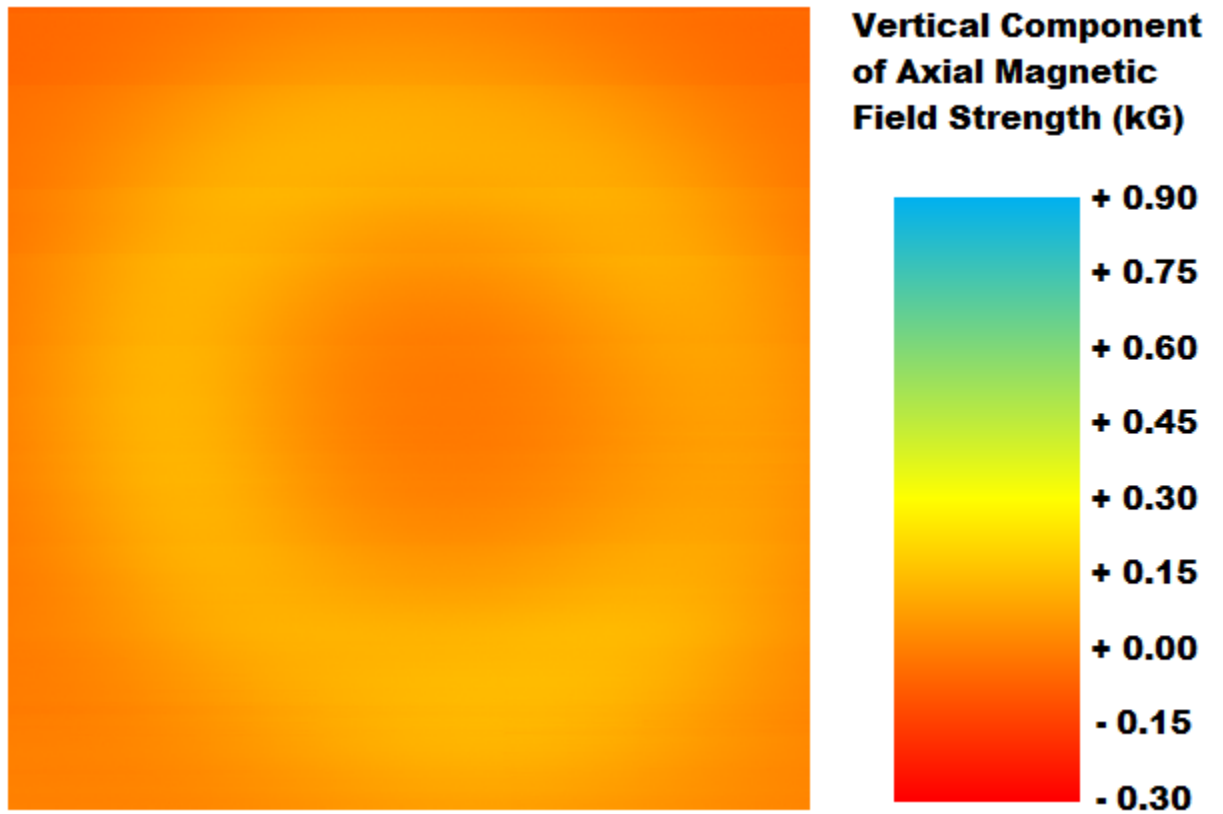


Figure A.3: Ring Magnet Axial Field at $z = 19.8$ mm.

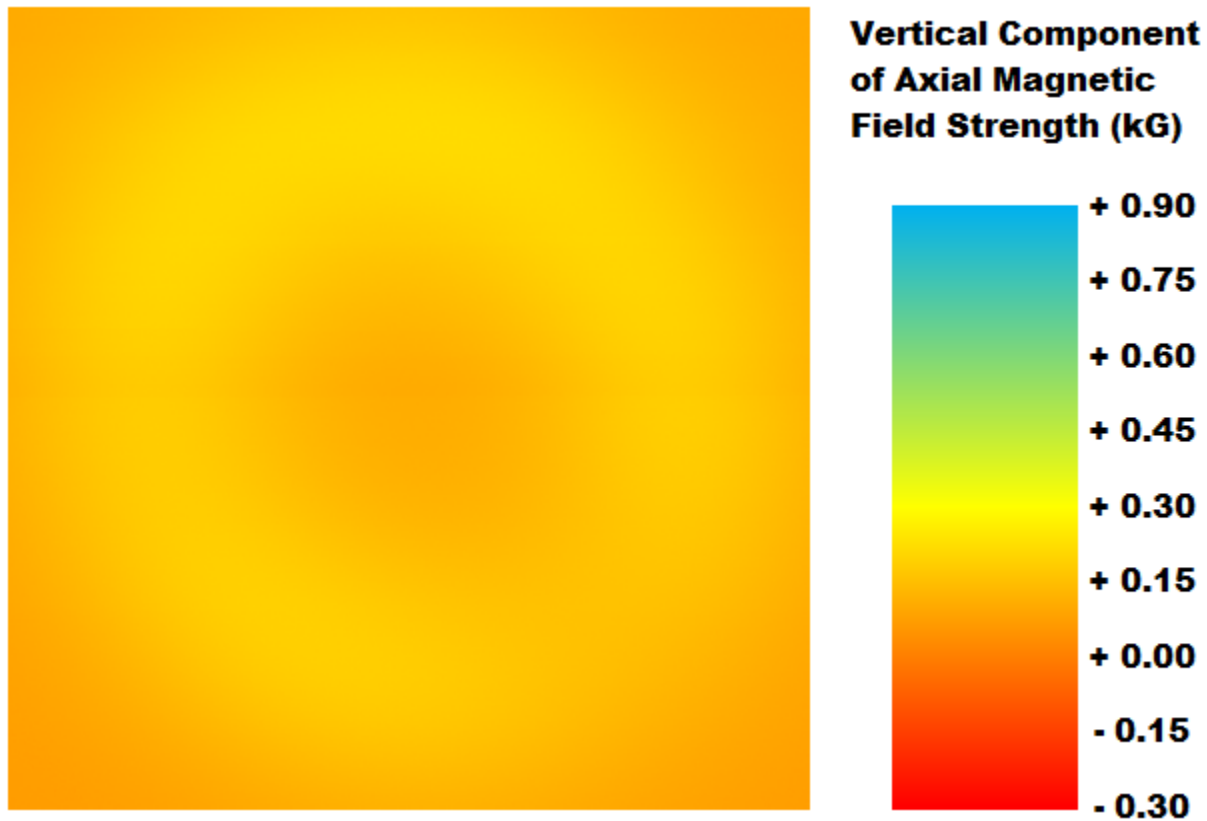


Figure A.4: Ring Magnet Axial Field at $z = 27.2$ mm.

A.2 Puck Magnet Axial Component

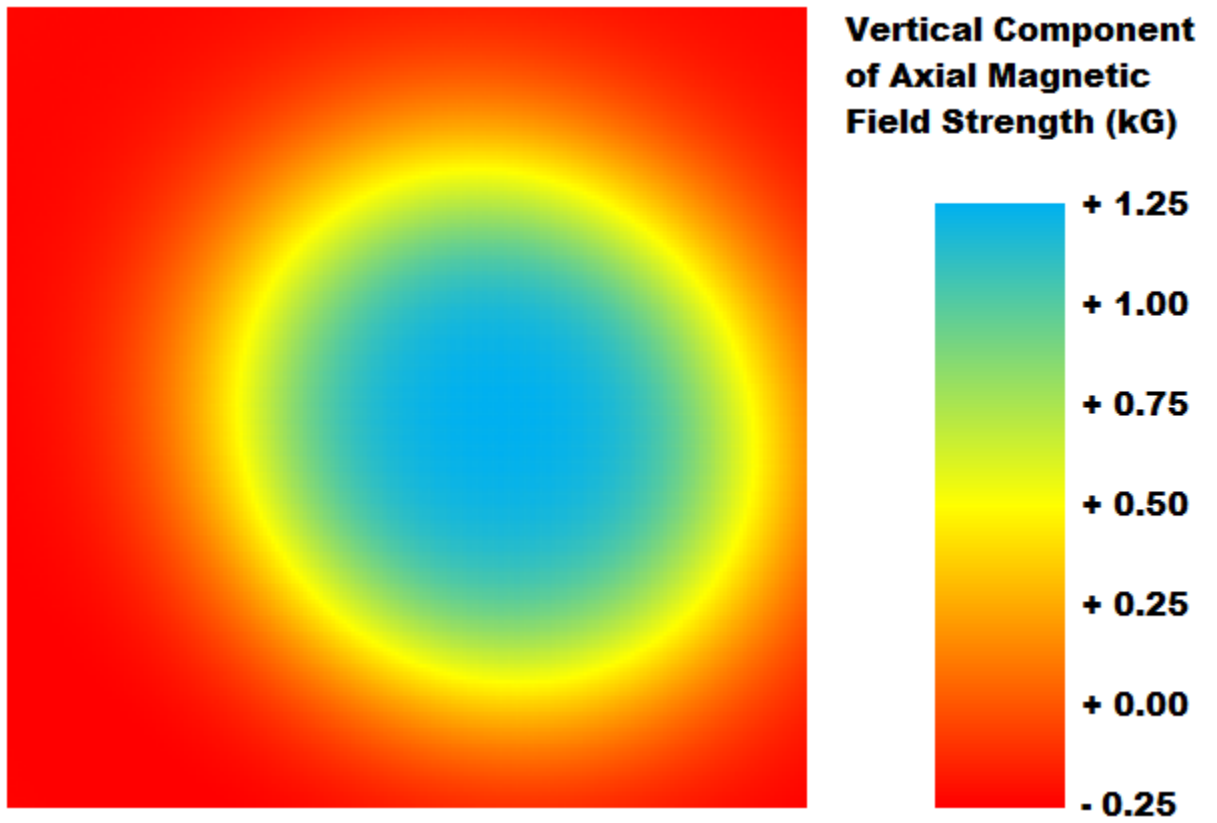


Figure A.5: Puck Magnet Axial Field at $z = 6.3$ mm.

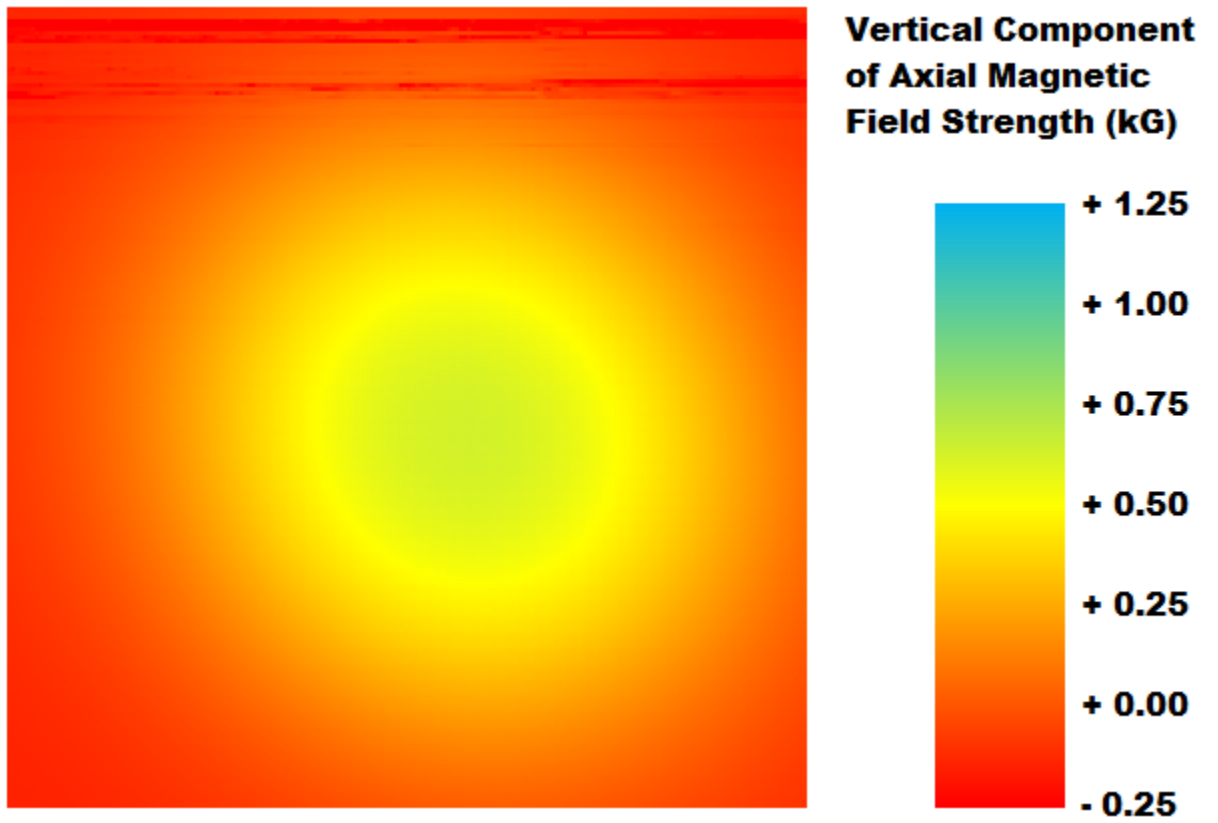


Figure A.6: Puck Magnet Axial Field at $z = 13.2$ mm.

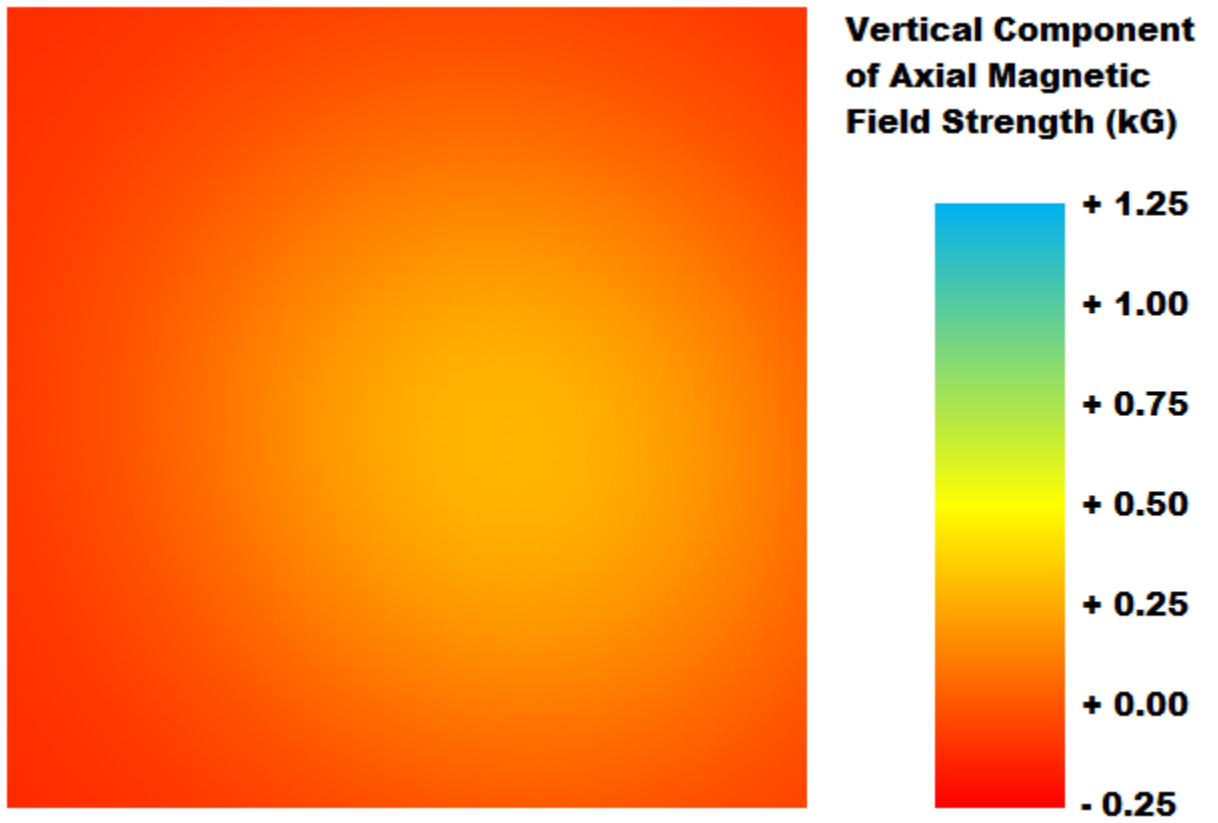


Figure A.7: Puck Magnet Axial Field at $z = 19.1$ mm.

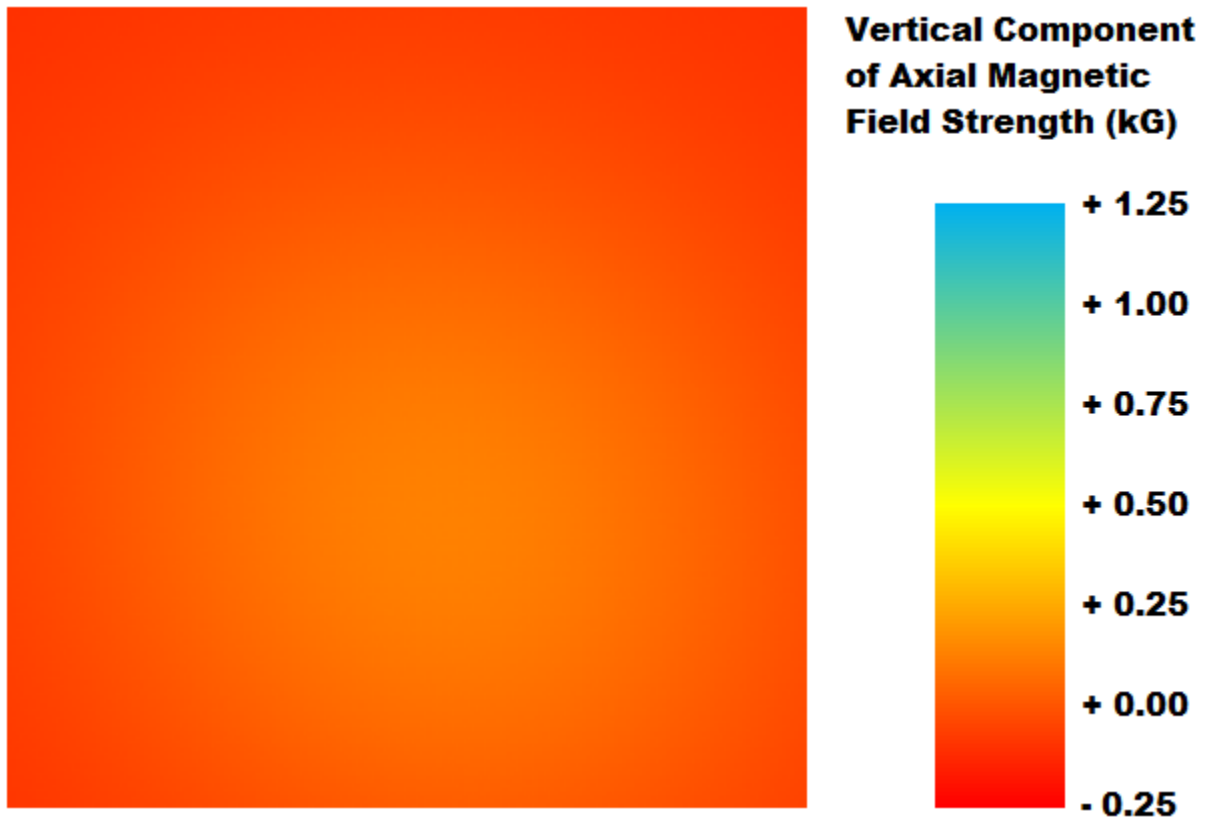


Figure A.8: Puck Magnet Axial Field at $z = 24.4$ mm.

A.3 Puck Magnet Radial Component

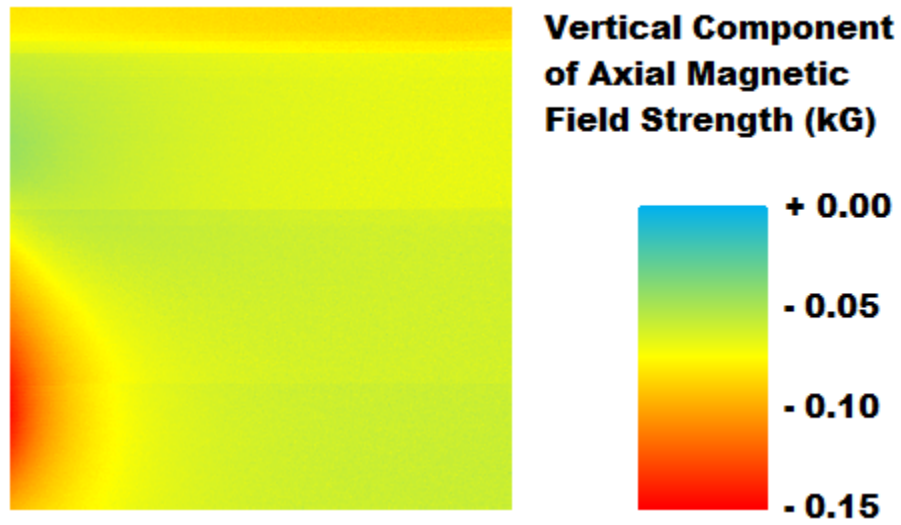


Figure A.9: Puck Magnet Radial Field at $z = 19.1$ mm.

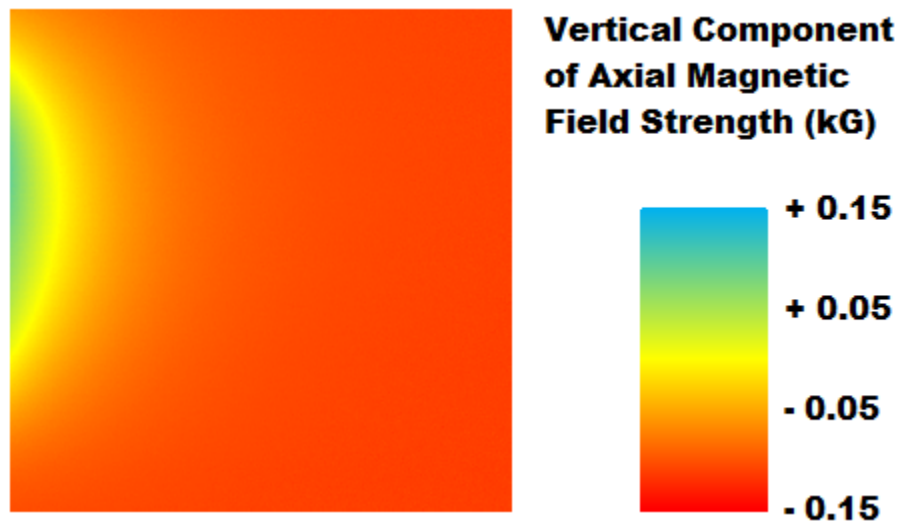


Figure A.10: Puck Magnet Radial Field at $z = 23.6$ mm.

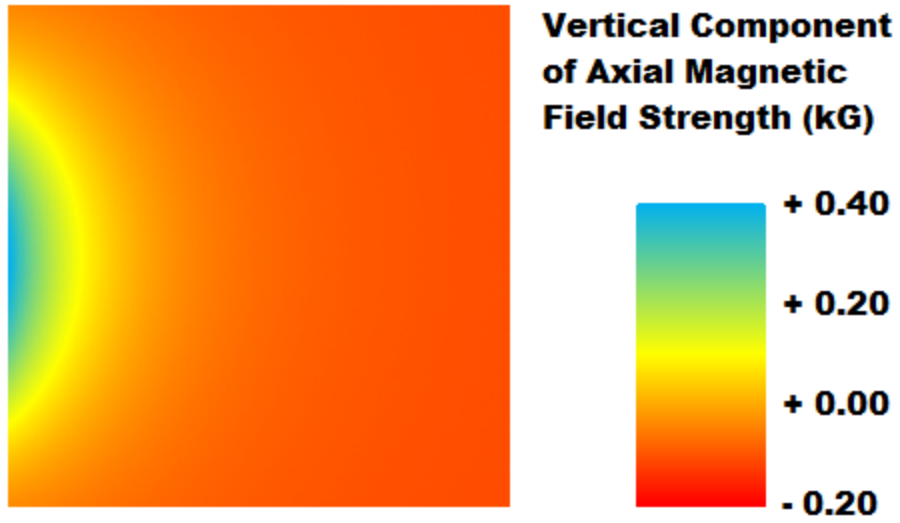


Figure A.11: Puck Magnet Radial Field at $z = 34.5$ mm.

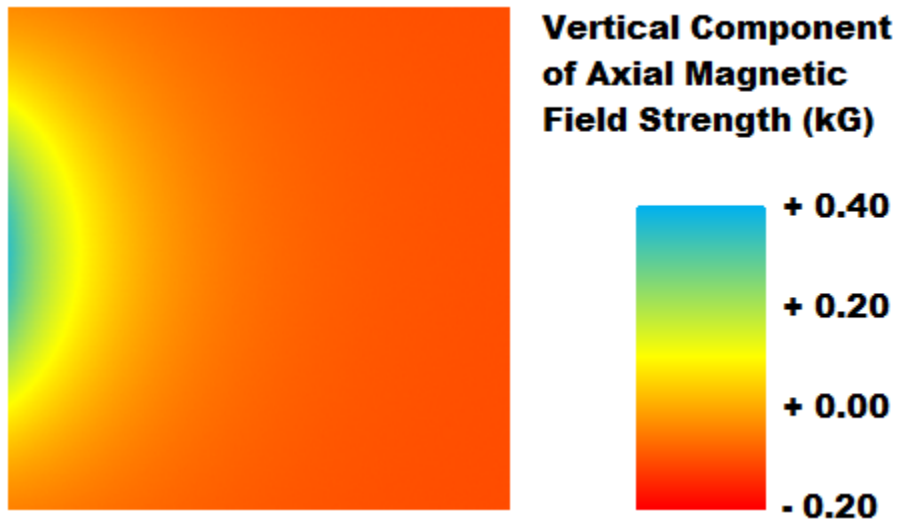


Figure A.12: Puck Magnet Radial Field at $z = 44.2$ mm.

Appendix B

Magnetic Field MATLAB Analysis Code

The LakeShore magnetic field sensor system provided us with large files of tabulated data describing the magnetic fields of our ring and puck magnets. We imported these data to MATLAB and wrote various scripts and functions in order to process and analyze our results [54]. The following pages present the code used for this MATLAB analysis.

```

function [B] = femm_input(file)
% Import data from text file:
% Script for importing data from the following text file:
%   C:\Users\Shawn\Documents\College\Maglev\Bzflipped_NdFe37.txt
% To extend the code to different selected data or a different text file,
% generate a function instead of a script.
% Auto-generated by MATLAB on 2016/03/16 11:52:20

% Initialize variables:
filename = file;
delimiter = '\t';
startRow = 3;

% Format string for each line of text:
formatSpec = '%f%f%[\n\r]';
%   column1: double (%f)
%   column2: double (%f)
% For more information, see the TEXTSCAN documentation.

% Open the text file:
fileID = fopen(filename,'r');

% Read columns of data according to format string.
% This call is based on the structure of the file used to generate this
% code. If an error occurs for a different file, try regenerating the code
% from the Import Tool.
dataArray = textscan(fileID,formatSpec,'Delimiter',delimiter, ...
    'HeaderLines',startRow-1,'ReturnOnError',false);

% Close the text file:
fclose(fileID);

% Post processing for unimportable data:
% No unimportable data rules were applied during the import, so no post
% processing code is included. To generate code which works for unimport-
% able data, select unimportable cells in a file and regenerate the script.

% Create output variabl:
B = [dataArray{1:end-1}];

% Clear temporary variables:
clearvars filename delimiter startRow formatSpec fileID dataArray ans;
end

```

```

function [B] = flipdata(file)
% Import data from text file:
% Script for importing data from the following text file:
%   C:\Users\Shawn\Documents\College\Maglev\Bzflipped_NdFe37.txt
% To extend the code to different selected data or a different text file,
% generate a function instead of a script.
% Auto-generated by MATLAB on 2016/03/16 11:52:20

% Initialize variables:
filename = file;
delimiter = '\t';
startRow = 3;

% Format string for each line of text:
formatSpec = '%f%f%[\n\r]';
%   column1: double (%f)
%   column2: double (%f)
% For more information, see the TEXTSCAN documentation.

% Open the text file:
fileID = fopen(filename,'r');

% Read columns of data according to format string:
% This call is based on the structure of the file used to generate this
% code. If an error occurs for a different file, try regenerating the code
% from the Import Tool.
dataArray = textscan(fileID,formatSpec,'Delimiter',delimiter, ...
    'HeaderLines',startRow-1,'ReturnOnError',false);

% Close the text file:
fclose(fileID);

% Post processing for unimportable data:
% No unimportable data rules were applied during the import, so no post
% processing code is included. To generate code which works for unimport-
% able data, select unimportable cells in a file and regenerate the script.

% Create output variable:
B = [dataArray{1:end-1}];

% Clear temporary variables:
clearvars filename delimiter startRow formatSpec fileID dataArray ans;
B(1:num_pt,2)=-B(num_pt:-1:1,2);
end

```

```

function [m,b,P] = magnet_mapping_cal(varargin)
% Get Matlab's Measured Field:
len = length(varargin);

for i = 1:len
    avg(i) = mean(mean(varargin{i}));
    stdvi(i) = std(std(varargin{i}));
    stdv(i) = stdvi(i)/sqrt(len);
end

% Get Actual Field in kG:
for i = 1:len
    inputs{i}=inputname(i);
end

for i = 1:len
    if (inputs{i}(16:18) == 'neg')
        int = str2num(inputs{i}(19));
        dec = str2num(inputs{i}(21:25));
        act(i) = -(int+dec*10^-5);
        int_unc = str2num(inputs{i}(31));
        dec_unc = str2num(inputs{i}(33:37));
        act_unc(i) = (int_unc+dec_unc*10^-5);
    else
        int = str2num(inputs{i}(16));
        dec = str2num(inputs{i}(18:22));
        act(i) = (int+dec*10^-5);
        int_unc = str2num(inputs{i}(28));
        dec_unc = str2num(inputs{i}(30:34));
        act_unc(i) = (int_unc+dec_unc*10^-5);
    end
end

% Create Fit:
data = [act' avg' stdv'];
Results = weightedfit(data); % 'weightedfit' coded by Ebo Ewusi-Annan,
A = Results.slope;           % University of Florida, 2011.
B = Results.Intercept;
y = @(x) A.*x+B;
for i = 1:len
    chi2i(i)=y(act(i))/stdv(i);
end
chi2sum = sum(chi2i);
v = len-2;
P = 1-chi2cdf(chi2sum,v);
m = 1/A;
b = -B/A;
field = @(counts) counts*m+b;
end

```

```

function [xLoc, yLoc, maxB, list] = max_B_loc(B_vals)
    highB = max(max(B_vals));
    area = size(B_vals);
    Xlength = area(1);
    Ylength = area(2);
    list = zeros(10,3);
    nextL = 1;
    for i = 1:Xlength
        for j = 1:Ylength
            if B_vals(i,j) > highB - 2
                if nextL <= 10
                    list(nextL,1) = i;
                    list(nextL,2) = j;
                    list(nextL,3) = B_vals(i,j);
                    nextL = nextL + 1;
                else
                    for k = 1:10
                        if B_vals(i,j) > list(k,3)
                            list(k,1) = i;
                            list(k,2) = j;
                            list(k,3) = B_vals(i,j);
                            break;
                        end
                    end
                end
            end
        end
    end
end
maxB = max(list(:,3));
for n = 1:10
    if list(n,3) == maxB
        xLoc = list(n,1);
        yLoc = list(n,2);
    end
end
end

```

```

function [Br] = plot_horiz_Br(r1,z1,r2,filename)
% Plots B_r along a line running from (r1,z1) to (r1,r2). Can be an array of r1, z1, and r2.
% Br is a two-element array where the first column is z and the second column is Br.

% Open File:
if (exist('filename')) % Add ability to specify file name.
    flen = length(filename);
    if (strcmp(filename(flen-2:flen),'FEM') || strcmp(filename(flen-2:flen),'ans'))
        filegood = 1; openfemm;
        simdir = 'C:\Users\Shawn\Documents\College\Maglev\femm simulations\';
        opendocument([simdir,filename]);
        if (strcmp(filename(flen-2:flen),'FEM'))
            mi_createmesh; mi_showmesh;
            mi_analyze; mi_loadsolution;
        end
    end
end

% Store Data:
mo_clearcontour;

% If only given one value for r1 or r2, use that value for all entries in the array:
if (length(r1) == 1), r1 = r1*ones(1,length(z1)); end
if (length(r2) == 1), r2 = r2*ones(1,length(z1)); end
line_len = abs(r2-r1);
num_pt = line_len*1000 + 1; % 1000 points per inch, include both end points.
num_cell = length(z1);
Br = cell(1,num_cell);
dir = 'C:\Users\Shawn\Documents\College\Maglev\femm results\';
for i = 1:length(z1)
    mo_addcontour(r1(i),z1(i));
    mo_addcontour(r2(i),z1(i));
    if (exist('filegood'))
        name{i} = [filename(1:flen-4),' Br horiz data r1 = ',num2str(r1(i)), ...
            ', z1 = ',num2str(z1(i)),', r2 = ',num2str(r2(i))];
    else
        name{i} = ['Br horiz data r1 = ',num2str(r1(i)),', z1 = ', ...
            num2str(z1(i)),', r2 = ',num2str(r2(i))];
    end
    mo_makeplot(3,num_pt(i),[dir,name{i}],0);
    Br{i} = femm_input([dir,name{i}],num_pt(i));
    Br_i = Br{i}; save([dir,name{i}],' .mat','Br_i')
    figure; plot(Br{i}(:,1),Br{i}(:,2),'b-');
    xlabel(['Horizontal Distance from r1 = ',num2str(r1(i))]);
    ylabel('Br (T)'); title(name{i});
    mo_clearcontour;
end

```

```

function [Bz] = plot_horiz_Bz(r1,z1,r2,filename)
% Plots B_z along a line running from (r1,z1) to (r2,z1). Can be an array of r1, z1, and r2.
% Bz is a two-element array where the first column is z and the second column is Bz.

% Open File:
if (exist('filename')) % Add ability to specify file name.
    flen = length(filename);
    if (strcmp(filename(flen-2:flen),'FEM') || strcmp(filename(flen-2:flen),'ans'))
        filegood = 1; openfemm;
        simdir = 'C:\Users\Shawn\Documents\College\Maglev\femm simulations\';
        opendocument([simdir,filename]);
        if (strcmp(filename(flen-2:flen),'FEM'))
            mi_createmesh; mi_showmesh;
            mi_analyze; mi_loadsolution;
        end
    end
end

% Store Data:
mo_clearcontour;

% If only given one value for r1 or r2, use that value for all entries in the array:
if (length(r1) == 1), r1 = r1*ones(1,length(z1)); end
if (length(r2) == 1), r2 = r2*ones(1,length(z1)); end
line_len = abs(r2-r1);
num_pt = line_len*1000 + 1; % 1000 points per inch, include both end points.
num_cell = length(z1);
Bz = cell(1,num_cell);
dir = 'C:\Users\Shawn\Documents\College\Maglev\femm results\';
for i = 1:length(z1)
    mo_addcontour(r1(i),z1(i));
    mo_addcontour(r2(i),z1(i));
    if (exist('filegood'))
        name{i} = [filename(1:flen-4), ' Bz horiz data r1 = ',num2str(r1(i)), ...
            ', z1 = ',num2str(z1(i)), ', r2 = ',num2str(r2(i))];
    else
        name{i} = ['Bz horiz data r1 = ',num2str(r1(i)), ', z1 = ',num2str(z1(i)), ...
            ', r2 = ',num2str(r2(i))];
    end
    mo_makeplot(2,num_pt(i),[dir,name{i}],0);
    Bz{i} = femm_input([dir,name{i}],num_pt(i));
    Bz_i = Bz{i};
    save([dir,name{i}],'Bz_i.mat','Bz_i')
    figure; plot(Bz{i}(:,1),Bz{i}(:,2),'b-');
    xlabel(['Horizontal Distance from r1 = ',num2str(r1(i))]);
    ylabel('Bz (T)'); title(name{i});
    mo_clearcontour;
end

```

```

function [x,y,data_adj] = plot_surf(data)
titsurf = 'Magnetic Field of Puck Magnet at Levitation Height';
titcont = 'Contour Plot of Puck Magnet Field at Levitation Height';
load('cal_data.mat'); % Adjust raw data to reflect calibration:
[m, b] = magnet_mapping_cal(cal3o50000kGnom0o00105kGunc0o00001kGr10x10, ...
    cal3o50000kGnom0o00387kGunc0o00001kGr10x10, ...
    cal3o50000kGnom0o52371kGunc0o00001kGr10x10, ...
    cal3o50000kGnom1o87496kGunc0o00001kGr10x10, ...
    cal3o50000kGnomneg0o00116kGunc0o00001kGr10x10, ...
    cal3o50000kGnomneg0o00120kGunc0o00001kGr10x10, ...
    cal3o50000kGnomneg0o51963kGunc0o00001kGr10x10, ...
    cal3o50000kGnomneg0o73362kGunc0o00001kGr10x10);
data_adj = data.*m + b;

% Generate a contour plot:
x = 0:0.01:(length(data_adj(1,:))-1)/100; length(x);
y = 0:0.01:(length(data_adj(:,1))-1)/100; length(y);
size(data_adj); close('all'); figure;
xlabel('x-axis (in)', 'Fontname', 'Times', 'FontSize', 12);
ylabel('y-axis (in)', 'Fontname', 'Times', 'FontSize', 12);
title(titcont, 'Fontname', 'Times', 'FontSize', 12);
contour(x,y,data_adj); axis('tight');
set(gcf, 'color', 'white');
set(gcf, 'PaperPosition', [0,0,4/4*3,3/4*3]);

% Generate a 3D surface plot:
figure; surf(x,y,data_adj);
grid('on'); box('on'); axis('tight');
xlabel('x-axis (in)', 'Fontname', 'Times', 'FontSize', 12);
ylabel('y-axis (in)', 'Fontname', 'Times', 'FontSize', 12);
zlabel('Magnetic Field (kG)', 'Fontname', 'Times', 'FontSize', 12);
title(titcont, 'Fontname', 'Times', 'FontSize', 12);
set(gcf, 'color', 'white');
set(gca, 'Fontname', 'Times', 'FontSize', 12);
set(gcf, 'PaperPosition', [0,0,4/4*3,3/4*3]);
end

```

```

function [Br] = plot_vert_Br(r1,z1,z2,filename)
% Plots B_r along a line running from (r1,z1) to (r1,z2). Can be an array of r1, z1, and z2.
% Br is a two-element array where the first column is z and the second column is Br.

% Open File:
if (exist('filename')) % Add ability to specify file name.
    flen = length(filename);
    if (strcmp(filename(flen-2:flen),'FEM') || strcmp(filename(flen-2:flen),'ans'))
        filegood = 1; openfemm;
        simdir = 'C:\Users\Shawn\Documents\College\Maglev\femm simulations\';
        opendocument([simdir,filename]);
        if (strcmp(filename(flen-2:flen),'FEM'))
            mi_createmesh; mi_showmesh;
            mi_analyze; mi_loadsolution;
        end
    end
end

% Store Data:
mo_clearcontour;

% If only given one value for z1 or z2, use that value for all entries in the array.
if (length(r1) == 1), z1 = z1*ones(1,length(r1)); end
if (length(z2) == 1), z2 = z2*ones(1,length(r1)); end
line_len = abs(z2-z1);
num_pt = line_len*1000 + 1; % 1000 points per inch, include both end points.
num_cell = length(r1);
Br = cell(1,num_cell);
dir = 'C:\Users\Shawn\Documents\College\Maglev\femm results\';
for i = 1:length(r1)
    mo_addcontour(r1(i),z2(i));
    mo_addcontour(r1(i),z1(i));
    if (exist('filegood'))
        name{i} = [filename(1:flen-4), ' Br vert data r1 = ',num2str(r1(i)), ...
            ', z1 = ',num2str(z1(i)), ', z2 = ',num2str(z2(i))];
    else
        name{i} = ['Br vert data r1 = ',num2str(r1(i)), ', z1=',num2str(z1(i)), ...
            ', z2 = ',num2str(z2(i))];
    end
    mo_makeplot(2,num_pt(i),[dir,name{i}],0);
    Br{i} = flipdata([dir,name{i}],num_pt(i));
    Br_i = Br{i};
    save([dir,name{i}],'mat','Br_i');
    figure; plot(Br{i}(:,1),Br{i}(:,2),'b-');
    xlabel(['Vertical Distance from z1 = ',num2str(z1(i))]);
    ylabel('Br (T)'); title(name{i});
    mo_clearcontour;
end

```

```

function [Bz] = plot_vert_Bz(r1,z1,z2,filename)
% Plots B_z along a line running from (r1,z1) to (r1,z2). Can be an array of r1, z1, and z2.
% Bz is a two-element array where the first column is z and the second column is Bz.

% Open File:
if (exist('filename')) % Add ability to specify file name.
    flen = length(filename);
    if (strcmp(filename(flen-2:flen),'FEM') || strcmp(filename(flen-2:flen),'ans'))
        filegood = 1; openfemm;
        simdir = 'C:\Users\Shawn\Documents\College\Maglev\femm simulations\';
        opendocument([simdir,filename]);
        if strcmp(filename(flen-2:flen),'FEM')
            mi_createmesh; mi_showmesh;
            mi_analyze; mi_loadsolution;
        end
    end
end

% Store Data:
mo_clearcontour;

% If only given one value for r1 or z2, use that value for all entries in the array.
if (length(r1) == 1), z1 = z1*ones(1,length(r1)); end
if (length(z2) == 1), z2 = z2*ones(1,length(r1)); end
line_len = abs(z2-z1);
num_pt = line_len*1000 + 1; % 1000 points per inch, include both end points.
num_cell = length(r1);
Br = cell(1,num_cell);
dir = 'C:\Users\Shawn\Documents\College\Maglev\femm results\';
for i = 1:length(r1)
    mo_addcontour(r1(i),z2(i));
    mo_addcontour(r1(i),z1(i));
    if (exist('filegood'))
        name{i} = [filename(1:flen-4),' Bz vert data r1 = ',num2str(r1(i)), ...
            ', z1 = ',num2str(z1(i)),' , z2 = ',num2str(z2(i))];
    else
        name{i} = ['Bz vert data r1 = ',num2str(r1(i)),' , z1 = ', ...
            num2str(z1(i)),' , z2 = ',num2str(z2(i))];
    end
    mo_makeplot(3,num_pt(i),[dir,name{i}],0);
    Bz{i} = flipdata([dir,name{i}],num_pt(i));
    Bz_i = Bz{i};
    save([dir,name{i}],'Bz_i');
    figure; plot(Bz{i}(:,1),Bz{i}(:,2),'b-');
    xlabel(['Vertical Distance from z1 = ',num2str(z1(i))]);
    ylabel('Bz (T)'); title(name{i});
    mo_clearcontour;
end

```

```

% Open Data File:
load('C:\Users\Shawn\Documents\College\Maglev\matlab femm functions\magnet
mapping\brz_puck.mat');
close all; % Note: The units of B are Tesla (T)

for i = 1:length(brz_puck)
    % Set-up fitype and Options:
    ft = fitype('poly2');
    opts = fitoptions('Method','LinearLeastSquares');
    opts.Lower = [-Inf, 0, -Inf];
    opts.Upper = [Inf, 0, Inf];

    % Fit Model to Data:
    [fr{i}, gf{i}] = fit( brz_puck{i}(1:762,2),brz_puck{i}(1:762,1),ft,opts);

    % Plot Fit and Data:
    figure; h = plot( fr{i},brz_puck{i}(1:762,2),brz_puck{i}(1:762,1));
    legend(h,'data','fit','Location','NorthEast' );
    ylabel('magnetic field (kg)'); xlabel('radial position (in)');
    title(['puck ',num2str(brz_puck{i}(1,3)),' in']); grid('on');

    mu{i} = fr{i}.p1*brz_puck{i}(1,3)^5/-6; % mu parameter
    mu_unc{i} = mu{i}*5*0.05./brz_puck{i}(1,3)^4; % unc due to hight uncertainty
    mu_unc_rel{i} = mu_unc{i}/mu{i}; % relative uncertainty
    p1{i} = fr{i}.p1;
end

```

```

load('puckrdata.mat'); % load variables
pr = [puckrh1o36r250x250, puckrh1o74r250x250, puckrho75r200x200t1, ...
      puckrho75r250x250t1, puckrho75r250x250t2, puckrho93r250x250];

% Part 1
[data_adj,x,y] = plot_surf(puckrh1o74r250x250);
FieldAlongYAxis = data_adj(:,1);
YmaxIndex = find(FieldAlongYAxis == max(FieldAlongYAxis)); % Finds Index of min in the y vector.
CenterOfField = y(YmaxIndex(1)); % Sometimes two indices contain minimum values.
                                % Arbitrarily choose the first one.

% Part 2
LevitationHeight = 1;
LevitationHeightIndex = find(x == LevitationHeight);
FieldAtLevitationHeight = data_adj(:,LevitationHeightIndex);
figure; plot(y,FieldAtLevitationHeight);
title('Field Strength vs Y coordinate, at levitation height');
xlabel('Y Coordinate'); ylabel('Field Strength');

%Part 3
CentralPoint = data_adj(YmaxIndex(1),LevitationHeightIndex);

%Part 4
StrengthAtCenterOfField = data_adj(YmaxIndex(1),:);
figure; plot(x,StrengthAtCenterOfField);
title('Field Strength vs X Coordinate, at the center of the puck');
xlabel('X Coordinate');
ylabel('Field Strength');

```

```

% Open Data File:
load('C:\Users\Shawn\Documents\College\Maglev\matlab femm functions\Bring.mat');
close all % Note: The units of B are Tesla (T)

% Set-up fitype and Options:
ft = fitype('poly2');
opts = fitoptions('Method','LinearLeastSquares');
opts.Lower = [-Inf, 0, -Inf];
opts.Upper = [Inf, 0, Inf];

% Fit model to data.
[fitresult,gof] = fit(Bring{1}(:,1),Bring{1}(:,2),ft,opts);

% Plot Fit and Data:
figure; h = plot(fitresult,Bring{1}(:,1),Bring{1}(:,2));
legend(h,'data','fit','Location','NorthEast');
ylabel('magnetic field (T)'); xlabel('radial position (in)');
title('ring 0.7 in'); grid('on');
a = fitresult.p1;

```

```
function [ ] = surf_w_contour(data)
%SURF_W_CONTOUR takes magnet mapping data, makes a surf plot and contour
% plot, and overlays them to make a new plot.

    close all;
    figure; hold('on');
    surf(data);
    contour(data);
    title(inputname(1));
    saveas(gcf,sprintf('%s_surf_w_contour.fig',get(gca,'title'),'string'));
end
```

```

% Puck Radial Field Tracking:
% Starts at z = 0, goes to z = 2 in.
% Radius goes from r = 0 to r = 0.5 in.
% Resolution is 1000 pt/in. 3D Array Br_puck.
% 1st index is radial distance from puck
% 2nd index is axial distance from puck
% 3rd index is for radial distance or magnetic field
    % (1 for radial distance and 2 for magnetic field strength in tesla).
z = 0:0.001:2;
r1 = 0; r2 = 0.5;
Br_puck_cell = plot_horiz_Br(r1,z,r2,'puck with high carbon steel NdFeB 52 MGOe.FEM');

% Convert From Cell Array to Array:
for i = 1:length(Br_puck_cell)
    Br = Br_puck_cell{i};
    Br_puck(:,i,:) = Br;
end

% Puck Axial Filed Height:
% Starts at z = 0 goes to z = 2 in.
% Radius at r = 0 in.
% Resolution is 1000 pt/in. 2D Array Bz0_puck.
% 1st index is axial distance from puck.
% 2nd index is for axial distance or magnetic field
    % (1 for radial distance and 2 for magnetic field strength in tesla).
z1 = 0; z2 = 2; r = 0;
Bz0_puck_cell = plot_vert_Bz(r,z1,z2,'puck with high carbon steel NdFeB 52 MGOe.FEM');
Bz0_puck = Bz0_puck_cell{1};

% Save Results:
dir = 'C:\Users\Shawn\Documents\College\Maglev\matlab femm functions/';
name = 'tracking_puck.mat';
save([dir,name],'Br_puck','Bz0_puck')

```

Appendix C

Micro-controller Code

All code is written in C

C.1 Main Code ADC

```
/*
 * main.c
 */

// Include files
#include "F28x_Project.h"

// Function Prototypes.
void ConfigureADC(void);
void SetUpADCSoftware(void);
void sample(void);
void controlCode(Uint16 data);

// Global Variables
Uint16 HPdata;

int main(void) {
    // The following is standard set up code for any
    // application on this TI Launchpad. This set up
    // sequence can be found in most if not all the
    // example programs in ControlSUITE
```

```

InitSysCtrl();
InitGpio();
DINT;
InitPieCtrl();
IER = 0x0000;
IFR = 0x0000;
InitPieVectTable();
EINT;
ERTM;
// End Setup Code

// Set up ADC-A
ConfigureADC();

// Choose ADC channel and acquisition window
SetUpADCSoftware();

// Enter primary loop. This is an infinite loop
// that will handle all of the processing of our
// program.
while(1) {
    sample();
    controlCode();
    DELAY_US(25000); // delay for 25ms
}
return 0;
}

void ConfigureADC(void) {
    EALLOW;
    AdcaRegs.ADCCTL2.bit.PRESCALE = 6; // Set ADCCLK divider to /4
    // Set resolution of ADC-A
    AdcSetMode(ADC_ADCA, ADC_RESOLUTION_12BIT, ADC_SIGNALMODE_SINGLE);
    // Set Pulse Position to Late
    AdcaRegs.ADCCTL1.bit.INTPULSEPOS = 1;
    // Power up ADC
    AdcaRegs.ADCCTL1.bit.ADCPWDNZ = 1;
    // delay 1ms to allow enough time for power up
    DELAY_US(1000);
}

```

```

void SetUpADCSoftware(void) {
    Uint16 acqps = 14; // time in which ADC can read data from
                       // input pin (75ns)

    EALLOW;
    AdcaRegs.ADCSOC1CTL.bit.CHSEL = 1; // Sets input channel to ADC-in1
    AdcaRegs.ADCSOC1CTL.bit.ACQPS = acqps;
    // configures HWI for channel 1 of the ADC
    AdcaRegs.ADCINTSEL1N2.bit.INT1SEL = 1; // end of SOC1 will set INT1 flag
    AdcaRegs.ADCINTSEL1N2.bit.INT1E = 1; // enable INT1 flag
    AdcaRegs.ADCINTFLGCLR.bit.ADCINT1 = 1; // make sure INT1 flag is cleared
}

// Function that reads in data from ADC
void sample(void) {
    // Forces SOC1 to alert ADC-A channel 1 to read in data
    AdcaRegs.ADCSOCFRC1.all = 0x0002;

    // This register is a hardware interrupt that will
    // alert us as to when the ADC is finished reading in data.
    // The value will be set to 1 automatically by the hardware
    // when the data acquisition is complete
    while(AdcaRegs.ADCINTFLG.bit.ADCINT1 == 0);
    // This will clear the ADCINT1 value so that the ADC
    // can read in more values at a later time
    AdcaRegs.ADCINTFLGCLR.bit.ADCINT1 = 1;
    // store the data we just collected
    HPdata = AdcaResultRegs.ADCRESULT1;
}

```

C.2 DAC-ADC Test Code

```
/*
 * main.c
 * Adds a DAC configuration and a DAC test
 */

// Include files
#include "F28x_Project.h"
#include "F2837xS_adc.h"
#include "F2837xS_dac.h"

// Function Prototypes.
void ConfigureADC(void);
void SetUpADCSoftware(void);
void sample(void);

//Global Variables
Uint16 HPdata;
void configureDAC(Uint16 dac_num)
{
    EALLOW;

    CpuSysRegs.PCLKCR16.bit.DAC_A = 1; // enable DAC_A clock

    DacRegs.DACCTL.bit.DACREFSEL = 1; // use ADC VREFHI, not external signal
    DacRegs.DACCTL.bit.LOADMODE = 0; // load on SysClk (PWM not yet enabled)
    DacRegs.DACOUTEN.bit.DACOUTEN = 1; // enable output
    DacRegs.DACVALS.all = 0; // output = 0
    DELAY_US(10); // Delay for buffered DAC to power up

    EDIS;
}

/*
 * Sets the DAC's analog voltage based on value
 * Equation used:
 *     With DACVALS = DACVALA = value -->
 *     VDAC = (DACVALA * DACREF) / 4096
 *

```

```

* With VREFHI from ADC the DACREF value should be 3.3V.
* This gives a range for DACVALA of 0 to 1241
*/

void SetDAC(uint16_t DAC, uint16_t value)
{
    DacRegs.DACVALS.all = value;
    DELAY_US(2);
}

void TestDAC()
{
    uint16_t limit = 1024;
    uint16_t v;
    uint16_t DACA = 61;
    // ramp up
    for (v = 0; v < limit; v++)
        SetDAC(DACA, v);

    // ramp down
    for (v = limit; v > 0; v--)
        SetDAC(DACA, v);
}

int main(void) {
    // The following is standard set up code for any
    // application on this TI Launchpad. This set up
    // sequence can be found in most if not all the
    // example programs in ControlSUITE
    InitSysCtrl();
    InitGpio();
    DINT;
    InitPieCtrl();
    IER = 0x0000;
    IFR = 0x0000;
    InitPieVectTable();
    EINT;
    ERTM;
    // End Setup Code
}

```

```

// Set up ADC-A
ConfigureADC();

// Set up DAC-A
ConfigureDAC();

// Choose ADC channel and acquisition window
SetUpADCSoftware();

// Enter primary loop. This is an infinite loop
// that will handle all of the processing of our
// program.
while(1) {
    sample();
    DELAY_US(25000); //delay for 25ms
}
}

void ConfigureADC(void) {
    EALLOW;
    AdcaRegs.ADCCTL2.bit.PRESCALE = 6; // Set ADCCLK divider to /4
    // Set resolution of ADC-A
    AdcSetMode(ADC_ADCA, ADC_RESOLUTION_12BIT, ADC_SIGNALMODE_SINGLE);
    // Set Pulse Position to Late
    AdcaRegs.ADCCTL1.bit.INTPULSEPOS = 1;
    // Power up ADC
    AdcaRegs.ADCCTL1.bit.ADCPWDNZ = 1;
    // delay 1ms to allow enough time for power up
    DELAY_US(1000);
}

void SetUpADCSoftware(void) {
    Uint16 acqps = 14; // time in which ADC can read data from input pin (75ns)

    EALLOW;
    AdcaRegs.ADCSOC1CTL.bit.CHSEL = 1; // Sets input channel to ADC-in1
    AdcaRegs.ADCSOC1CTL.bit.ACQPS = acqps;
    // configures HWI for channel 1 of the ADC
    AdcaRegs.ADCINTSEL1N2.bit.INT1SEL = 1; // end of SOC1 will set INT1 flag
    AdcaRegs.ADCINTSEL1N2.bit.INT1E = 1; // enable INT1 flag

```

```

    AdcaRegs.ADCINTFLGCLR.bit.ADCINT1 = 1; // make sure INT1 flag is cleared
}

// Function that reads in data from ADC
void sample(void) {
    // Forces SOC1 to alert ADC-A channel 1 to read in data
    AdcaRegs.ADCSOCFRC1.all = 0x0002;

    // This register is a hardware interrupt that will
    // alert us as to when the ADC is finished reading in data.
    // The value will be set to 1 automatically by the hardware
    // when the data acquisition is complete
    while(AdcaRegs.ADCINTFLG.bit.ADCINT1 == 0);
    // This will clear the ADCINT1 value so that the ADC
    // can read in more values at a later time
    AdcaRegs.ADCINTFLGCLR.bit.ADCINT1 = 1;
    // store the data we just collected
    HPdata = AdcaResultRegs.ADCRESULT1;
}

```

C.3 Control Code

```
/*
 * control.c
 *
 */

#include <stdio.h>
#include <stdlib.h>
#include <math.h>
#include "control.h"
#include "dmat.h"

double findPos(double i, double u, double c, double c2) {
    double Bpuck[] = {-0.0977, 0.1215, -0.0011};
    double Bhall = i*c;
    double Bs = u*c2;
    double firstRoot;
    double secondRoot;
    double y = 0;

    int hasImagRoots = solve_quadratic(Bpuck[0], Bpuck[1], Bpuck[2] -
                                       Bhall - Bs, &firstRoot, &secondRoot);

    if(!hasImagRoots) {
        if (firstRoot < secondRoot) {
            y = firstRoot;
        } else {
            y = secondRoot;
        }
    }

    return y;
}

double control(double yd, double y, dmat *x, dmat *A, dmat *B, dmat *C,
               double D, unsigned int size) {
    double e = yd - y;

    dmat cx_prod_matrix;
```

```

    dmat ax_prod_matrix;
    dmat be_prod_matrix;

    dmat result_matrix;

    int i;

    dmat_mul(&cx_prod_matrix, C, x);
    double cx_prod_num = cx_prod_matrix.data[0][0];

    dmat_mul(&ax_prod_matrix, A, x);

    dmat_mul_s(&be_prod_matrix, B, e);

    dmat_add(&result_matrix, &be_prod_matrix, &ax_prod_matrix);

    for (i = 0; i < size; i++) {
        (x -> data)[i][0] = result_matrix.data[i][0];
    }

    return cx_prod_num + (D*e);
}

int solve_quadratic(double a, double b, double c, double *firstRoot,
                   double *secondRoot) {
    int hasImagRoots = 0;

    double discrim = (b*b) - (4*a*c);
    if (discrim >= 0) {
        *firstRoot = ((-1 * b) + sqrt(discrim)) / (2*a);
        *secondRoot = ((-1 * b) - sqrt(discrim)) / (2*a);
    } else {
        hasImagRoots = 1;
    }

    return hasImagRoots;
}

```

Appendix D

Schematics and Design Drawings

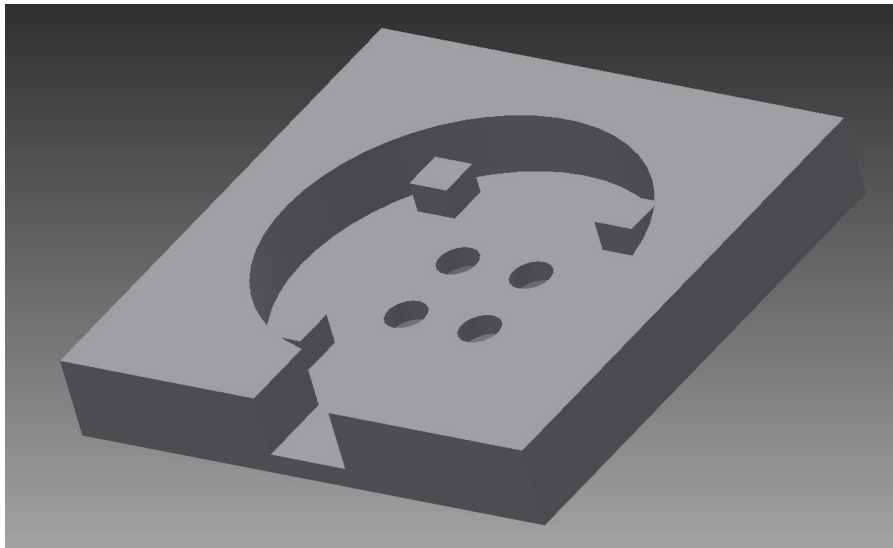


Figure D.1: A CAD drawing of the protective case we built and used to house the base of our system.

See Section 3.5 for more details on the protective case design and fabrication.

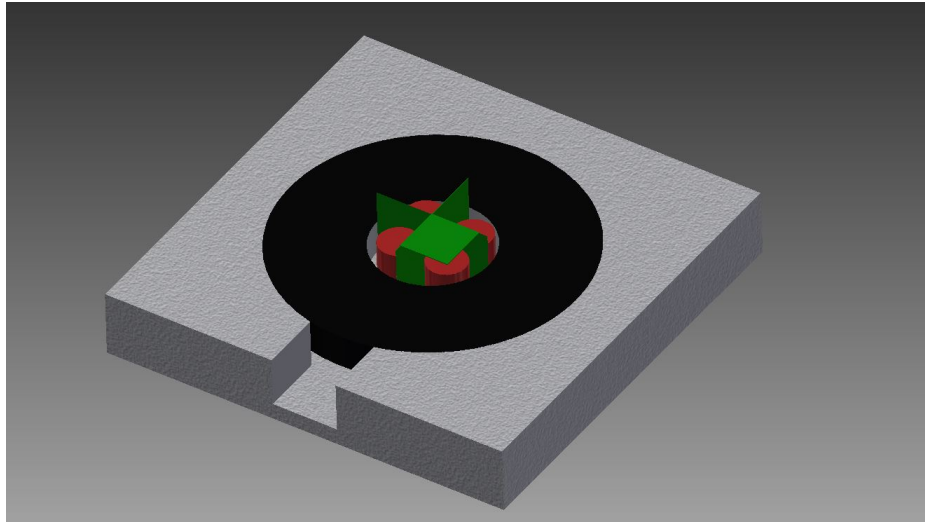


Figure D.2: A drawing that illustrates the placement of the ring magnet, solenoids, and PCB.

The data sheet beginning on the following page details the Darlington pair transistor the team used the circuit design [66]. A circuit diagram is provided in Figure 3.5.

2N6387, 2N6388

Plastic Medium-Power Silicon Transistors

These devices are designed for general-purpose amplifier and low-speed switching applications.

Features

- High DC Current Gain – $h_{FE} = 2500$ (Typ) @ $I_C = 4.0$ Adc
- Collector–Emitter Sustaining Voltage – @ 100 mAdc
 $V_{CE(sus)} = 60$ Vdc (Min) – 2N6387
 $= 80$ Vdc (Min) – 2N6388
- Low Collector–Emitter Saturation Voltage –
 $V_{CE(sat)} = 2.0$ Vdc (Max) @ I_C
 $= 5.0$ Adc – 2N6387, 2N6388
- Monolithic Construction with Built–In Base–Emitter Shunt Resistors
- TO–220AB Compact Package
- These Devices are Pb–Free and are RoHS Compliant*

MAXIMUM RATINGS (Note 1)

Rating	Symbol	Value	Unit
Collector–Emitter Voltage	2N6387 2N6388	V_{CEO} 60 80	Vdc
Collector–Base Voltage	2N6387 2N6388	V_{CB} 60 80	Vdc
Emitter–Base Voltage		V_{EB} 5.0	Vdc
Collector Current – Continuous – Peak		I_C 10 15	Adc
Base Current		I_B 250	mAdc
Total Power Dissipation @ $T_C = 25^\circ\text{C}$ Derate above 25°C		P_D 65 0.52	W W/ $^\circ\text{C}$
Total Power Dissipation @ $T_A = 25^\circ\text{C}$ Derate above 25°C		P_D 2.0 0.016	W W/ $^\circ\text{C}$
Operating and Storage Junction, Temperature Range		T_J, T_{stg} –65 to +150	$^\circ\text{C}$

Stresses exceeding those listed in the Maximum Ratings table may damage the device. If any of these limits are exceeded, device functionality should not be assumed, damage may occur and reliability may be affected.

1. Indicates JEDEC Registered Data.

THERMAL CHARACTERISTICS

Characteristics	Symbol	Max	Unit
Thermal Resistance, Junction–to–Case	$R_{\theta JC}$	1.92	$^\circ\text{C}/\text{W}$
Thermal Resistance, Junction–to–Ambient	$R_{\theta JA}$	62.5	$^\circ\text{C}/\text{W}$

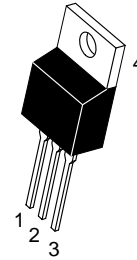
*For additional information on our Pb–Free strategy and soldering details, please download the ON Semiconductor Soldering and Mounting Techniques Reference Manual, SOLDERRM/D.



ON Semiconductor®

www.onsemi.com

DARLINGTON NPN SILICON POWER TRANSISTORS 8 AND 10 AMPERES 65 WATTS, 60 – 80 VOLTS



TO–220
CASE 221A
STYLE 1

MARKING DIAGRAM



2N638x = Device Code
x = 7 or 8
G = Pb–Free Package
A = Assembly Location
Y = Year
WW = Work Week

ORDERING INFORMATION

Device	Package	Shipping
2N6387G	TO–220 (Pb–Free)	50 Units / Rail
2N6388G	TO–220 (Pb–Free)	50 Units / Rail

2N6387, 2N6388

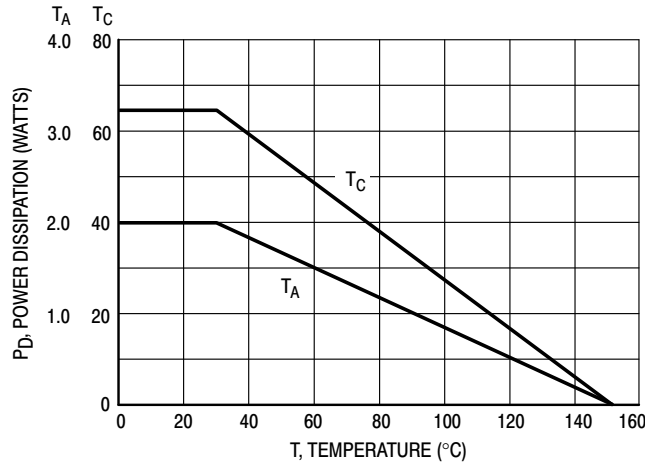


Figure 1. Power Derating

ELECTRICAL CHARACTERISTICS ($T_C = 25^\circ\text{C}$ unless otherwise noted) (Note 2)

Characteristic	Symbol	Min	Max	Unit	
OFF CHARACTERISTICS					
Collector–Emitter Sustaining Voltage (Note 3) ($I_C = 200\text{ mA dc}$, $I_B = 0$)	2N6387 2N6388	$V_{CEO(sus)}$	60 80	– –	Vdc
Collector Cutoff Current ($V_{CE} = 60\text{ Vdc}$, $I_B = 0$) ($V_{CE} = 80\text{ Vdc}$, $I_B = 0$)	2N6387 2N6388	I_{CEO}	– –	1.0 1.0	mAdc
Collector Cutoff Current ($V_{CE} = 60\text{ Vdc}$, $V_{EB(off)} = 1.5\text{ Vdc}$) ($V_{CE} = 80\text{ Vdc}$, $V_{EB(off)} = 1.5\text{ Vdc}$) ($V_{CE} = 60\text{ Vdc}$, $V_{EB(off)} = 1.5\text{ Vdc}$, $T_C = 125^\circ\text{C}$) ($V_{CE} = 80\text{ Vdc}$, $V_{EB(off)} = 1.5\text{ Vdc}$, $T_C = 125^\circ\text{C}$)	2N6387 2N6388 2N6387 2N6388	I_{CEX}	– – – –	300 300 3.0 3.0	μAdc mAdc
Emitter Cutoff Current ($V_{BE} = 5.0\text{ Vdc}$, $I_C = 0$)		I_{EBO}	–	5.0	mAdc
ON CHARACTERISTICS (Note 3)					
DC Current Gain ($I_C = 5.0\text{ Adc}$, $V_{CE} = 3.0\text{ Vdc}$) ($I_C = 10\text{ Adc}$, $V_{CE} = 3.0\text{ Vdc}$)	2N6387, 2N6388 2N6387, 2N6388	h_{FE}	1000 100	20,000 –	–
Collector–Emitter Saturation Voltage ($I_C = 5.0\text{ Adc}$, $I_B = 0.01\text{ Adc}$) ($I_C = 10\text{ Adc}$, $I_B = 0.1\text{ Adc}$)	2N6387, 2N6388 2N6387, 2N6388	$V_{CE(sat)}$	– –	2.0 3.0	Vdc
Base–Emitter On Voltage ($I_C = 5.0\text{ Adc}$, $V_{CE} = 3.0\text{ Vdc}$) ($I_C = 10\text{ Adc}$, $V_{CE} = 3.0\text{ Vdc}$)	2N6387, 2N6388 2N6387, 2N6388	$V_{BE(on)}$	– –	2.8 4.5	Vdc

DYNAMIC CHARACTERISTICS

Small–Signal Current Gain ($I_C = 1.0\text{ Adc}$, $V_{CE} = 5.0\text{ Vdc}$, $f_{test} = 1.0\text{ MHz}$)	$ h_{fe} $	20	–	–
Output Capacitance ($V_{CB} = 10\text{ Vdc}$, $I_E = 0$, $f = 1.0\text{ MHz}$)	C_{ob}	–	200	pF
Small–Signal Current Gain ($I_C = 1.0\text{ Adc}$, $V_{CE} = 5.0\text{ Vdc}$, $f = 1.0\text{ kHz}$)	h_{fe}	1000	–	–

Product parametric performance is indicated in the Electrical Characteristics for the listed test conditions, unless otherwise noted. Product performance may not be indicated by the Electrical Characteristics if operated under different conditions.

2. Indicates JEDEC Registered Data.

3. Pulse Test: Pulse Width $\leq 300\ \mu\text{s}$, Duty Cycle $\leq 2.0\%$.

2N6387, 2N6388

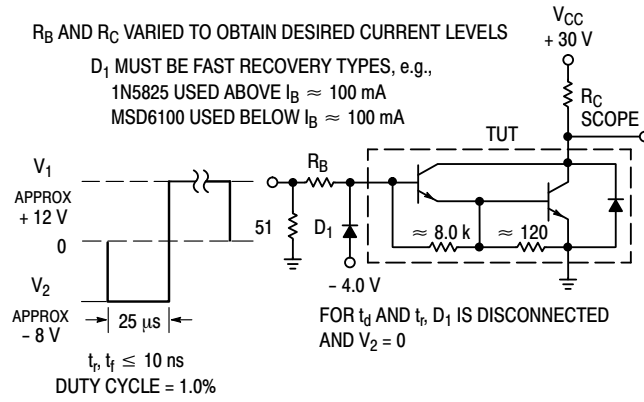


Figure 2. Switching Times Test Circuit

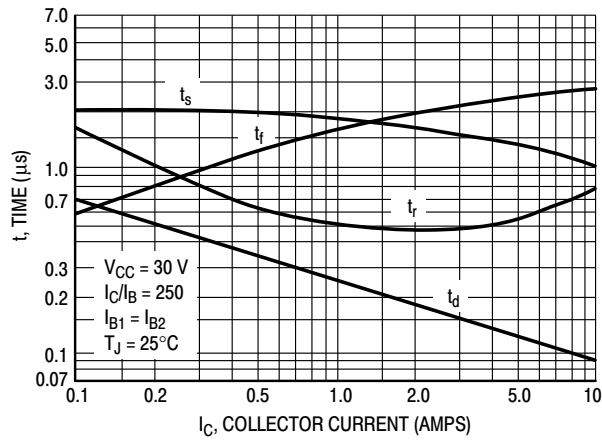


Figure 3. Switching Times

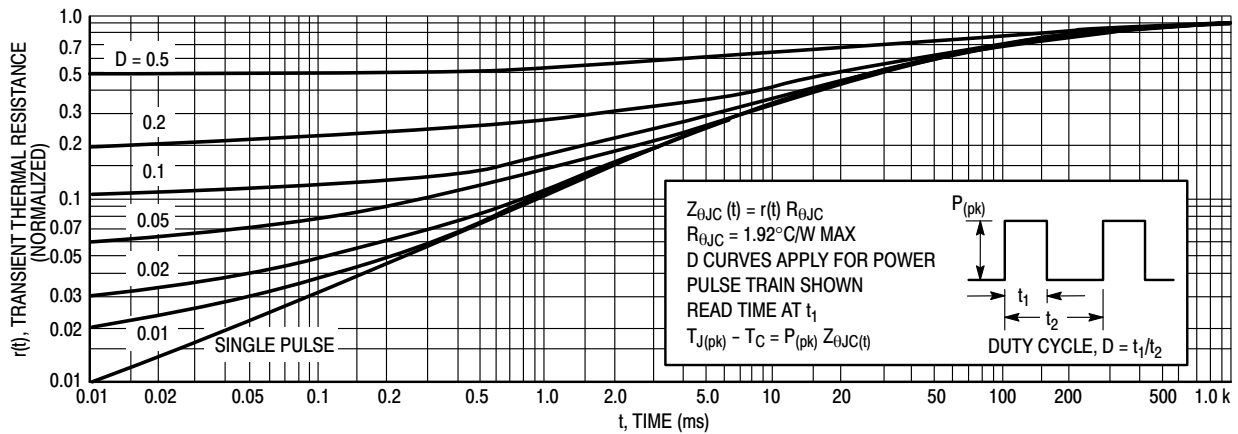


Figure 4. Thermal Response

2N6387, 2N6388

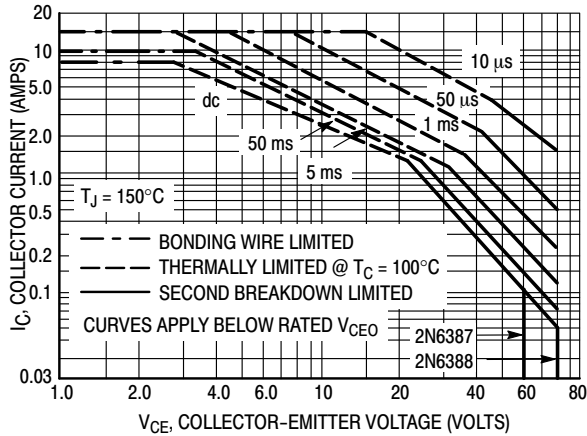


Figure 5. Active-Region Safe Operating Area

There are two limitations on the power handling ability of a transistor: average junction temperature and second breakdown. Safe operating area curves indicate $I_C - V_{CE}$ limits of the transistor that must be observed for reliable operation; i.e., the transistor must not be subjected to greater dissipation than the curves indicate.

The data of Figure 5 is based on $T_{J(pk)} = 150^\circ\text{C}$; T_C is variable depending on conditions. Second breakdown pulse limits are valid for duty cycles to 10% provided $T_{J(pk)} < 150^\circ\text{C}$. $T_{J(pk)}$ may be calculated from the data in Figure 4. At high case temperatures, thermal limitations will reduce the power that can be handled to values less than the limitations imposed by second breakdown

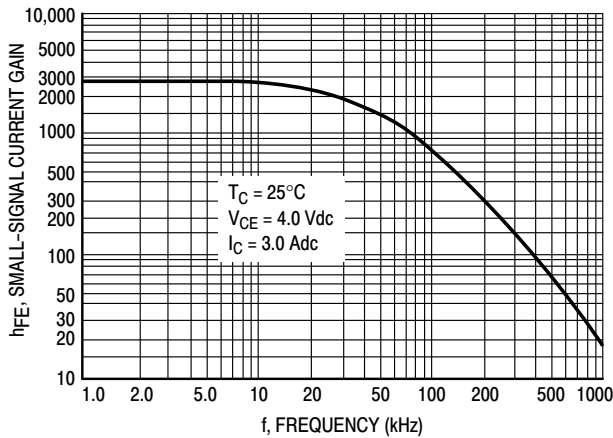


Figure 6. Small-Signal Current Gain

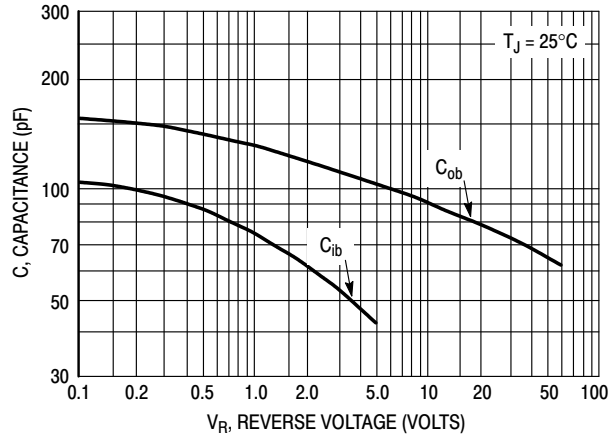


Figure 7. Capacitance

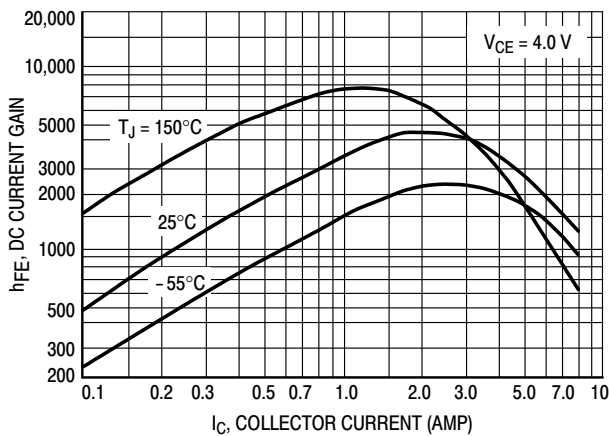


Figure 8. DC Current Gain

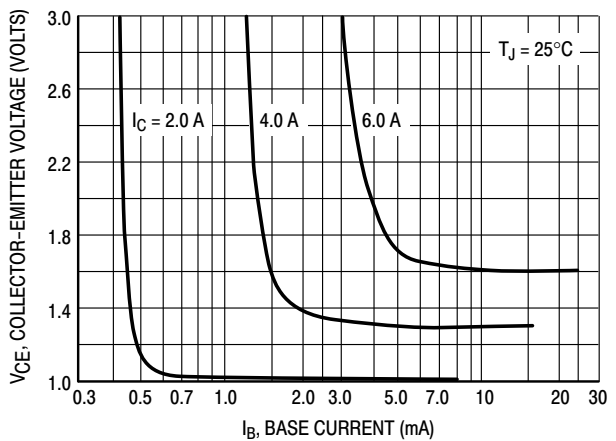


Figure 9. Collector Saturation Region

2N6387, 2N6388

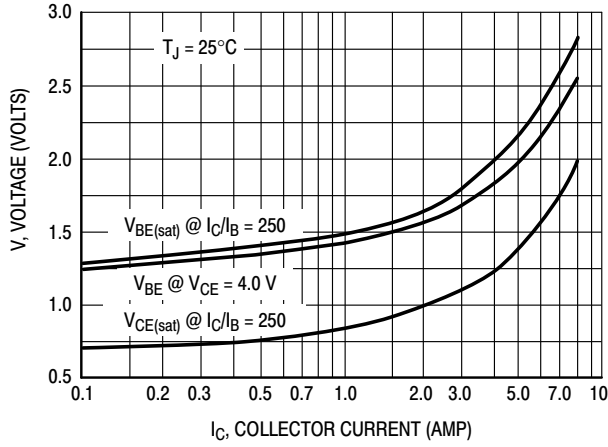


Figure 10. "On" Voltages

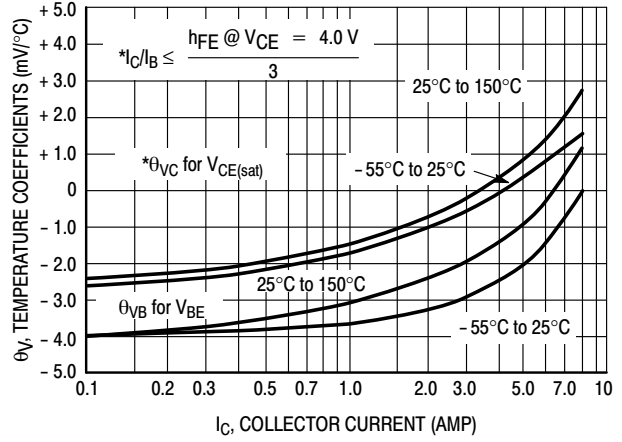


Figure 11. Temperature Coefficients

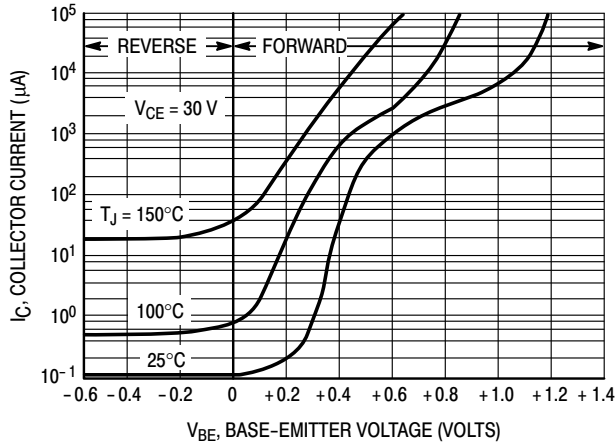


Figure 12. Collector Cut-Off Region

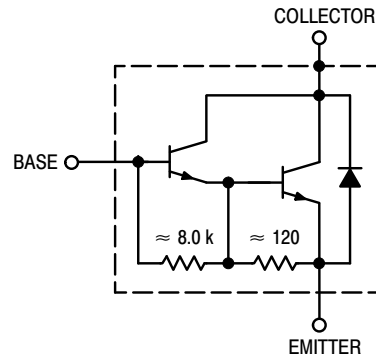
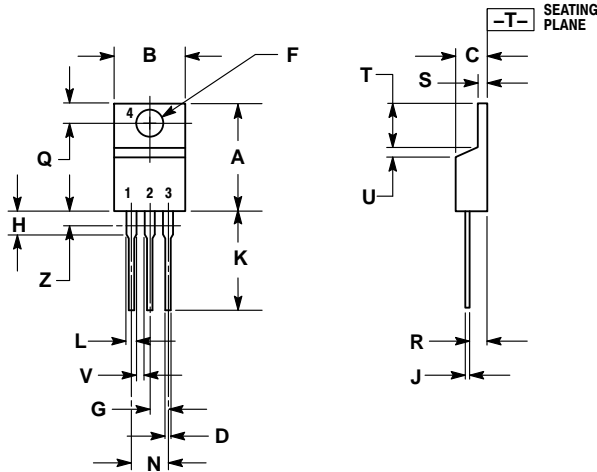


Figure 13. Darlington Schematic

2N6387, 2N6388

PACKAGE DIMENSIONS

TO-220
CASE 221A-09
ISSUE AH



NOTES:

1. DIMENSIONING AND TOLERANCING PER ANSI Y14.5M, 1982.
2. CONTROLLING DIMENSION: INCH.
3. DIMENSION Z DEFINES A ZONE WHERE ALL BODY AND LEAD IRREGULARITIES ARE ALLOWED.

DIM	INCHES		MILLIMETERS	
	MIN	MAX	MIN	MAX
A	0.570	0.620	14.48	15.75
B	0.380	0.415	9.66	10.53
C	0.160	0.190	4.07	4.83
D	0.025	0.038	0.64	0.96
F	0.142	0.161	3.61	4.09
G	0.095	0.105	2.42	2.66
H	0.110	0.161	2.80	4.10
J	0.014	0.024	0.36	0.61
K	0.500	0.562	12.70	14.27
L	0.045	0.060	1.15	1.52
N	0.190	0.210	4.83	5.33
Q	0.100	0.120	2.54	3.04
R	0.080	0.110	2.04	2.79
S	0.045	0.055	1.15	1.39
T	0.235	0.255	5.97	6.47
U	0.000	0.050	0.00	1.27
V	0.045	---	1.15	---
Z	---	0.080	---	2.04

STYLE 1:

- PIN 1. BASE
2. COLLECTOR
3. EMITTER
4. COLLECTOR

ON Semiconductor and the  are registered trademarks of Semiconductor Components Industries, LLC (SCILLC) or its subsidiaries in the United States and/or other countries. SCILLC owns the rights to a number of patents, trademarks, copyrights, trade secrets, and other intellectual property. A listing of SCILLC's product/patent coverage may be accessed at www.onsemi.com/site/pdf/Patent-Marking.pdf. SCILLC reserves the right to make changes without further notice to any products herein. SCILLC makes no warranty, representation or guarantee regarding the suitability of its products for any particular purpose, nor does SCILLC assume any liability arising out of the application or use of any product or circuit, and specifically disclaims any and all liability, including without limitation special, consequential or incidental damages. "Typical" parameters which may be provided in SCILLC data sheets and/or specifications can and do vary in different applications and actual performance may vary over time. All operating parameters, including "Typicals" must be validated for each customer application by customer's technical experts. SCILLC does not convey any license under its patent rights nor the rights of others. SCILLC products are not designed, intended, or authorized for use as components in systems intended for surgical implant into the body, or other applications intended to support or sustain life, or for any other application in which the failure of the SCILLC product could create a situation where personal injury or death may occur. Should Buyer purchase or use SCILLC products for any such unintended or unauthorized application, Buyer shall indemnify and hold SCILLC and its officers, employees, subsidiaries, affiliates, and distributors harmless against all claims, costs, damages, and expenses, and reasonable attorney fees arising out of, directly or indirectly, any claim of personal injury or death associated with such unintended or unauthorized use, even if such claim alleges that SCILLC was negligent regarding the design or manufacture of the part. SCILLC is an Equal Opportunity/Affirmative Action Employer. This literature is subject to all applicable copyright laws and is not for resale in any manner.

PUBLICATION ORDERING INFORMATION

LITERATURE FULFILLMENT:

Literature Distribution Center for ON Semiconductor
P.O. Box 5163, Denver, Colorado 80217 USA
Phone: 303-675-2175 or 800-344-3860 Toll Free USA/Canada
Fax: 303-675-2176 or 800-344-3867 Toll Free USA/Canada
Email: orderlit@onsemi.com

N. American Technical Support: 800-282-9855 Toll Free
USA/Canada

Europe, Middle East and Africa Technical Support:

Phone: 421 33 799 2940
Japan Customer Focus Center
Phone: 81-3-5817-1050

ON Semiconductor Website: www.onsemi.com

Order Literature: <http://www.onsemi.com/orderlit>

For additional information, please contact your local Sales Representative

Mouser Electronics

Authorized Distributor

Click to View Pricing, Inventory, Delivery & Lifecycle Information:

[ON Semiconductor:](#)

[2N6387](#) [2N6387G](#) [2N6388](#) [2N6388G](#)

References

- [1] G. Abbascia, K. Asenso, and A. White, “Magnetically Levitated Vertical-Axis Wind Turbine,” B.S. thesis, Worcester Polytechnic Institute, Worcester, Massachusetts, 2009 [Online]. Available: <https://web.wpi.edu/Pubs/E-project/Available/E-project-043009-111617/unrestricted/MagneticallyLevitatedVerticalAxisWindTurbine.pdf>
- [2] M. Asadzadeh. (2010). *An Introduction to the Finite Element Method (FEM) for Differential Equations* [Online]. Available: http://www.math.chalmers.se/~mohammad/teaching/Fourier/LectureNotes_A3/draft_1.pdf (accessed Jun. 11, 2016). DOI: 10.13140/2.1.4865.3128
- [3] S. I. Babic and C. Akyel, “Improvement in the Analytical Calculation of the Magnetic Field Produced by Permanent Magnet Rings,” in *Progress In Electromagnetics Research C*, vol. 5, pp. 71-82, Nov. 2008 [Online]. Available: <http://jpieer.org/PIERC/pier.php?paper=08101501>
- [4] J. Bardeen, L. N. Cooper, and J. R. Schrieffer, “Theory of Superconductivity,” in *Phys. Rev.*, vol. 108, no. 5, pp. 1175-204, Dec. 1957. DOI: 10.1103/physrev.108.1175
- [5] S. Basovich, S. Arogeti, Y. Menaker, and Z. Brand, “Magnetically Levitated Six-DOF Precision Positioning Stage With Uncertain Payload,” in *IEEE/ASME Trans. on Mechatronics*, vol. 21, no. 2, pp. 660-73, Apr. 2016. DOI: 10.1109/TMECH.2015.2489928
- [6] S. Benacchio, A. Malher, J. Boisson, and C. Touzé, “Design of Magnetic Vibration Absorber with Tunable Stiffness,” in *Nonlinear Dyn.*, vol. 85, no. 2, pp. 893-911, Jul. 2016. DOI: 10.1007/s11071-016-2731-3

- [7] M. V. Berry, “The Levitron™: An Adiabatic Trap for Spins,” in *Proc. R. Soc. Lond. A*, vol. 452, no. 1948, pp. 1207-20, May 1996. DOI: 10.1098/rspa.1996.0062
- [8] M. V. Berry and A. K. Geim, “Of Flying Frogs and Levitrons,” in *Eur. J. Phys.*, vol. 18, no. 4, pp. 307–13, Jan. 1997. DOI: 10.1088/0143-0807/18/4/012
- [9] S. Bhattacharjee. (2013, Apr. 30) *Lateral Bracing System* [Online]. Available: <http://seasoft022.blogspot.com/2013/04/lateral-bracing-system.html>
- [10] D. Blanding, *Exact Constraint: Machine Design Using Kinematic Principles*. New York, NY, USA: ASME Press, 1999. ISBN: 978-0791800850
- [11] E. H. Brandt, “Levitation in Physics,” in *Science*, vol. 243, no. 4889, pp. 349-55, Jan. 1989. DOI: 10.1126/science.243.4889.349
- [12] Y. Cai and D. M. Rote, “Review of Dynamic Stability of Repulsive-Force Maglev Suspension Systems,” in *IEEE Trans. Magn.*, vol. 38, no. 2, pp. 1383-90, Mar. 2002. DOI: 10.1109/20.996030
- [13] W. C. Caruso, K. M. Cintorino, B. D. McPheron, and Roger Williams. (2016). *A Procedure for Analyzing a Magnetic Levitation Toy* [Online]. Available: <http://egr.uri.edu/wp-uploads/asee2016/36-443-1-RV.pdf> (accessed Jun. 3, 2016).
- [14] L. D. Cohen and I. Cohen, “Finite Elements for Active Contour Models and Balloons for 2D and 3D Images,” in *IEEE Trans. Pattern Anal. Mach. Intell.*, vol. 15, no. 11, pp. 1131-47, Nov. 1993. DOI: 10.1109/34.244675
- [15] E. Comay, “A Difference between Solenoid and Magnetic Spin,” in *J. Magn. Magn. Mater.*, vol. 43, no. 1, pp. 59–60, Jun. 1984. DOI: 10.1016/0304-8853(84)90274-9
- [16] S. Earnshaw, “On the Nature of the Molecular Forces which Regulate the Constitution of the Luminiferous Ether,” in *Trans. Camb. Phil. Soc.*, vol. 7, pp. 97-112, 1842 [Online]. Available: https://ia800700.us.archive.org/33/items/cbarchive_36266_onthenatureofthemolecularforce1833/onthenatureofthemolecularforce1833.pdf

- [17] A. El Hajjaji and M. Ouladsine, “Modeling and Nonlinear Control of Magnetic Levitation Systems,” in *IEEE Trans. Ind. Electron.*, vol. 48, no. 4, pp. 831-838, Aug. 2001. DOI: 10.1109/ICMSAO.2011.5775532
- [18] A. V. Filatov, E. H. Maslen, and George T. Gillies, “A Method of Noncontact Suspension of Rotating Bodies using Electromagnetic Forces,” in *J. Appl. Phys.*, vol. 91, no. 4, pp. 2355-71, Feb. 2002. DOI: 10.1063/1.1432113
- [19] D. G. Fink and D. Christiansen, *Electronics Engineers Handbook*, 3rd ed. New York, NY, USA: McGraw Hill, 1989. ISBN: 978-0070209824
- [20] T. P. Fries and T. Belytschko, “The Extended/Generalized Finite Element Method: An Overview of the Method and its Applications,” in *Int. J. Numer. Meth. Engng.*, vol. 84, no. 3, pp. 253-304, Oct. 2010. DOI: 10.1002/nme.2914
- [21] J. García-Martín, J. Gómez-Gil, and E. Vázquez-Sánchez, “Non-Destructive Techniques Based on Eddy Current Testing,” in *Sensors*, vol. 11, pp. 2525-65, Feb. 2011. DOI: 10.3390/s110302525
- [22] D. J. Griffiths, *Introduction to Electrodynamics*, 3rd ed. Upper Saddle River, NJ, USA: Prentice Hall, 1999. ISBN: 978-0138053260
- [23] M. Grillakis. MATH462. Lecture Notes, “The Finite Element Method.” University of Maryland, College Park, MD, May 2, 2016.
- [24] I. Groning, S. Butz, and G. Henneberger, “Design of a Microcontroller-Based State Control for a Magnetic Levitation Transport System,” in *IECON '98: Proceedings of the 24th Annual Conference of the IEEE Industrial Electronics Society*, Aachen, Germany, 1998, pp. 1658-62. DOI: 10.1109/IECON.1998.722919
- [25] Y. Guo, J. X. Jin, J. G. Zhu, and H. Y. Lu, “Design and Analysis of a Prototype Linear Motor Driving System for HTS Maglev Transportation,” in *IEEE Trans. Appl. Supercond.*, vol. 17, no. 2, pp. 2087-90, Jun. 2007. DOI: 10.1109/TASC.2007.898185
- [26] G. S. Gupta and S. C. Mukhopadhyay, “Embedded Microcontroller Based Magnetic Levitation,” in *Embedded Microcontroller Interfacing: Designing Integrated Projects*. New York, NY, USA: Springer, 2010, ch. 7, pp. 127–55. ISBN: 978-3642136351

- [27] X. Hai-Jun and S. Jian, “Failure Analysis and Optimization Design of a Centrifuge Rotor,” in *Eng. Fail. Anal.*, vol. 14, no. 1, pp. 101-09, Jan. 2007. DOI: 10.1016/j.engfailanal.2005.12.007
- [28] L. Heinzle, “Eddy Current Testing Using the Bode 100,” OMICRON Lab, Putnam, CT, 2011. Available: https://www.omicron-lab.com/fileadmin/assets/customer_examples/Article_Eddy_Current_Testing_v1_0.pdf
- [29] R. J. A. Hill and L. Eaves., “Nonaxisymmetric Shapes of a Magnetically Levitated and Spinning Water Droplet,” in *Phys. Rev. Lett.*, vol. 101, no. 23, pp. 234501-04, Dec. 2003. DOI: 10.1103/PhysRevLett.101.234501
- [30] R. L. Hollis and S. E. Salcudean, “Input/ Output System for Computer use Interface Using Magnetic Levitation,” U.S. Patent 5 146 566, Sep. 8, 1992.
- [31] International Rectifier, “HEXFET Power MOSFET,” IRLB8721PbF datasheet, Apr. 2009. Available: <https://cdn-shop.adafruit.com/datasheets/irlb8721pbf.pdf>
- [32] D. Ishak, Z. Q. Zhu, D. Howe, “Eddy-Current Loss in the Rotor Magnets of Permanent-Magnet Brushless Machines Having a Fractional Number of Slots per Pole,” in *IEEE Trans. Magn.*, vol. 41, no. 9, pp. 2462-69, Sep. 2005. DOI: 10.1109/TMAG.2005.854337
- [33] Y. Iwasa and H. Lee, “‘Electromaglev’—Magnetic Levitation of a Superconducting Disc with a DC Field Generated by Electromagnets: Part 1. Theoretical and experimental results on operating modes, lift-to-weight ratio, and suspension stiffness,” in *Cryogenics*, vol. 37, no. 12, pp. 807–16, Dec. 1997. DOI: 10.1016/S0011-2275(97)00082-9
- [34] V. S. Jesna and S. Ushakumari, “Stabilization of Three pole Active Magnetic Bearing by Sliding Mode Control Techniques,” in *International Conference on Green Technologies*, Trivandrum, Kerala, India, 2012, pp. 147-54. DOI: 10.1109/ICGT.2012.6477963
- [35] T. B. Jones, M. Washizu, and R. Gans, “Simple Theory for the Levitron[®],” in *J. Appl. Phys.*, vol. 82, no. 2, pp. 883-88, July 1997. DOI: 10.1063/1.365856

- [36] R. V. Jones. (2001). *Laplace Transforms and Circuit Analysis* [Online]. Available: http://people.seas.harvard.edu/~jones/es154/lectures/lecture_0/laplace/laplace.html (accessed Jun. 3, 2016).
- [37] W. Jones, “Earnshaw’s Theorem and the Stability of Matter,” in *Eur. J. Phys.*, vol. 1, no. 2, pp. 85-88, Apr. 1980. DOI: 10.1088/0143-0807/1/2/004
- [38] Y. Kato, T. Yoshida, K. Ohniwa, “Self-Sensing Active Magnetic Bearings with Zero-Bias-Current Control,” in *Electr. Eng. Jpn.*, vol. 165, no. 2, pp. 69-76, Nov. 2008. DOI: 10.1002/eej.20616
- [39] S. Katzen, *The Quintessential PIC[®] Microcontroller*, 2nd ed. London, UK: Springer-Verlag, 2005. ISBN: 978-1852339425
- [40] S. Kazadi, A. Li, A. An, B. Shen, and A. Pyun, “A Levitating Motor Based on Passive Magnetic Levitation Supports,” in *2015 IEEE 10th Conference on Industrial Electronics and Applications*, Auckland, New Zealand, 2015, pp. 2046-49. DOI: 10.1109/ICIEA.2015.7334450
- [41] W. Kim and D. L. Trumper, “Linear Motor-Levitated Stage for Photolithography,” in *CIRP Ann.*, vol. 46, no. 1, pp. 447-50, Jan. 1997. DOI: 10.1016/S0007-8506(07)60862-2
- [42] W. Kim and D. L. Trumper, “High-Precision Magnetic Levitation Stage for Photolithography,” in *Precis. Eng.*, vol. 22, no. 2, pp. 66-77, Apr. 1998. DOI: 10.1016/S0141-6359(98)00009-9
- [43] W. Kim, S. Verma, and H. Shakir, “Design and Precision Construction of Novel Magnetic-Levitation-Based Multi-Axis Nanoscale Positioning Systems,” in *Precis. Eng.*, vol. 31, no. 4, pp. 337-50, Oct. 2007. DOI: 10.1016/j.precisioneng.2007.02.001
- [44] R. D. Knight, “Electromagnetic Induction,” in *Physics for Scientists and Engineers: A Strategic Approach*, 3rd ed. New York, NY, USA: Pearson, 2013, ch. 33, pp. 962-1002. ISBN: 978-0321740908
- [45] Z. Kohari and I. Vajda, “Spin-down Measurements and Loss Calculation of Multi-Layer, Multi-Pole HTS Magnetic Bearings,” in *Supercond. Sci. Technol.*, vol. 18, no. 2, pp. S105-S110, Feb. 2005. DOI: 10.1088/0953-2048/18/2/023

- [46] R. Krechetnikov and J. E. Marsden, “On Destabilizing Effects of Two Fundamental Non-conservative Forces,” in *Physica D*, vol. 214, pp. 25-32, Feb. 2006. DOI: 10.1016/j.physd.2005.12.003
- [47] T. R. Kuphaldt, “Inductors,” in *Lessons in Electric Circuits, Volume One: DC*, 5th ed. [Online]. Boise, ID: EETech, 2006, ch. 15, pp. 481-500. Available: <http://www.ibiblio.org/kuphaldt/electricCircuits/DC/DC.pdf>
- [48] V. Labinac, N. Erceg, and D. Kotnik-Karuza, “Magnetic Field of a Cylindrical Coil,” in *Amer. J. Phys.*, vol. 74, no. 7, pp. 621-27, July 2006. DOI: 10.1119/1.2198885
- [49] Q. Li, L. Wan, L. Zhu, and Z. Xu, “Decoupling Control for a Magnetic Suspension Stage,” in *2007 IEEE International Conference on Control and Automation*, Guangzhou, China, 2007, pp. 323-28. DOI: 10.1109/ICCA.2007.4376372
- [50] D. L. Logan, “Introduction,” in *A First Course of the Finite Element Method*, 4th ed. Toronto, Ontario, Canada: Cengage, 2007, ch. 1, pp. 1-27. ISBN: 0-534552986
- [51] K. Lum, V. T. Coppola, and D. S. Bernstein, “Adaptive Autocentering Control for an Active Magnetic Bearing Supporting a Rotor with Unknown Mass Imbalance,” in *IEEE Trans. Control Syst. Technol.*, vol. 4, no. 5, pp. 587-97, Sept. 1996. DOI: 10.1109/87.531925
- [52] K. B. Ma, Y. V. Postrekhin, and W. K. Chu, “Superconductor and Magnetic Levitation Devices,” in *Rev. Sci. Instrum.*, vol. 74, no. 12, pp. 4989-5017, Dec. 2003. DOI: 10.1063/1.1622973
- [53] B. P. Mann and N. D. Sims, “Energy Harvesting from the Nonlinear Oscillations of Magnetic Levitation,” in *J. Sound Vib.*, vol. 319, no. 1, pp. 515-30, Jan. 2009. DOI: 10.1016/j.jsv.2008.06.011
- [54] MathWorks. (2016, Sep. 14) MATLAB R2016b, version 9.1. [Online]. Available: <https://www.mathworks.com/products/matlab.html>
- [55] D. Meeker. (2015, Oct. 25) *Finite Element Method Magnetics Version 4.2 User’s Manual* [Online]. Available: <http://www.femm.info/Archives/doc/manual42.pdf> (accessed Jun. 13, 2016).

- [56] D. Meeker. (2016, Jan. 12) Finite Element Method Magnetics, version 4.2. [Online]. Available: <http://www.femm.info/wiki/Download>
- [57] F. C. Moon and P. Chang, *Superconducting Levitation: Applications to Bearing and Magnetic Transportation*. Weinheim, Germany: Wiley, 2008. ISBN: 978-3527617531
- [58] G. Mur and A. T. de Hoop, "A Finite Element Method for Computing Three-Dimensional Electromagnetic Fields in Inhomogeneous Media," in *IEEE Trans. Magn.*, vol. 21, no. 6, pp. 2188-91, Nov. 1985. DOI: 10.1109/TMAG.1985.1064256
- [59] T. Nakata, N. Takahashi, K. Fujiwara, and A. Ahagon, "3-D Finite Element Method for Analyzing Magnetic Fields in Electrical Machines Excited from Voltage Sources," in *IEEE Trans. Magn.*, vol. 24, no. 6, pp. 2582-84, Nov. 1988. DOI: 10.1109/20.92180
- [60] National Science Foundation (n.d.) *The Hysteresis Loop and Magnetic Properties* [Online]. Available: <https://www.nde-ed.org/EducationResources/CommunityCollege/MagParticle/Physics/HysteresisLoop.htm>
- [61] C. R. Nave, "Condensed Matter," in *HyperPhysics* [Online]. Atlanta, GA: Georgia State University, 2016. Available: <http://hyperphysics.phy-astr.gsu.edu/hbase/emcon.html#emcon> (accessed Oct. 10, 2016).
- [62] C. R. Nave, "Electricity and Magnetism," in *HyperPhysics* [Online]. Atlanta, GA: Georgia State University, 2016. Available: <http://hyperphysics.phy-astr.gsu.edu/hbase/emcon.html#emcon> (accessed Jul. 13, 2016).
- [63] C. R. Nave, "Magnetic Properties of Ferromagnetic Materials," in *HyperPhysics* [Online]. Atlanta, GA: Georgia State University, 2016. Available: <http://hyperphysics.phy-astr.gsu.edu/hbase/Tables/magprop.html> (accessed Apr. 27, 2017).
- [64] D. Nedelkovski, "What is Hall Effect and How Hall Effect Sensors Work," in *How To Mechatronics* [Online]. Available: <http://howtomechatronics.com/how-it-works/electrical-engineering/hall-effect-hall-effect-sensors-work/> (accessed Mar. 3, 2017).

- [65] J. W. Nilsson and S. Riedel, *Electric Circuits*, 9th ed. New York, NY, USA: Pearson, 2010. ISBN: 978-0137050512
- [66] ON Semiconductor, “Plastic Medium-Power Silicon Transistors,” 2N6387 datasheet, Nov. 2014 [Rev. 15]. Available: <http://www.mouser.com/ds/2/308/2N6387-D-102357.pdf>
- [67] J. B. Peterson. (1941, Oct.) “Damping Characteristics of Dashpots,” National Bureau of Standards, Washington, DC, USA. [Online]. Available: <http://ntrs.nasa.gov/archive/nasa/casi.ntrs.nasa.gov/19930084797.pdf>
- [68] N. P. Plakhtienko, “Modeling a Vibrating Mechanical System with an Acceleration-Feedback Controlled Frictional Electromagnetic Damper,” in *Int. Appl. Mech.*, vol. 47, no. 1, pp. 97-106, Jun. 2011. DOI: 10.1007/s10778-011-0447-0
- [69] E. M. Purcell and D. J. Morin, *Electricity and Magnetism*, 3rd ed. Cambridge, MA, USA: Cambridge University Press, 2013. ISBN: 978-1107014022
- [70] E. Ramsden, *Hall-Effect Sensors: Theory and Applications*, 2nd ed. Burlington, MA, USA: Elsevier. ISBN: 978-0750679343
- [71] G. P. Rao, J. L. Kirtley, D. C. Meeker, and K. J. Donegan, “Hybrid Permanent Magnet/Homopolar Generator and Motor,” U.S. Patent 6 097 124, Aug. 1, 2000.
- [72] R. Ravaud, G. Lemarquand, V. Lemarquand, and C. Depollier, “Analytical Calculation of the Magnetic Field Created by Permanent-Magnet Rings,” in *IEEE Trans. Magn.*, vol. 44, no. 8, pp. 1982-89, Aug. 2008. DOI: 10.1109/TMAG.2008.923096
- [73] F. E. Reed, “Dynamic Vibration Absorbers and Auxiliary Mass Dampers,” in *Shock and Vibration Handbook*, 3rd ed. C. M. Harris, Ed. New York, NY, USA: McGraw Hill, 1988, ch. 6. ISBN: 978-0070268012.
- [74] T. G. Reese, O. Heid, R. M. Weisskoff, and V. J. Wedeen, “Reduction of Eddy Current-Induced Distortion in Diffusion MRI Using a Twice-Refocused Spin Echo,” in *Magn. Reson. Med.*, vol. 49, no. 1, pp. 177-82, Jan. 2003. DOI: 10.1002/mrm.10308

- [75] M. Reisinger, S. Silber, J. Sloupenský, M. Moravec, W. Amrhein, and P. Dirnberger, “Magnetically Levitated Rotor Spinning Drive System with High System Stability,” in *2015 IEEE 11th International Conference on Power Electronics and Drive Systems*, Sydney, NSW, 2015, pp. 1184-89. DOI: 10.1109/PEDS.2015.7203541
- [76] S. Rosofsky, “Numerically Modeling the Magnetic Fields of a Puck and a Ring Magnet,” May 2016, unpublished.
- [77] S. Ryf, T. Wolber, F. Duru, and R. Luechinger, “Interference of Neodymium Magnets with Cardiac Pacemakers and Implantable Cardioverter-Defibrillators: An in vitro Study,” in *Technol. Health Care*, vol. 16, no. 1, pp. 13-18, Jan. 2008.
- [78] N. Sadowski, Y. Lefèvre, M. Lajoie-Mazenc, and J. Cros, “Finite Element Torque Calculation in Electrical Machines while Considering the Mouvement,” in *IEEE Trans. Magn.*, vol. 28, no. 2, pp. 1410-13, Mar. 1992. DOI: 10.1109/20.123957
- [79] W. M. Saslow, “Maxwell’s Theory of Eddy Currents in Thin Conducting Sheets and Applications to Electromagnetic Shielding and MAGLEV,” in *Am. J. Phys.*, vol. 60, no. 8, pp. 693-711, Aug. 1992. DOI: 10.1119/1.17101
- [80] C. Schott, R. S. Popovic, S. Alberti, and M. Q. Tran, “High Accuracy Magnetic Field Measurements with a Hall Probe,” in *Rev. Sci. Instrum.*, vol. 70, no. 6, pp. 2703-26, Feb. 1999. DOI: 10.1063/1.1149831
- [81] P. D. Shanmuga, A. Cinitha, P. K. Umesh, and R. I. Nagesh, “Enhancing the Seismic Response of Buildings with Energy Dissipation Methods: An Overview,” in *J. of Civ. Eng. Res.*, vol. 4, no. 2A, pp. 17-22, 2014. DOI: 10.5923/c.jce.201401.04
- [82] M. D. Simon, L. O. Heflinger, and L. K. Geim, “Diamagnetically Stabilized Magnetic Levitation,” in *Am. J. Phys.*, vol. 69, no. 6, pp. 702-13, Jun. 2001. DOI: 10.1119/1.1375157
- [83] M. D. Simon, L. O. Heflinger, and S. L. Ridgway, “Spin Stabilized Magnetic Levitation,” in *Am. J. Phys.*, vol. 65, no. 4, pp. 286-92, Apr. 1997. DOI: 10.1119/1.18488
- [84] M. Spizzuoco, A. Occhiuzzi, and G. Serino, “Performance of a Semi-Active MR Control System for Earthquake Protection” in *13th World*

- Conference on Earthquake Engineering* Vancouver, B.C., Canada, 2004. Available: http://www.iitk.ac.in/nicee/wcee/article/13_2525.pdf
- [85] W. A. Strauss, “Computation of Solutions,” in *Partial Differential Equations: An Introduction*, 2nd ed. Hoboken, NJ, USA: Wiley, 2008, ch. 8, pp. 199-227. ISBN: 978-0470054567
- [86] M. D. Symans, M. C. Constantinou, D. P. Taylor, and K. D. Gargnajt, “Semi-Active Fluid Viscous Dampers for Seismic Response Control” in *Proc. of the First World Conference on Structural Control* Los Angeles, CA, 1994. Available: <http://www.taylordevices.com/Tech-Paper-archives/literature-pdf/23-Semi-ActiveFVD.pdf>
- [87] H. Toda, Z. P. Xia, J. B. Wang, K. Atallah, and D. Howe, “Rotor Eddy Current Loss in Permanent Magnet Brushless Machines,” in *IEEE Trans. Magn.*, vol. 40, no. 4, pp. 2104-06, Apr. 2004. DOI: 10.1109/TMAG.2004.832481
- [88] D. L. Trumper, S. M. Olson and P. K. Subrahmanyam, “Linearizing Control of Magnetic Suspension Systems,” in *IEEE Trans. Control Syst. Technol.*, vol. 5, no. 4, pp. 427-38, July 1997. DOI: 10.1109/87.595924
- [89] D. Utrata and D. Enyart. (2016). *Eddy Current Inspection* [Online]. Available: <http://www.iprt.iastate.edu/assistance/nde/tools/eddycurrent> (accessed Jun. 23, 2016).
- [90] J.G. Van Bladel, *Electromagnetic Fields*, 2nd ed. Hoboken, NJ, USA: Wiley, 2007. ISBN: 978-0471263883
- [91] Y. Wang, K. T. Chau, C. C. Chan, and J. Z. Jiang, “Transient Analysis of a New Outer-Rotor Permanent-Magnet Brushless DC Drive Using Circuit-Field-Torque Coupled Timestepping Finite Element Method,” in *IEEE Trans. Magn.*, vol. 38, no. 2, pp. 1297-300, Mar. 2002. DOI: 10.1109/20.996331
- [92] Z. Wang, Z. Chen, and J. Wang, “Feasibility Study of a Large-Scale Tuned Mass Damper with Eddy Current Damping Mechanism,” in *Earthq. Eng. & Eng. Vib.*, vol. 11, no. 3, pp. 391-401, Sep. 2012. DOI: 10.1007/s11803-012-0129-x
- [93] A. C. Webster and R. Vaicaitis, “Application of Tuned Mass Dampers to Control Vibrations of Composite Floor Systems,” in *Eng. J. AISC*, vol.

- 29, no. 3, pp. 116-24, 1992. Available: <http://www.civil.umd.edu/~ccfu/ref/TunedMassDampersCompositeFloor.pdf>
- [94] H. Yaghoubi, “The Most Important Maglev Applications,” in *J. Eng.*, vol. 2013, Article ID 537986, 19 pp., 2013. DOI: 10.1155/2013/537986
- [95] S. D. Yang. (2014). *The Laplace Transform in Circuit Analysis* [Online]. Available: http://www.ee.nthu.edu.tw/~sdyang/courses/circuits/ch13_std.pdf (accessed Jun. 3, 2016).
- [96] Z. Zhang and C. Menq, “Six-Axis Magnetic Levitation and Motion Control,” in *IEEE Trans. Rob.*, vol. 23, no. 2, pp. 196-205, Apr. 2007. DOI: 10.1109/TRO.2007.892232
- [97] H. Zhu, T. Teo and C. Pang, “Design and Modeling of a Six-Degree-of-Freedom Magnetically Levitated Positioner Using Square Coils and 1-D Halbach Arrays,” in *IEEE Transactions on Industrial Electronics*, vol. 64, no. 1, pp. 440-450, Jan. 2017. href<http://doi.org/10.1109/TIE.2016.2598811>